ABSTRACT

Name: Anna Pla-Dalmau Department: Chemistry

Title: Design of Fluorescent Compounds for Scintillation Detection

Major: Chemistry Degree: Doctor of Philosophy

Approved by: Date:

Charles W. Spangler 8/7/90

Dissertation Director

NORTHERN ILLINOIS UNIVERSITY

AAB1674

FERMILAB
LIBRARY

ABSTRACT

Plastic scintillation detectors for high energy physics applications require the development of new fluorescent compounds to meet the demands set by the future generation of particle accelerators such as the Superconducting Supercollider (SSC). Plastic scintillators are commonly based on a polymer matrix doped with two fluorescent compounds: the primary dopant and the wavelength shifter. Their main characteristics are fast response time and high quantum efficiency. The exposure to larger radiation doses and demands for larger light output questions their survivability in the future experiments. A new type of plastic scintillator - intrinsic scintillator - has been suggested. It uses a single dopant as primary and wavelength shifter, and should be less susceptible to radiation damage.

Organic fluorescent compounds exhibiting a large spectral separation between absorption and fluorescence spectra such as 2-(2'-hydroxyphenyl)benzothiazole (HBT) and 3-hydroxyflavone (3HF) have been studied in polystyrene as dopants for intrinsic scintillators. HBT and 3HF undergo excited state proton transfer upon excitation by UV or ionizing radiation, thus showing a shift between absorption and emission spectra. In order to improve their quantum yield, several derivatives of both compounds have been prepared by substitution in the phenyl ring. A relationship structure-quantum yield has been observed. In HBT, the quantum yield increased using substituents with an electron-withdrawing or resonance

character. In 3HF, the para-substituted derivatives showed higher quantum yields than the ortho-derivatives.

Radiation damage studies have been performed on polystyrene doped with HBT and 3HF, as well as for the undoped polymer. The irradiation results indicate that HBT forms a conformational isomer absorbing at a longer wavelength, thus reducing the initial Stokes shift. 3HF does not undergo any substantial damage. Polystyrene shows the formation of transient excited species that are quenched in the presence of oxygen. Permanent damage to the polymer is observed at about 400 nm.

NORTHERN ILLINOIS UNIVERSITY

DESIGN OF FLUORESCENT COMPOUNDS FOR SCINTILLATION DETECTION

A DISSERTATION SUBMITTED TO THE GRADUATE SCHOOL
IN PARTIAL FULFILLMENT OF THE REQUIREMENTS
FOR THE DEGREE
DOCTOR OF PHILOSOPHY

DEPARTMENT OF CHEMISTRY

BY

ANNA PLA-DALMAU

DEKALB, ILLINOIS

AUGUST 1990

Certification: In accordance with departmental and Graduate School policies, this dissertation is accepted in partial fulfillment of degree requirements.

Charles W Spangler

Dissertation Director

8/7/90

Date

ACKNOWLEDGEMENTS

I wish to express my sincerest gratitude to my major professor, Dr. Charles W. Spangler, not only for his help and advice during the performance of this research, but also for his kindness and friendship. I am deeply grateful to Dr. Alan D. Bross, in charge of the scintillating fiber detector development in the Particle Detector Group at Fermi National Accelerator Laboratory, a physicist who agreed to be one of my advisors, although it "only was for a chemistry dissertation". I appreciate their help and guidance throughout the course of this work, as well as their ability to extend bridges between chemistry and physics.

I want to extend my gratitude to Dr. David F. Anderson, head of the Particle Detector Group at Fermilab, for his unconditional support during my three years in the PDG. Also, his understanding made possible a flexible schedule that permitted me to complete the coursework requirements and numerous trips to DeKalb.

I also want to thank Dr. David Piatak, Dr. Steven Gray, Dr. Steven Bachrach, and Dr. Daniel Kaplan for their help in serving as committee members. Dr. Bachrach provided valuable suggestions and guidance for the energy calculation studies.

I am indebted to Fermi National Accelerator Laboratory and to the Graduate School of Northern Illinois University for their financial support.

I am thankful for the help, advice, and camaraderie of former and current members of the PDG at Fermilab: Mark Lundin, Kerry Mellott, and especially Brian Kross, who also added optimism and good humor.

I extend my appreciation to the members of Charley's group at NIU for their assistance on numerous occasions: Kathleen Havelka, Tom Hall, and Pei-Kang Liu.

Very special thanks are due to my parents, Josep and Consol, and my sister Marta for their love and encouragement. My sincerest gratitude is due to my dear friend Jordi who has endured with good humor and patience the long hours I have spent in the laboratory. This dissertation is dedicated to them.

TABLE OF CONTENTS

	Page
LIST OF TABLES	vii
LIST OF FIGURES	viii
LIST OF APPENDICES	xiii
I. INTRODUCTION	1
A. Scintillation Detectors	2
B. Status of Plastic Scintillators	6
1. Advances in Polymer Development	7
2. Advances in Dopant Development	9
3. Radiation Damage in Plastic Scintillators	18
C Fluorescent Compounds with Large Stokes Shift	23
1. Photophysics of 2-(2'-Hydroxyphenyl)benzothiazole (HBT)	25
2. Photophysics of 3-Hydroxyflavone (3HF)	31
3. Methodology for HBT and 3HF Syntheses	35
II. RESULTS AND DISCUSSION	37
A. Radiation Damage Studies on Polystyrene	37
1. Irradiation in Different Environments	44
2. Irradiation of Samples with Different Molecular Weights	46
3. Irradiation of Samples of Different Monomer Purification Processes	50
B. HBT and Its Derivatives	51

		Page
	C. 3HF and Its Derivatives	60
	D. Fluorescence as a Function of Temperature	70
	1. HBT and Its Derivatives	72
	2. 3HF and Its Derivatives	75
	E. Absolute Quantum Yield Measurements for 3HF	81
	F. Radiation Damage Studies on HBT- and 3HF-Doped Scintillators	82
	1. Irradiation Results for HBT	84
	2. Irradiation Results for 3HF	91
III.	CONCLUSIONS	95
IV.	EXPERIMENTAL SECTION	101
	A. General Considerations	101
	1. Instrumentation	101
	2. Fluorescence Measurements	101
	3. Polymerizations	102
	4. Radiation Damage Studies	103
	5. Quantum Yield Determinations	104
	6. Molecular Orbital Calculations	105
	B. Starting Materials	105
	1. Preparation of 3-Fluorosalicylic Acid	106
	C. Products: Fluorescent Compounds	107
	1. 2-(2'-Hydroxyphenyl)benzothiazole Derivatives	107
	2. 3-Hydroxyflavone Derivatives	112
REFERENCES		122
APPENDICES		128

LIST OF TABLES

		Page
Table 1.	List of HBT derivatives studied	55
Table 2.	Photophysical characteristics of HBT and its derivatives in a polystyrene matrix	56
Table 3.	Relative quantum yields of HBT and its derivatives	59
Table 4.	List of 3HF derivatives studied	65
Table 5.	Photophysical characteristics of 3HF and its derivatives in a polystyrene matrix	66
Table 6.	Relative quantum yields of 3HF and its derivatives	69
Table 7.	Absolute quantum yield values for HBT and 3HF derivatives in polystyrene	83

LIST OF FIGURES

		Page
Figure 1.	p-Terphenyl (PTP)	10
Figure 2.	p-Quaterphenyl (PQP)	11
Figure 3.	1,4-Bis(4-methyl-5-phenyloxazol-2-yl)benzene (DMPOPOP)	11
Figure 4.	2,5-Diphenyloxazole (PPO)	11
Figure 5.	2-(4-Biphenylyl)-5-(4-tert-butylphenyl)-1,3,4-oxadiazole (BPBD)	11
Figure 6.	2-(4-Biphenylyl)-5-phenyl-1,3,4-oxadiazole (PBD)	12
Figure 7.	7H-Benzimidazo[2,1-a]benz[de]isoquinoline-7-one (BBQ)	12
Figure 8.	2,5-Bis(5-tert-butyl-2-benzoxazolyl)thiophene (BBOT)	12
Figure 9.	2-(p-n-Decyloxyphenyl)-5-phenyl-1,3,4-oxadiazole (R-PDP)	14
Figure 10.	p-Bis(2-p-n-decyloxyphenyl)-1,3,4-oxadiazol--5-yl)benzene (R-PDPDP-R)	14
Figure 11	2',2''-Dimethyl-p-terphenyl	14
Figure 12.	syn-Indenofluorene (SIF)	14
Figure 13.	Oligo 408	15
Figure 14.	Oligo 373	15
Figure 15.	1-Phenyl-3-mesityl-2-pyrazoline (PMP)	16

		Page
Figure 16.	2,2'-Bipyridyl-3,3'-diol (BPD)	17
Figure 17.	3-Hydroxyflavone (3HF)	17
Figure 18.	2-(2'-Hydroxyphenyl)-benzothiazole (HBT)	17
Figure 19.	General scheme for excited-state intramolecular proton transfer	24
Figure 20.	Excited-state intramolecular proton transfer for HBT	26
Figure 21.	Resonant contributions to the ionic form of HBT	28
Figure 22.	Excited-state intramolecular proton transfer for 3HF	32
Figure 23.	Resonance structures for the 3HF tautomer	33
Figure 24.	Polystyrene transmittance immediately after irradiation	39
Figure 25.	Fluorescence of irradiated polystyrene	41
Figure 26.	Polystyrene transmittance after oxygen annealing	42
Figure 27.	High molecular weight polystyrene irradiated at 10 Mrad	48
Figure 28.	Low molecular weight polystyrene irradiated at 10 Mrad	49
Figure 29.	Absorption and fluorescence spectra of HBT in PS	52
Figure 30.	Resonance forms delocalizing the charges created by proton transfer in HBT	53
Figure 31.	Absorption and fluorescence spectra of 3HF in PS	61
Figure 32.	Differences between absorption and fluorescence spectra of 2M3HF and 4P3HF in PS	67
Figure 33.	Changes in fluorescence yield of HBF and its derivatives as a function of temperature	73

Page

Figure 34.	Changes in fluorescence yield as a function of temperature for HBT and its derivatives relative to each value at room temperature	74
Figure 35.	Changes in fluorescence yield of 3HF and its ortho-derivatives as a function of temperature	76
Figure 36.	Changes in fluorescence yield of 3HF and its para-derivatives as a function of temperature	77
Figure 37.	Changes in fluorescence yield as a function of temperature for 3HF and its derivatives relative to each yield at room temperature	78
Figure 38.	Comparison of changes in fluorescence yield as function of temperature between ortho- and para-substituted 3HF derivatives relative to each yield at room temperature	79
Figure 39.	Absorption spectra of irradiated HBT in PS	85
Figure 40.	HBT fluorescence immediately after irradiation	87
Figure 41.	Formation of the trans-keto HBT isomer	88
Figure 42.	Relative energy diagram for HBT isomers	91
Figure 43.	Absorption spectra of irradiated 3HF in PS	92
Figure 44.	Absorption and emission spectra of 3FHBT in PS	129
Figure 45.	Absorption and emission spectra of 3CHBT in PS	130
Figure 46.	Absorption and emission spectra of 3PHBT in PS	131
Figure 47.	Absorption and emission spectra of 4MHBT in PS	132
Figure 48.	Absorption and emission spectra of 5CHBT in PS	133
Figure 49.	Absorption and emission spectra of 5MHBT in PS	134
Figure 50.	Absorption and emission spectra of 5PHBT in PS	135

Page

Figure 51. Absorption and emission spectra of 2C3HF in PS 136

Figure 52. Absorption and emission spectra of 4C3HF in PS 137

Figure 53. Absorption and emission spectra of 2F3HF in PS 138

Figure 54. Absorption and emission spectra of 4F3HF in PS 139

Figure 55. Absorption and emission spectra of 4M3HF in PS 140

Figure 56. Absorption and emission spectra of 25M3HF in PS 141

Figure 57. Absorption and emission spectra of 2MO3HF in PS 142

Figure 58. Absorption and emission spectra of 4MO3HF in PS 143

Figure 59. Absorption and emission spectra of 4MS3HF in PS 144

Figure 60. Absorption and emission spectra of 4PO3HF in PS 145

Figure 61. Absorption spectra of irradiated 3CHBT/PS 147

Figure 62. Fluorescence spectra of irradiated 3CHBT/PS 148

Figure 63. Absorption spectra of irradiated 3PHBT/PS 149

Figure 64. Fluorescence spectra of irradiated 3PHBT/PS 150

Figure 65. Absorption spectra of irradiated 4MHBT/PS 151

Figure 66. Fluorescence spectra of irradiated 4MHBT/PS 152

Figure 67. Absorption spectra of irradiated 5MHBT/PS 153

Figure 68. Fluorescence spectra of irradiated 5MHBT/PS 154

Figure 69. Absorption spectra of irradiated 5PHBT/PS 155

Figure 70. Fluorescence spectra of irradiated 5PHBT/PS 156

Figure 71. Absorption spectra of irradiated 2M3HF/PS 157

Page

Figure 72. Absorption spectra of irradiated 4M3HF/PS 158

Figure 73. Absorption spectra of irradiated 25M3HF/PS 159

Figure 74. Absorption spectra of irradiated 2C3HF/PS 160

Figure 75. Absorption spectra of irradiated 4C3HF/PS 161

LIST OF APPENDICES

		Page
APPENDIX A.	Absorption and Emission Spectra of HBT and 3HF Derivatives in Polystyrene	128
APPENDIX B.	Absorption and Emission Spectra of Irradiated HBT and 3HF Derivatives in Polystyrene	146

I. INTRODUCTION

The new generation of high energy particle accelerators, such as the Superconducting Supercollider (SSC), raises a challenge to existing particle detector technology, since fast response detectors with the ability to withstand exposure to large radiation doses will be required. A short response time is exhibited by plastic scintillation detectors. These are based on a polymer matrix doped with an organic fluorescent compound and will emit light when exposed to ionizing radiation. The key issue is whether they will be resilient to the radiation damage produced by the large radiation doses received. There is an ongoing project at the Department of Energy's Fermi National Accelerator Laboratory in Batavia, Illinois, that focuses on the investigation of radiation resistant plastic scintillators. Its goal is to identify and quantify the damage caused by the radiation and improve the plastic scintillators accordingly. The results reported in this study are part of this ongoing investigation.

Two fluorescent organic compounds, 3-hydroxyflavone (3HF) and 2-(2'-hydroxyphenyl)benzothiazole (HBT) have been studied as dopants for plastic scintillators in a polystyrene matrix. They exhibit a large spectral shift between absorption and emission spectra because of the excited state intramolecular proton transfer process that they undergo upon excitation. They absorb in the UV region and fluoresce in the green region of the visible spectrum. Thus, plastic scintillators doped with such compounds should be less sensitive to polymer degradation, one of the

principal consequences of radiation damage. Under irradiation, the polymer matrix suffers permanent damage, with the creation of some chemical species that absorb in the blue region of the spectrum, thus causing a decrease in the scintillation efficiency of the detector.

Several 3HF and HBT derivatives have been prepared and investigated in the search for a scintillation detector with a high light output and a large spectral shift to longer wavelengths in fluorescence, which would make the detectors more resistant to irradiation. The subject of the present study is a comparative analysis of these derivatives and the characterization of their fluorescence spectra and quantum yields. Radiation damage studies have also been performed in order to obtain an overall evaluation of the respective merits of the derivatives as scintillation detectors

A. Scintillation Detectors

Nuclear and high energy physics experiments often use scintillators as detection devices. Scintillation detectors are based on the property of certain materials (in solid, liquid, or gas phase) to emit a photon of light when a charged particle or electromagnetic radiation interacts with them. A typical detector consists of a scintillation material coupled to a photomultiplier tube, which converts the quanta of light into electrical pulses. Measurement and analysis of the electrical signal provides information about the incident radiation (1, 2).

Plastic scintillators used in high energy physics experiments are expected to detect a variety of particles over a wide energy range. When

high energy electrons or positrons pass through a scintillator, they can lose energy by ionization of the polymer, or through the bremsstrahlung effect, consisting of the emission of a photon by the electron (positron) when it undergoes rapid acceleration through interaction with the electric field of the atoms in the polymer. Heavier charged particles, such as protons, muons, and pions lose energy through ionization loss and through inelastic collisions with the atoms of the polymer. Neutrons dissipate their energy through collisions with the nuclei. Photons can interact through three different processes, depending on their energy and the medium:

1. Photoelectric effect where the photon transfers all its energy to an orbital electron, which is ejected from the atom;
2. Compton scattering, in which the photon partially transfers its energy to an orbital electron, which is ejected, and the rest of the energy is carried away by the scattered photon; and
3. Pair production, where the photon is transformed into an electron-positron pair.

In organic materials, Compton scattering is the dominant photon energy transfer mechanism.

Two major applications of scintillation detectors in high energy physics include calorimetry and particle selection or triggering. Calorimeters are often made of dense metal plates such as iron or lead interspersed with plates of scintillator. These are used to determine the energy of the incoming radiation. In particle selection or triggering, scintillators are used in horoscopes that discriminate ionizing radiation or particles under certain criteria.

Scintillation detectors were first used in 1903 when Crookes built an instrument with a screen coated with ZnS that scintillated when struck by α-particles. The weak scintillations were detected with the naked eye, using a microscope in a dark room. This procedure was tedious compared to the other detection techniques available at the time. For this reason, scintillators fell into disuse until the mid-1940s, when a replacement for the human eye, the photomultiplier tube, was developed. Further improvements made scintillation detectors very reliable and convenient for a variety of uses.

Six types of scintillation materials currently exist: organic crystals, organic liquids, plastics, inorganic crystals, gases, and glasses. Of those based on organic materials, plastic scintillators are the most widely used because they offer an extremely fast response, and a high light output. Other major advantages include their commercial availability and price. In addition, plastics can be easily machined into many different forms and sizes, and an experimenter can usually choose among several types for any given application.

Common plastic scintillators are ternary systems. They consist of three basic components: a polymer matrix such as polystyrene (PS) or polyvinyltoluene (PVT) and two solutes or dopants, usually referred to as the primary and the secondary dopants. The secondary dopant, also referred to as a wavelength shifter, is used because the primary solute generally fluoresces in the deep blue (short wavelength) and the absorption of the polymer matrix is large in that region of the spectrum. Without the presence of a wavelength shifter, much of the light produced

by the primary dopant would be reabsorbed within a short distance, rendering it unavailable for detection purposes.

The scintillation mechanism involves three main processes:

1. Energy transfer from the incident radiation or particle to the excited states of the polymer. The concentrations of the primary and secondary dopants are sufficiently small to neglect their direct excitation. Shifting of the π-electrons into excited singlet states is the major excitation process, since π-electron ionization, and excitation and ionization of electrons in other shells, only occurs to a small extent (1).
2. Energy transfer from the excited state of the polymer to the primary dopant. This process follows the Förster mechanism of non-radiative energy transfer (3-6). The energy transfer is described by a dipole-dipole interaction in which non-radiative energy transfer occurs between the first excited π-singlet state of the polymer and the primary dopant. The strength of this interaction (k) is given by:

$$k = \frac{1}{(\tau_{os})_o} \left(\frac{R_o}{R}\right)^6,$$

where $(\tau_{os})_o$ is the natural fluorescence lifetime of the polymer, R is the mean separation between polymer and primary molecules, and R_0 is a constant proportional to the overlap integral between the polymer fluorescence distribution and the dopant absorption. Using the optimum primary dopant concentration (from 0.75% to 1.25% by weight), this process can dominate over emission or quenching of the

excited states of the polymer. This is a very efficient process (7) which does not depend upon the polymer radiative quantum yield. For example, polystyrene with only a 3% quantum yield (8) makes a good scintillator when used with a dopant of high radiative quantum yield.

3. Energy transfer from the primary excited state to the secondary dopant through emission and reabsorption of a photon. This final process involves deexcitation of the primary dopant to the ground state by emission of a photon, followed by absorption of this photon by the secondary dopant, which in turn relaxes to the ground state by emitting a second photon. Although most of the dopants have a quantum yield near 1.0 (radiative deexcitation is the main relaxation process), this transfer process does not provide an overall photon yield of 1.0, mainly because of the overlap between the absorption and emission spectra of the secondary dopant. The secondary dopant reabsorbs some of the light that it emits, an effect known as self-absorption. In large scintillation counters, the self-absorption effect leads to considerable light losses.

B. Status of Plastic Scintillators

The progress made in development of plastic scintillators is presented in this section. Each component of a plastic scintillator - the polymer and dopants - is treated separately.

1. Advances in Polymer Development

Plastic scintillators were considered only after liquid scintillators had met with some success. Since the alkyl benzenes are the most efficient liquid solvents, their polymeric derivatives were studied and they proved to be the most efficient plastics. The polymers have higher fluorescence quantum efficiencies than their liquid counterparts. However, the non-radiative energy transfer between the polymer and the dopant is less efficient than between the liquid solvent and the solute.

Polystyrene was used for the initial plastic scintillator studies (9). Later, polyvinyltoluene was shown to have between 10% and 20% higher efficiency than polystyrene (10). Consequently, a variety of alkyl-substituted styrene derivatives were studied (11, 12). These studies showed that the polyvinylxylenes had the highest scintillation efficiency, and the results were analyzed with the Hammett and Taft equations (11), which verified that the scintillation efficiency improved with the electron-donating capacity of the substituent. A plausible explanation for this effect is that the absorption shifts to the red by substituting the ring with electron-donating groups, thus decreasing the energy gap between ground state and excited states.

Several polymerization methods were investigated for polystyrene-based plastic scintillators (9, 13):

1. Mixing of the dopant in molten polystyrene;
2. Polymerization of styrene solution at 50 °C using benzoyl peroxide as catalyst;

3. Polymerization of styrene solution at 125-140 °C for several days, without a catalyst;
4. Polymerization of styrene solution at 200 °C for 12-15 hours without a catalyst.

Method 1 has been used when the dopant is of such a nature that copolymerization would occur if one of the other methods were used (14). Otherwise, method 3 has been more generally adopted, since further research has shown that catalysts, mold-releasing agents, and impurities tend to decrease the scintillation efficiency (15).

Other studies (16) focussed on the effects that the polymer molecular weight and the amount of unreacted monomer have on the scintillation efficiency. The results indicated that the scintillation efficiency increased with increasing molecular weight until approximately 100,000 amu, but further increases in molecular weight did not affect its efficiency. In addition, the presence of unreacted monomer was found to be harmful to the scintillation efficiency.

In the past few years, new demands for scintillators and the increasing awareness of the susceptibility of scintillators to radiation damage have prompted studies on a variety of polymers, such as polycarbonates, polysulfones, polysiloxanes, and epoxies (17, 18). In general, other polymers studied have shown more resistance to radiation damage than polystyrene. In addition to radiation hardness, there are other criteria, however, that need be considered when designing a plastic scintillation detector, among them the limitations imposed by the manufacturing process. Recent experiments have shown that the use of fibers instead of sheets of plastic scintillators can result in a more precise

and compact detector (19). Fibers can be extruded or drawn, but drawn fibers are of a higher optical quality. Since drawn polystyrene-based fibers have been industrially available for a long time, high-quality PS fibers can be obtained easily and inexpensively. On the other hand, polyvinyltoluene fibers are difficult to draw, thus making PVT, in spite of its higher efficiency, a second choice for scintillating fibers.

Another example of how the existing technology affects the choice of scintillation materials can be found in the polysiloxanes. Experimental results indicated that certain polysiloxanes are more resilient to radiation damage than polystyrene (17). However, due to the rubbery nature of polysiloxanes, fibers cannot be drawn with present technology, and new methods must be developed before these polymers can be successfully used in scintillating fiber detectors.

2. Advances in Dopant Development

A large number of organic compounds have been tested as dopants for scintillators. The first studies were concerned with incorporation of the dopants in liquid scintillators. Later studies progressed toward using them in plastic scintillation materials. The first efficient solute discovered was 1,1',4,4'-tetraphenylbutadiene (TPB) (20). Analyses of other compounds indicated that p-terphenyl (PTP) provided a more efficient scintillator than anthracene, a widely used and efficient organic scintillating crystal. This fact prompted the use and study of compounds with linear aromatic chain structures over those with condensed aromatic structures. Therefore, after the p-terphenyl results, p-quaterphenyl was

analyzed (21). p-Quaterphenyl turned out to be an efficient fluor, but presented solubility problems that would tend to increase for analog compounds with increasing aromatic chain length. Hayes et al. (22) then found that the solubility improved without negatively affecting the scintillation efficiency when a phenyl group was replaced by an oxazole or an oxadiazole group. This prompted the synthesis of a series of 2,5-diaryloxazoles and 2,5-diaryl-1,3,4-oxadiazoles. Encouraged by the results, other research groups made various modifications and prepared a series of new compounds, such as 2,5-diarylthiazoles (23), 2-aryl and 2,7-diarylfluorenes (24), and 3,6-diaryl-2-pyrones (25). These compounds are still utilized in commercial scintillators as either primary dopants, at 1-1.5% concentration by weight, or as secondary dopants in 0.01-0.02% concentration by weight, depending upon their absorption and emission characteristics. Complete names, abbreviations, and chemical structures of the compounds listed above are shown in Figures 1 to 8.

Figure 1. p-Terphenyl (PTP).

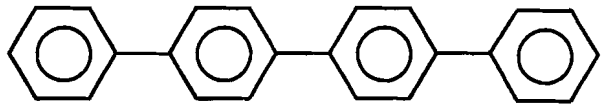

Figure 2. p-Quaterphenyl (PQP).

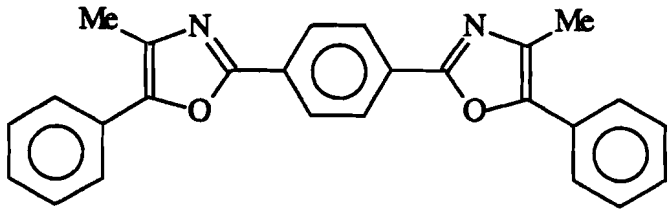

Figure 3. 1,4-Bis(4-methyl-5-phenyloxazol-2-yl)benzene (DMPOPOP).

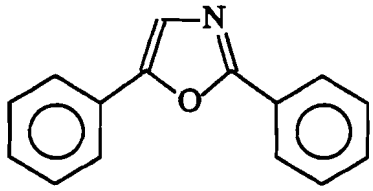

Figure 4. 2,5-Diphenyloxazole (PPO).

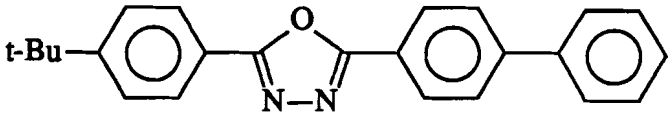

Figure 5. 2-(4-Biphenylyl)-5-(4-<u>tert</u>-butylphenyl)-1,3,4-oxadiazole (BPBD).

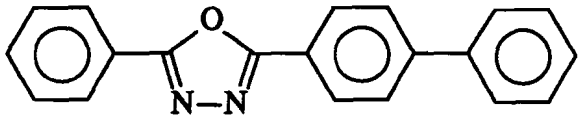

Figure 6. 2-(4-Biphenylyl)-5-phenyl-1,3,4-oxadiazole (PBD).

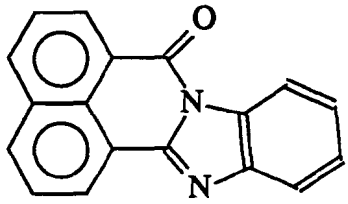

Figure 7. 7H-Benzimidazo[2,1-a]benz[de]isoquinoline-7-one (BBQ).

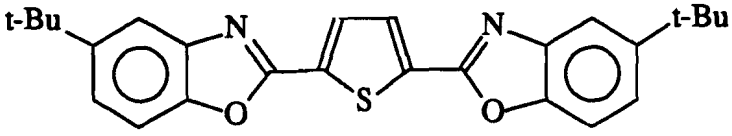

Figure 8. 2,5-Bis(5-tert-butyl-2-benzoxazolyl)thiophene (BBOT).

In hope of improving the spectral match between the primary and secondary dopants, and of improving their solubility in the polymers, other oxadiazole derivatives have been tested in these past few years (18). Two of the recently developed oxadiazole derivatives, shown in Figures 9 and 10, are 2-(p-n-decyloxyphenyl)-5-phenyl-1,3,4-oxadiazole (R-PDP), and p-bis(2-(p-n-decyloxyphenyl)-1,3,4-oxadiazol-5-yl)benzene (R-PDPDP-R). They have been tried with polysiloxane scintillators as a possible solution to the insolubility of other fluors in these polymers (18).

It has been mentioned above that the p-oligophenylenes presented increasing solubility problems as the chain augmented; hence, p-quaterphenyl was considerably less soluble than p-terphenyl. However, these compounds could be modified to improve their solubility without exchanging a phenyl group for a heteroaromatic group, but rather by addition of alkyl or alkoxy groups on the phenyl ring. Nonetheless, substitution along the phenyl rings created another problem in certain compounds, that of the loss of coplanarity. The phenyl rings were out of plane if the substituents were too bulky, thus affecting the absorption and emission spectra (8). A plausible solution was to bridge the rings to force coplanarity on the system. Based on these principles, several substituted p-oligophenylenes were synthesized (26) and evaluated in liquid and plastic scintillators. Recently, new p-oligophenylene derivatives (27-29), originally intended as laser dyes, have also been tested as solutes for polysiloxane-based scintillators (18). Some examples of these new derivatives are shown in Figures 11 to 14.

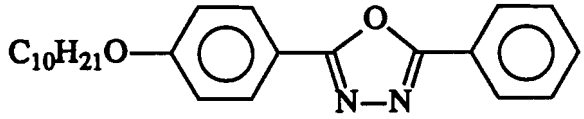

Figure 9. 2-(p-n-Decyloxyphenyl)-5-phenyl-1,3,4-oxadiazole (R-PDP).

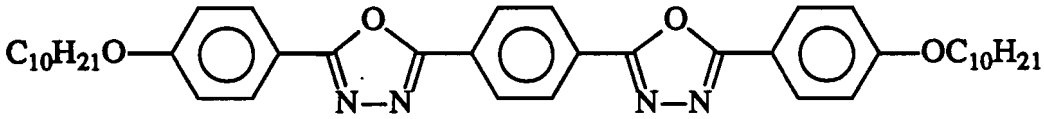

Figure 10. p-Bis(2-p-n-decyloxyphenyl)-1,3,4-oxadiazol-5-yl)benzene (R-PDPDP-R).

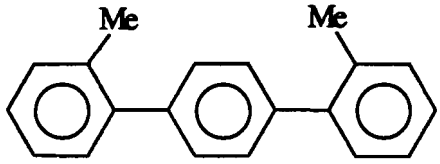

Figure 11. 2',2"-Dimethyl-p-terphenyl.

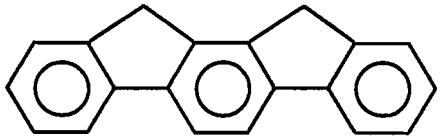

Figure 12. syn-Indenofluorene (SIF).

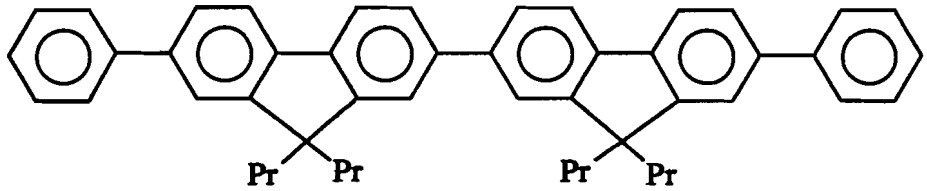

Figure 13. Oligo 408.

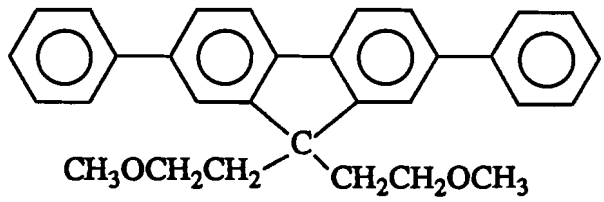

Figure 14. Oligo 373.

Research carried out with these dopants indicated several problems, among them:

1. The overlap between absorption and emission spectra was the cause of a considerable amount of lost light.
2. The permanent damage in the irradiated polymer occurred at about 400 nm, where most of the primary dopants emitted light. Thus, the species created under irradiation compete with the secondary dopant in absorbing the light emitted by the primary (30).

A possible solution to both problems has recently been pursued by using dopants that exhibit a large spectral separation between absorption and emission wavelengths, that is, a large Stokes shift. Moreover, the use

of such compounds gives the option of having an efficient plastic scintillator with a single dopant. Plastic scintillators using a single dopant with a large Stokes shift have been named intrinsic scintillators (30), since they couple directly to the polymer and, at the same time, act as wavelength shifters. A number of compounds with such characteristics have recently been studied, in particular: 1-phenyl-3-mesityl-2-pyrazoline (PMP) (31, 32), 2,2'-bipyridyl-3,3'-diol (BPD) (33, 34), 3-hydroxyflavone (3HF) (35-37), and 2-(2'-hydroxyphenyl)-benzothiazole (HBT) (30, 38). These are represented in Figures 15 to 18. The work presented here, and performed at Fermi National Accelerator Laboratory, involved the study and development of plastic scintillators using 3HF, HBT, and their respective derivatives. A separate section is dedicated to the review of these two families of compounds.

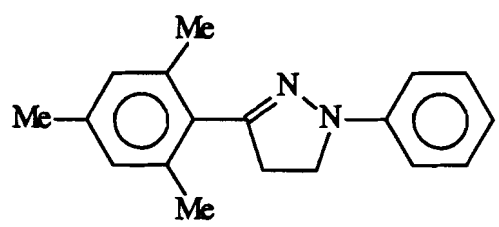

Figure 15. 1-phenyl-3-mesityl-2-pyrazoline (PMP).

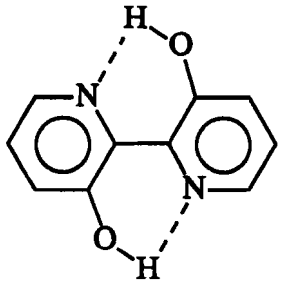

Figure 16. 2,2'-Bipyridyl-3,3'-diol (BPD).

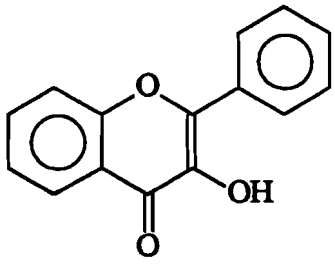

Figure 17. 3-Hydroxyflavone (3HF).

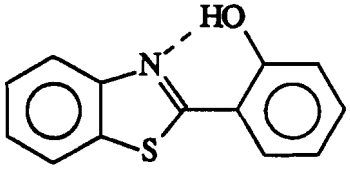

Figure 18. 2-(2'-hydroxyphenyl)-benzothiazole (HBT).

3. Radiation Damage in Plastic Scintillators

Radiation damage in polymers has been investigated for many years (17), since numerous applications exist where polymeric materials are exposed to ionizing radiation, notably in nuclear power plants and in space vehicles. However, in such cases, the studies were concerned with the changes in mechanical, rather than optical properties of the polymers when exposed to radiation.

Several experiments on plastic scintillators (39, 40) are currently underway to gather information on the optical changes produced by exposure to radiation. The radiation hardness of plastic scintillators has become an important aspect in their development, since new applications, such as their use in the new generation of particle accelerators (e.g., SSC), will expose them to doses in excess of 1 Mrad/year.

Plastic scintillators used in high energy physics measurements are expected to detect a variety of particles. The detection is possible because the particles cause the dopants to fluoresce, but they also cause damage to the plastic material. Prolonged exposure to high energy radiation damages both the polymer and the dopants (17), resulting in a reduction in the light output of plastic scintillators during extended use (39). Radiation damage to the polymer creates color centers which will extend the polymer matrix absorption band to longer wavelengths. The longer absorption tail of the polymer will absorb light emitted by the fluors (39). An alteration of the polymer structure can also affect the energy transfer from the polymer to the dopant. Damage to the fluor implies a decrease in its concentration in the polymer matrix. With a

concentration below the optimum, the energy transfer between polymer and fluor will be less efficient (1). Furthermore, damage to the dopant will also result in the formation of additional color centers in the polymer. The extent of the damage depends upon different factors, such as the structure of the polymer and fluors, the dose rate of the incident radiation, and the environment under which the scintillators are irradiated (17).

An effective study of radiation damage to plastic scintillators must involve the analysis of polymers as well as dopants. Damage to the polymer is generally detected by absorption and electron spin resonance (ESR) measurements. Damage to the dopants is detected by absorption and fluorescence measurements. The overall change can be monitored using Bi^{207}, a β-source, and recording the pulse height spectrum produced by the photodetector viewing the scintillation light. Under identical conditions of electrical signal processing, the pulse height (proportional to the light yield of the scintillator) will deteriorate as the detector accumulates radiation damage. In scintillating fibers, the change in light attenuation length is reported as indicative of this damage. Currently, the results published in the literature disagree with regard to the range of the damage produced in similar scintillators working under similar conditions (37, 39).

The deposition of radiation energy in an organic material leads to a complex set of events, as explained above. Regardless of which mechanism applies, the primary event in radiation damage is the ejection of a high energy electron:

$$R \longrightarrow R^{+} + e^{-}$$

This electron can cause ionization of other molecules, resulting in a chain reaction of ionization events:

$$e^{-} + R \longrightarrow R^{+} + 2e^{-}$$

Due to the coulombic attraction, there is recombination of electrons and positively charged ions yielding highly excited species:

$$e^{-} + R^{+} \longrightarrow R^{*}$$

If the energy transfer involved in the interaction is insufficient to cause ionization, it will still produce electronically excited molecules:

$$R \longrightarrow R^{*}$$

The excited molecules will undergo, depending on their nature, radiationless or radiative decay to their ground state. In organic materials, molecules in excited electronic states can also undergo homolytic bond cleavage, producing free radicals:

$$R - R \longrightarrow R'\bullet + R''\bullet$$

The radicals formed will follow reaction patterns already known in radical chemistry, with the difference that these radicals are not randomly dispersed, but normally form clusters. This highly localized environment will favor recombination over other reactions.

The reactions occurring under polymer irradiation can be listed as follows:

1. Homolytic bond cleavage to form radicals

$$- CH_2 - CH_2 - CH_2 - \longrightarrow - CH_2^{\bullet} + {}^{\bullet}CH_2 - CH_2 -$$

2. Radical recombination

$$- CH_2^{\bullet} + {}^{\bullet}CH_2 - CH_2 - \longrightarrow - CH_2 - CH_2 - CH_2 -$$

3. Recombination to form a crosslink

$$\begin{array}{l} - CH_2 - \underset{\bullet}{C}H - \\ - CH_2 - \overset{\bullet}{C}H - \end{array} \longrightarrow \begin{array}{l} - CH_2 - CH - \\ \qquad\qquad\quad | \\ - CH_2 - CH - \end{array}$$

4. Disproportionation, resulting in permanent cleavage of the polymer chain

$$-CH_2\bullet + \bullet CH_2CH_2- \longrightarrow -CH_3 + CH_2 = CH-$$

5. Addition to a double bond to form a crosslink

$$\begin{array}{l} -CH_2-\underset{\bullet}{C}H- \\ -CH=CH- \end{array} \longrightarrow \begin{array}{l} -CH_2-CH- \\ \qquad\quad | \\ -\dot{C}H-CH- \end{array}$$

6. Hydrogen abstraction (mostly in small radical chains)

$$-[CH_2-CH_2]^{*}- \longrightarrow -CH_2-\dot{C}H- + H\bullet$$

7. Formation of allylic radicals

$$\begin{array}{l} -CH_2-\dot{C}H-CH_2- \\ -CH_2-CH=CH_2 \end{array} \xrightarrow{\bullet} \begin{array}{l} -CH_2-CH_2-CH_2- \\ -\dot{C}H_2-CH=CH_2 \end{array}$$

8. Radical migration, through hydrogen abstraction

$$\begin{array}{l} -CH_2-\underset{\bullet}{C}H-CH_2- \\ -CH_2-CH_2-CH_2 \end{array} \longrightarrow \begin{array}{l} -CH_2-CH_2-CH_2- \\ -CH_2-CH_2-\underset{\bullet}{C}H- \end{array}$$

The analyses carried out at Fermi National Accelerator Laboratory (30) indicate that most of the fluors tested are not permanently damaged by radiation, but it is the damage to the polymer that causes the reduction in light output. If the polymer damage cannot be avoided, the use of dopants with a large Stokes shift will provide a partial solution to the problem. After irradiation, the polymer will show an absorption tail of up to 400 nm. Since dopants with large Stokes shift fluoresce at longer wavelengths, the emitted light will not be absorbed by the polymer tail. Thus, the scintillator becomes less affected by the radiation-induced changes in the polymer.

C. Fluorescent Compounds with Large Stokes Shift

3-Hydroxyflavone (3HF) and 2-(2'-hydroxyphenyl)benzothiazole (HBT) have been studied as dopants for plastic scintillators because they show a large Stokes shift between absorption and emission. This characteristic has been considered very important in order to decrease the self-absorption of the emitted light. Although the use of these compounds in scintillators is relatively new, they have been investigated in other areas for their complex behavior, namely, their ultrafast intramolecular proton transfer isomerization (41, 42). This ultrafast isomerization is responsible for the large spectral separation between the light absorbed and emitted. During the past decade, a major effort has been made to understand ultrafast reactions, that is, reactions for which the half-life is of the order of femtoseconds or picoseconds (42). This advance has been possible because of the development of picosecond and

femtosecond spectroscopy. Ultrafast isomerizations are important prototypes for fast processes in biology, such as photosynthesis and vision (41).

A general view of how the intramolecular proton transfer isomerization occurs is presented in Figure 19. The reaction is initiated by optically exciting the reactant from its ground state to its lowest excited singlet state. Subsequently, the excited reactant isomerizes to yield the product in its lowest excited singlet state. The excited product relaxes to the ground state by emitting a photon. In the ground state, the product isomerizes back to the reactant.

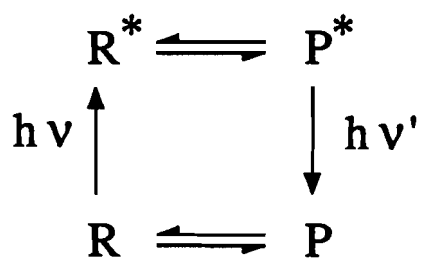

Figure 19. General scheme for excited-state intramolecular proton transfer.

Although both HBT and 3HF fall into the same excited-state intramolecular proton transfer (ESIPT) isomerization class, they behave differently under certain conditions. Therefore, the progress made over the years in understanding and characterizing their behavior will be reported here separately. Section 1 will review the physical and chemical properties of HBT, section 2 will review the same aspects of

3HF, and section 3 will review preparation methods for HBT as well as those for 3HF.

1. Photophysics of 2-(2'-Hydroxyphenyl)benzothiazole (HBT)

The first data on HBT were reported by Cohen and Flavian in 1967 (43) in a study of the photochromic behavior (reversible color change) of N-salicylideneaniline (SA) and related anils, such as HBT. They postulated that both compounds exhibited proton transfer in the excited state as an explanation for the spectral shift between absorption (λ_{max}=350 nm) and fluorescence (λ_{max}=525 nm). Excited-state proton transfer was possible due to the pronounced difference between the acidities at the excited and ground states. However, HBT is not a photochromic molecule, but a fluorescent one. After optical excitation, HBT fluoresces whereas SA has a geometrical rearrangement into a photochromic isomer (solid changes from yellow to red color) besides showing fluorescence (44-46).

There have been numerous studies on the excited-state proton transfer of HBT and its derivatives since the Cohen and Flavian study. Williams and Heller (47) suggested the model depicted in Figure 20, where the proton remains predominantly on the phenyl oxygen while in the ground state (enol form). Upon UV excitation, in the first excited singlet state, the phenol is a considerably stronger acid and the nitrogen is a stronger base. Thus, the proton is transferred from the oxygen site to the nitrogen site, and the isomer formed (Figure 20, S_1') is more stable than the isomer before proton transfer (Figure 20, S_1). S_1 can then be

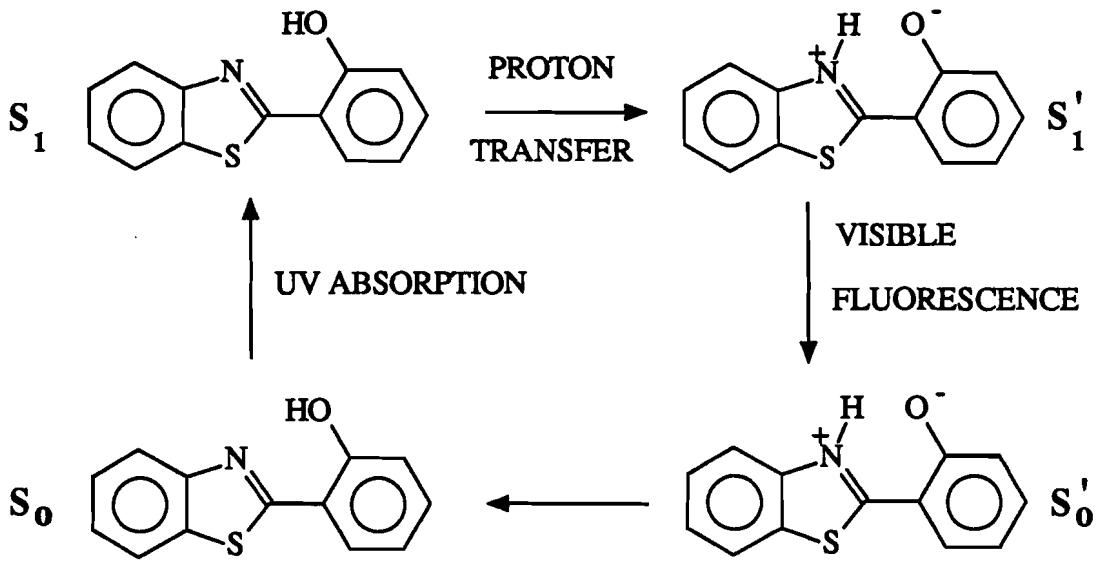

Figure 20. Excited-state intramolecular proton transfer for HBT.

regarded as a vibrationally excited form of S_1'. Then the molecule deexcites to the ground state, emitting a photon. In the ground state the enol form is again the more stable form and the proton will then transfer back to the oxygen. S_0' is also a vibrationally excited state of S_0.

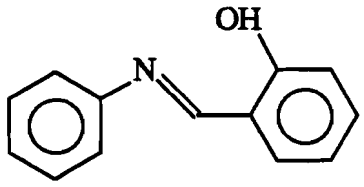

SA

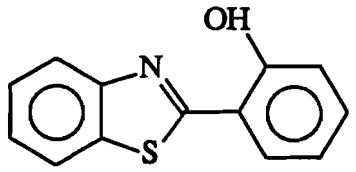

HBT

This model becomes more complicated once the possible conformers are taken into consideration. The ionic enol forms can be represented also as the keto or quinoid forms (see Figure 21). Williams and Heller also postulated that the cis ionic enol form and the trans keto or quinoid form could be the more stable ones. However, they did not isolate any quinoid product, but only the enol product form in the ground state. Furthermore, by replacing the proton for a methyl group, they proved the proton was necessary for obtaining the large Stokes shift, and to improve the UV stability of the benzothiazoles.

Substituted HBT derivatives have been of interest in studying the effect of electron-donating and electron-withdrawing groups on the rate of proton transfer. Electron-withdrawing substituents in the 2-phenyl ring can enhance the probability of the hydrogen transfer process by

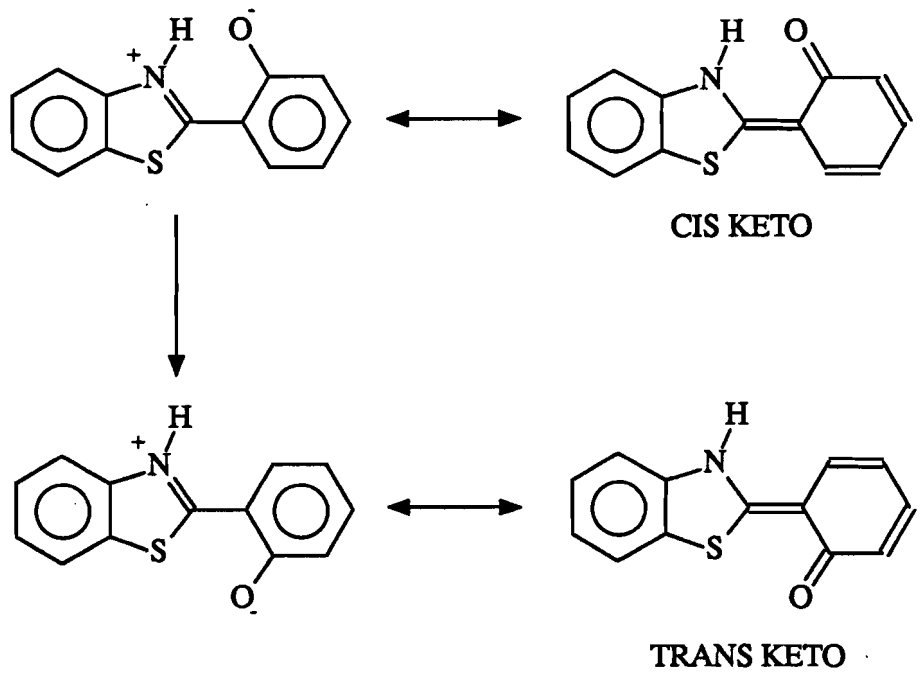

Figure 21. Resonant contributions to the ionic form of HBT.

making the hydroxyl group more acidic. However, given that the rate constant for this process had been calculated to be about 10^{11} s^{-1} (48), there would be no sensible overall effect in the quantum yield. Electron-donating substituents will reduce the acidity of the hydroxyl group and may decrease the rate constant for proton transfer sufficiently to enable other processes to compete, with a consequent decrease in the quantum yield. Several derivatives were prepared in order to quantify this effect, but no reliable data were obtained (49).

A key issue for the photophysics of HBT is to determine whether the excited-state intramolecular proton transfer is not inhibited by an energy barrier, or whether it occurs by tunneling effect. By means of picosecond spectroscopy, Barbara et al. (48, 50) studied the excited-state vibrational and conformational relaxation of HBT, first as a function of temperature in solution, and then at 12 K in argon. Their experiments identified and quantified three relaxation processes:

1. Proton transfer occurred within 5 ps of excitation at temperatures ranging from 4 K to 300 K.
2. The proton transfer rate ($k_{PT} > 10^{11}$ s^{-1}) actually exceeded vibrational relaxation rate ($k_{VR} \sim 10^{11}$ s^{-1}) at 4 K, and increased rapidly with temperature.
3. Radiationless decay (10^2 - 10^3 ps) is induced by large amplitude torsional motion in solution at T > 200 K.

Based on the extremely rapid rate of excited-state intramolecular proton transfer, they suggested that ESIPT may be a special type of vibrational relaxation for this molecule.

Recently, a novel experimental technique has been introduced, allowing the study of transient infrared spectra of electronically excited molecules on the picosecond time range. This technique has been used to analyze ESIPT in HBT (51), providing, for the first time, convincing evidence of the excited-state proton transfer. The stretching modes of the N-H and C-O group, which are formed by proton transfer (Figure 21, cis-keto form), were detected. These results also show the existence of a strong intramolecular hydrogen bond in the excited state, which indicates the formation of the cis-keto instead of the trans-keto form, as had been postulated by Williams and Heller.

The studies presented on HBT have dealt with the photophysics of the molecule in the solid state or in aprotic solvent solutions. The HBT behavior is more complicated when polar protic solvents are involved. In addition to the S_0-S_1 absorption band observed in non-polar solvents, a weak absorption at long wavelengths (around 400 nm) is found in polar solutions. These studies (52, 53) demonstrated that the anion HBT^- is formed in polar solvents containing OH^- ions or other hydrogen-bonding impurities. The anion absorption band is located at approximately 400 nm and the fluorescence maximum is at 470 nm, showing a small Stokes shift, since there is no proton transfer. In high-purity solvents the anion is not detected.

Recently, using transient electronic absorption, the background-state reaction from the keto to the enol form (Figure 20) has been shown to occur (54).

The current information on HBT provides a good description of the photochemistry and photophysics of this molecule in the solid state and

in solvents free of hydrogen-bonding impurities. However, more data are still required to characterize it in polar protic solvents.

2. Photophysics of 3-Hydroxyflavone (3HF)

3-Hydroxyflavone (3HF) and its derivatives show a large Stokes shift due to electronic distribution in the excited state after intramolecular proton transfer, which is favored by a basicity increase in the excited state of the carbonyl (Figure 22).

In 1979, Sengupta and Kasha (55) suggested the mechanism depicted in Figure 22 and assigned the green fluorescence at 520 nm to the excited tautomer (T) of 3HF formed after proton transfer, and the blue fluorescence at 400 nm to the normal (N) form of 3HF, since it showed a small Stokes shift indicative of fluorescence prior to proton transfer. They also pointed out the need for the phenyl ring to be coplanar with the rest of the molecule for the full basicity of the carbonyl to be developed, thereby permitting the proton transfer. Therefore, if torsion of the phenyl ring is prevented, such that the out-of-plane conformation is frozen in before excitation, then the tautomerization could be inhibited. Figure 23 shows the contribution of the pyrylium form to the tautomer stabilization.

McMorrow and Kasha (56) later demonstrated that in extremely dry and pure hydrocarbon solvents (e.g., methylcyclobutane) only fluorescence from the tautomer was observed, and that the proton transfer rate was very high, as has also been observed in other ESIPT systems ($k_{PT} > 10^{11}\ s^{-1}$). However, with traces of water present in the methylcyclohexane, three regions of fluorescence were observed:

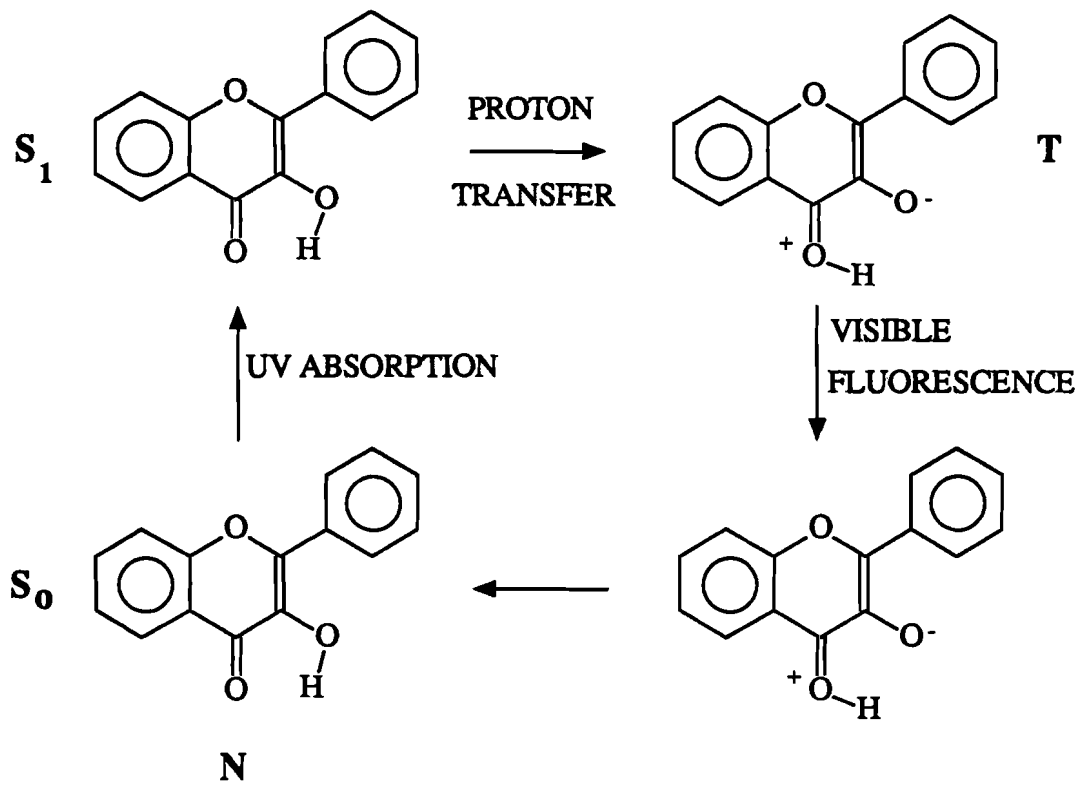

Figure 22. Excited-state intramolecular proton transfer for 3HF.

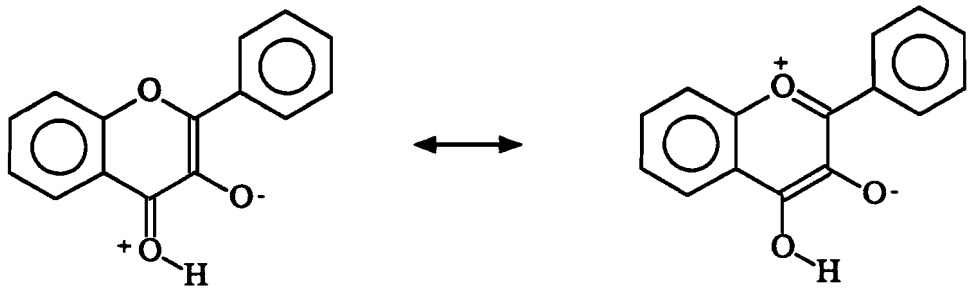

3HF TAUTOMER (T) PYRYLIUM STRUCTURE

Figure 23. Resonance structures for the 3HF tautomer.

1. A green fluorescence at 523 nm from the 3HF tautomer,
2. Another green fluorescence at 497 nm from the 3HF anion, and
3. A blue fluorescence at 400 nm from the normal electromer.

Studies of 3HF in hydrogen-bonding solvents (56, 57), such as alcohols and ethers, showed a slow proton transfer rate due to the solvation of the 3HF molecules, thus inhibiting the proton transfer. In other words, in pure alkane solvents, only unsolvated molecules exist and the proton transfer barrier is zero or small. However, in hydrogen-bonding solvents, a significant proton-transfer potential barrier exists.

Several additional studies (58-62) were performed to gather more information on the 3HF proton transfer mechanism: hydrogen/deuterium isotope effects, solvent effects, and structural effects due to substitution in the phenyl ring. The substitution studies revealed that the ortho derivatives were less basic and less hydrogen-bond donating than the para derivatives. The ortho derivatives also showed a weaker intra-

molecular bond and a greater activation energy. These findings support the hypothesis that the excited-state proton transfer in 3HF is dominated by energetic factors in the solute/solvent complex rather than relaxation effects involving the dynamics of the solvent.

A recent study of 3HF in solid argon (63) verified the fact that in the absence of water impurities, only fluorescence from the tautomer was observed, and that proton transfer was fast under such conditions. The proton transfer rate constant was estimated to be larger than 10^{12} s^{-1}.

In a different experiment (64), 3HF/solvent complexes of known stoichiometry were prepared; they proved to slow down the proton transfer rate. For $3HF{\bullet}(ROH)_1$ (R=H,Me,T) complexes the ESPT is still rapid (< 10 ps) due to the cyclic hydrogen-bonded structure that the alcohol or water are able to form with the hydroxyl and carbonyl groups. Nevertheless, the $3HF{\bullet}(Et_2O)_1$ complex undergoes ESPT in about 40 ps, and complexation of 3HF to two or more water or alcohol molecules inhibits ESPT at low temperatures.

It has been mentioned that the lack of planarity of the 3HF molecule would affect the proton transfer. Brucker and Kelley (65) carried out a comparison of 3-hydroxychromone (no 2-phenyl ring present) with 3HF and its substituted derivatives in order to determine if the effect of the torsion of the phenyl ring occurred before, during, or after the proton transfer. Their results indicated that proton transfer occurred very fast, as usual, and the phenyl torsion plus vibrational relaxation contributed to the deexcitation of the molecule after proton transfer. The deexcitation process takes place in approximately 15 ps. In an argon matrix at 10 K

the phenyl torsion is restricted and vibrational relaxation is the only deexcitation mode occurring in a time scale of the order of 100 ps.

3. Methodology for HBT and 3HF Syntheses

Preparation of HBT and its derivatives can be accomplished through three similar pathways:

1. o-Aminothiophenol and the corresponding salicylic acid derivative can be condensed in polyphosphoric acid at 200 °C until the reaction is complete (66).
2. o-Aminothiophenol and the corresponding salicylaldehyde derivative can be condensed in triethyl phosphate and glacial acetic acid at room temperature followed by oxidation with lead tetraacetate (67).
3. o-Aminothiophenol and the corresponding salicylic acid derivative can be condensed in phosphorous trichloride in refluxing toluene (68).

Synthesis of 3HF and its derivatives can be achieved by the Algar-Flynn-Oyamada procedure for the preparation of flavonols (69). The procedure consists of a two-step synthesis where the first reaction is an aldol condensation between o-hydroxyacetophenone and a benzaldehyde derivative. The second reaction involves the oxidation of the chalcone by hydrogen peroxide. Both reactions take place in strongly basic solutions. Some modifications to this procedure have been also used in the 3HF and derivatives syntheses:

1. Aldol condensation in acidic solution (HCl) is also reported for the chalcone formation of some bulky p-hydroxybenzaldehyde

derivatives (70). The corresponding chalcone is oxidized with hydrogen peroxide to yield the flavonol derivative.

2. Aldol condensation in basic solution followed by oxidation in hydrogen peroxide without the chalcone isolation (71).

A completely different synthetic pathway has also been described. Flavonols were obtained in high yields from the photolysis of nitrochromenes followed by acidic hydrolysis. The nitrochromenes are prepared from the condensation of o-hydroxyacetophenone and nitrostyrene derivatives (72).

II. RESULTS AND DISCUSSION

The following sections present the analyses performed in search of an intrinsic scintillator - i.e., a polymer matrix plus a dopant exhibiting a large Stokes shift - resistant to radiation and with a high light output. The studies carried out involve polystyrene as the polymer base for the scintillators, 2-(2'-hydroxyphenyl)benzothiazole (HBT) and its derivatives and 3-hydroxyflavone (3HF) and its derivatives as the dopants.

Radiation damage tests as well as fluorescence and quantum yield measurements were performed on the different scintillator materials prepared.

A. Radiation Damage Studies on Polystyrene

Polystyrene was the only polymer matrix studied in this project for the preparation of intrinsic scintillators. Polystyrene was singled out because of its suitability for drawing fibers, when compared with other polymer matrices available for scintillation detection. The use of scintillating fibers as opposed to sheets is desirable for calorimetry experiments and necessary for particle tracking experiments. Scintillation detectors built as ribbons of fibers are more efficient, when used in calorimetry experiments that require thin scintillation layers, than their precursors made of sheets of scintillating material. High resolution

is required in tracking experiments, and this can only be accomplished by using small-diameter fibers of a high light output.

In the preparation of the polymer matrix, styrene monomer was separated from the inhibitor, tert-butylcatechol, by column filtration (tert-butylcatechol removal column from Aldrich Chemical Co.), and purified by vacuum distillation. Pure polystyrene samples were prepared by polymerizing a given amount of styrene monomer in test tubes placed in a silicone oil bath. The test tubes were first silylated to allow for a quick release of the polymer. All test tube samples underwent three freeze-pump-thaw cycles to remove dissolved gases before they were polymerized. A standard polymerization cycle involved no initiator, but only heating at 125 °C for several days. At the end of the cycle, the temperature was raised to 140 °C for about 12 hours, to achieve a better monomer conversion. Finally, the temperature was slowly lowered below the glass transition temperature. The test tubes were then quenched in liquid nitrogen to avoid the formation of vacuum bubbles, which appeared when the test tubes were cooled at room temperature. The plastic samples obtained were then machined into slices of 1 cm in thickness or into cuvette pieces (dimensions: 1.24 x 1.24 x 4 cm).

To study the radiation damage on the polystyrene matrix, several polystyrene (PS) samples were irradiated at the Department of Energy's Idaho National Engineering Laboratory (INEL) in Idaho Falls. The PS samples were exposed to gamma/electron radiation doses of different magnitude, ranging from 1 to 50 Mrad. Figure 24 shows the effect of 1, 10, and 50 Mrad radiation doses on the polystyrene. It can be observed

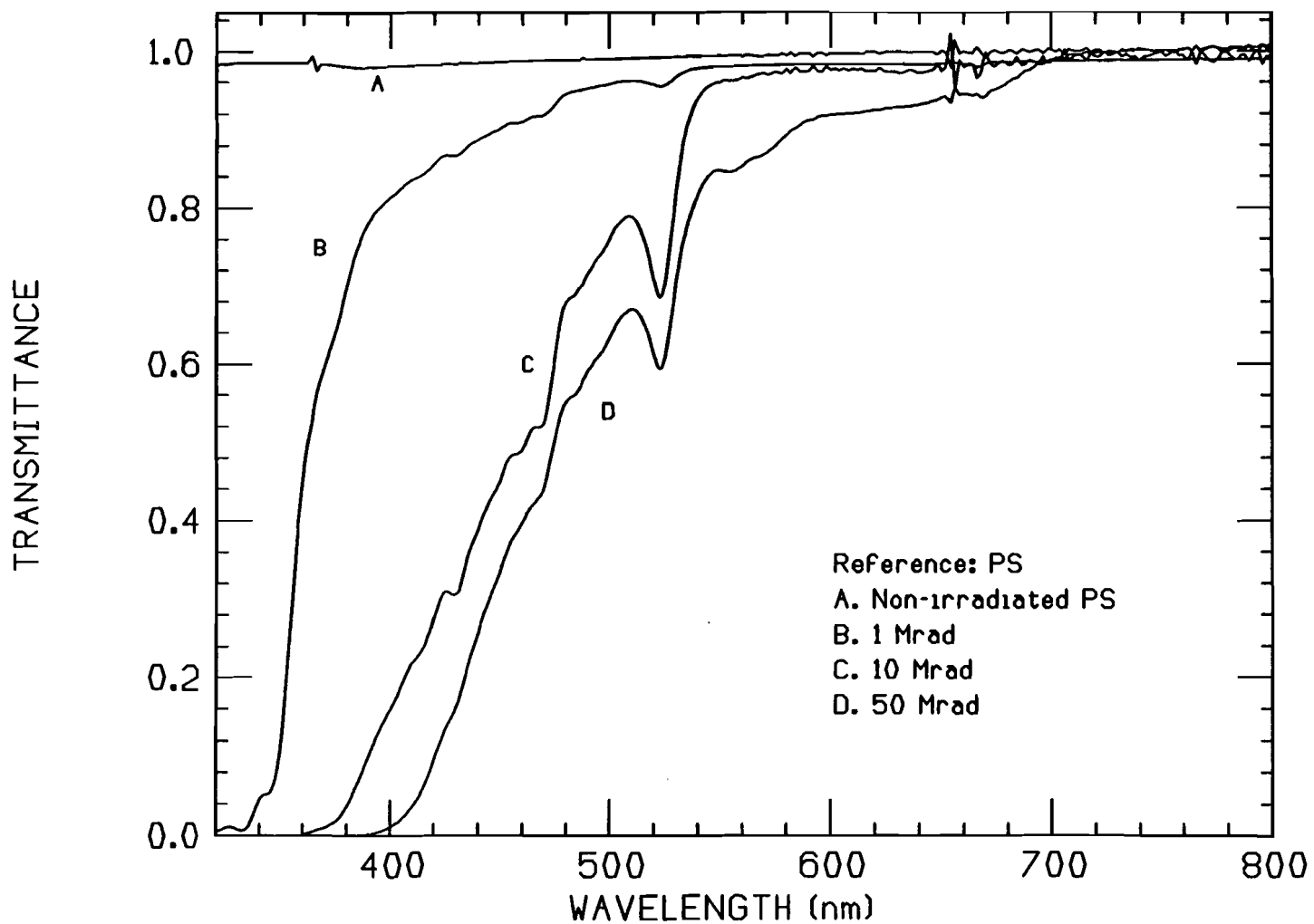

Figure 24. Polystyrene transmittance immediately after irradiation.

that considerable damage is already caused at the relatively low dose of 1 Mrad. The damage, as measured by the absorption area, does not present a linear relation with the dose received. Under irradiation, there is the formation of a new absorption band, which is only slightly detectable at 1 Mrad, but becomes quite large at doses of 50 Mrad. Polystyrene is less resistant to radiation than polyvinyltoluene and some polysiloxanes (17, 18). However, its performance under irradiation is higher than that of certain halogenated polymers.

It was also observed that the irradiated polystyrene samples would fluoresce in the green region of the visible spectrum when excited with a UV lamp (see Figure 25). This green fluorescence was present only after irradiation. Non-irradiated polystyrene exhibits only a small fluorescence peak at 360 nm, its normal fluorescence, when excited with a 313 nm light source.

Absorption measurements were performed before, immediately after, and 2 weeks after irradiation of the samples. Immediately after irradiation, polystyrene samples had a characteristic brownish color, and they showed a large absorption tail that, depending on the dose received, could extend up to 600 nm. The samples had a new absorption band at 530 nm and a new fluorescence peak at 550 nm.

Two weeks after the irradiation had taken place, however, the brown color of the PS samples had faded, and the radiation-induced absorption tail was considerably reduced in size (Figure 26). At the same time, the absorption band at 530 nm and the fluorescence peak at 550 nm had disappeared. Therefore both the absorption band at 530 nm and the fluorescence peak at 550 nm were credited to the same transient species

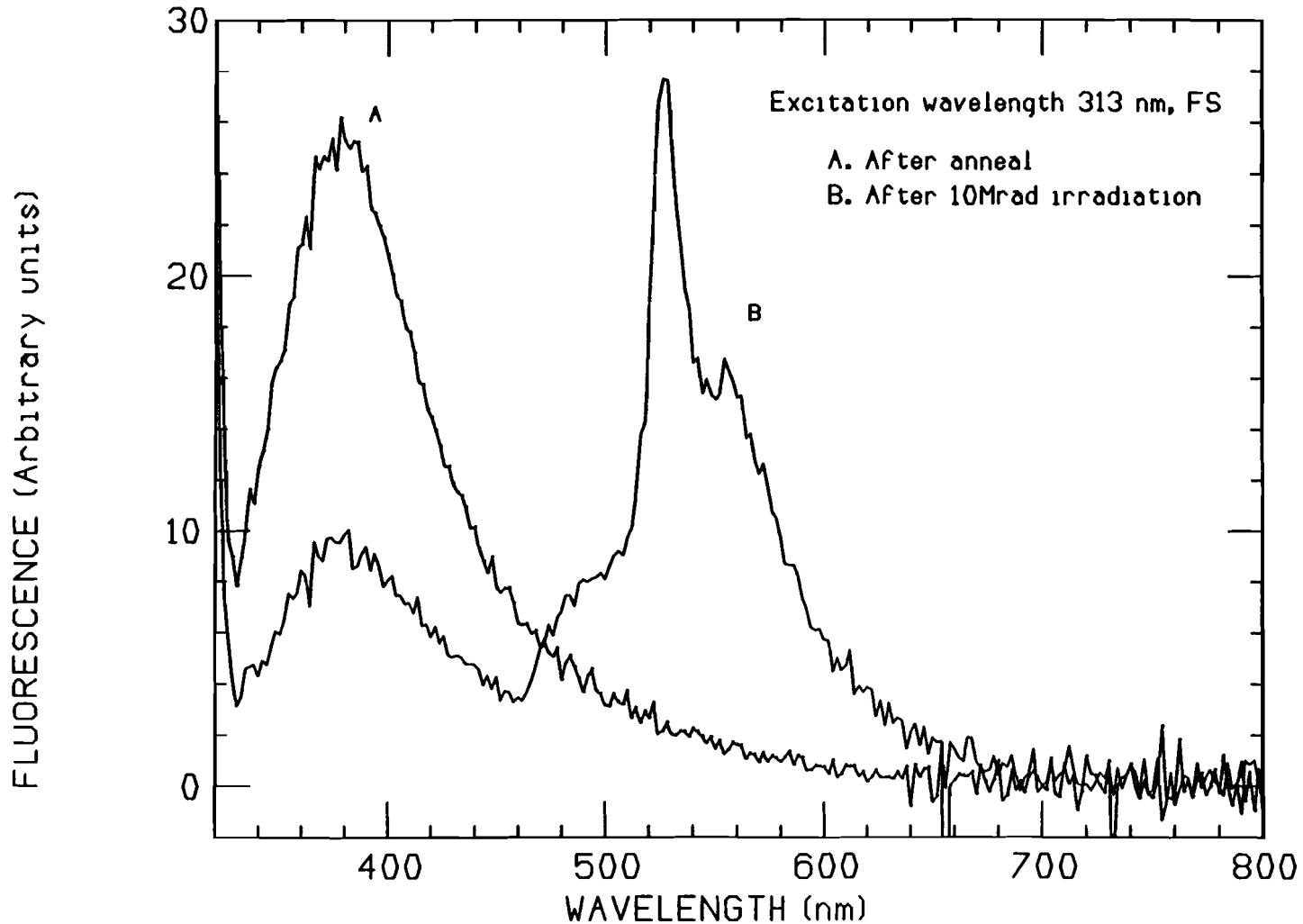

Figure 25. Fluorescence of irradiated polystyrene.

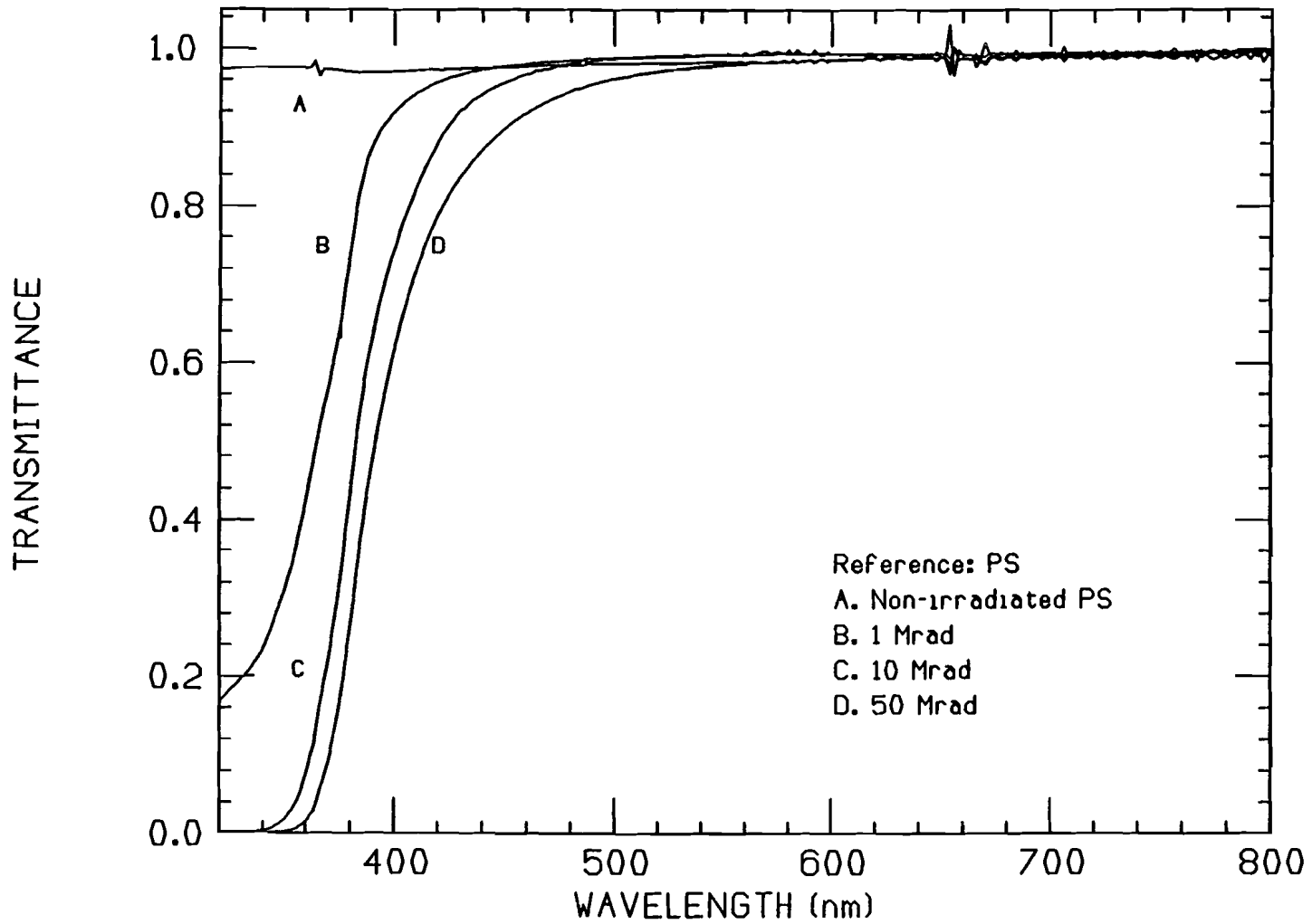

Figure 26. Polystyrene transmittance after oxygen annealing.

created under irradiation. This conclusion is supported by other experimental results published on polystyrene irradiation with X-rays (73), picosecond single electron pulse radiolysis (74, 75), and gamma irradiation (76). All these studies report the formation of a transient species which absorbs at approximately 530 nm (530 nm in dioxane solution, 515 nm in cyclohexane solution), and assign this absorption to be the singlet excimers of polystyrene (74), since the absorption spectrum is very similar to that of the excimers of benzene and alkyl-benzene reported previously (77).

An electron spin resonance (ESR) study (73) of X-ray irradiated polystyrene samples indicated the presence of various free radicals at different temperatures. At liquid nitrogen temperature, the radiation damage products were identified as cyclohexadienyl radical formed by transfer of a hydrogen atom from the main chain to the phenyl ring, in the meta position, in addition to the chain radical [- CH_2 - $C(C_6H_5)$ - CH_2 -], which is thermally more stable.

The increase in the polymer absorption after irradiation is caused by the presence of different species, since several processes can occur when a large amount of energy is deposited in the polymer. Both transient excited species and free radicals form, and in time the excited species relax and the free radicals recombine. Their formation and disappearance explains the reduction of the polystyrene absorption tail when measured a few weeks after irradiation. However, other processes taking place during irradiation such as photooxidation reactions, chain cleavage, and crosslinking, lead to permanent damage in the sample. These

processes are responsible for the remaining absorption measured weeks after irradiation.

The changes (partial recovery from radiation damage) that polystyrene undergoes from the time the irradiation ceases until 2 to 4 weeks later is referred to as the polystyrene annealing process. This annealing process has also been observed in other types of polymers (78), where it was also attributed to the relaxation of excited species formed under irradiation.

A series of additional irradiation studies were initiated in order to collect more information on both the annealing process, which in turn would provide insight into the recoverable radiation damage, and the permanent damage suffered by polystyrene when exposed to radiation. For investigating the annealing process, several polystyrene samples were irradiated in different environments, whereas to study the permanent damage issue, PS samples of different molecular weight as well as samples prepared from different monomer purification processes were irradiated.

1. Irradiation in Different Environments

Several polystyrene samples were irradiated in aluminum cans which had been evacuated and backfilled with different gases: oxygen, argon, or nitrogen. One set of samples was irradiated under vacuum conditions. The samples irradiated in nitrogen and argon exhibited the same characteristics and these results matched those seen in the initial set of samples irradiated. The PS had darkened and showed a green fluorescence in

addition to the pre-irradiation fluorescence in the blue spectral region. Similar behavior was observed for the PS samples irradiated under vacuum conditions.

Irradiation in oxygen proved to be the only condition to produce a different effect on the radiation damage in PS. When the samples irradiated in oxygen-filled cans were analyzed immediately after irradiation, they showed only a small dark spot in the center of the sample. This central region was the only part of the sample delivering the fluorescence in the green region.

The comparison of the behavior of the PS samples irradiated under different environments indicated that the presence of oxygen was responsible for the quenching of the excited species. To confirm this point, three samples that had been irradiated in argon and presented very little annealing were placed in three different aluminum cans backfilled with oxygen, argon, and air respectively. The three samples, which were all of the same thickness, exhibited different annealing rates, with the sample exposed to oxygen showing the highest rate, that in argon the lowest rate, and the sample exposed to air with an intermediate annealing rate. Furthermore, the annealing rate for the sample kept in the argon atmosphere was much lower than that of the samples in oxygen and air.

In light of the results obtained, all subsequent samples that were prepared to monitor the radiation-induced changes were irradiated in a nitrogen or argon environment. After the absorption and fluorescence measurements immediately after irradiation had been performed, the samples were returned to the cans, which were pressurized with oxygen,

while waiting for the measurements to take place two weeks later. The PS samples of a thickness between 1 and 1.24 cm had completely annealed after the 2-week period.

In addition to its role in the annealing issue, irradiation of the PS samples in the presence of nitrogen results in a good model for scintillating fibers when used in radiation detectors, where their being imbedded in lead or tungsten blocks prevents air circulation. The optimum conditions for using the fibers in a detector would be those that prevented the formation of the transient absorbing species altogether, since they cause a reduction in the light output characteristics of the detector. Although the PS irradiation results indicate that the samples in the presence of oxygen annealed faster, constantly flushing the detector with oxygen may not be a feasible option. Moreover, the constant presence of oxygen during prolonged radiation exposure of the detector may not even be a desirable option. The appearance of other processes, in particular an increase in the formation of undesirable photooxidation products, would defeat the beneficial effect of the annealing property of the oxygen by increasing the amount of permanent damage, which would also result in the reduction of the light output.

2. Irradiation of Samples with Different Molecular Weights

The polystyrene samples prepared by the standard polymerization cycle described above had an average molecular weight of approximately 350,000 amu. This information was obtained using gel permeation chromatography. The molecular weight of the polymer can be varied by

modifying the conditions of the polymerization. Thus, a fast process - for example 24 h at 180 °C - will yield a polymer with an average molecular weight between 10,000 and 20,000 amu (79). On the other hand, a slow polymerization - 3 weeks at 75 °C, for instance - will render a polymer with a high molecular weight, of approximately 1,000,000 amu.

Several polystyrene samples were prepared following the fast and slow polymerization cycles mentioned above. The samples were irradiated afterwards. The results of absorption and fluorescence after irradiation are shown in Figures 27 and 28. The transient absorption tail measured immediately after irradiation has approximately the same area regardless of the molecular weight of the polymer. The only significant difference resides in the intensity of the absorption band at 530 nm, which is barely formed in the irradiated sample of high molecular weight. The polymer of low molecular weight shows an absorption band of approximately the same area as that of the standard (intermediate molecular weight) polymer sample. The low molecular weight sample exhibited the characteristic green fluorescence that had been observed for the reference sample, while the polymer of high molecular weight showed no observable fluorescence when irradiated with a UV light.

The molecular weight ranges studied indicate that there is a slight gain in increasing the molecular weight of the polymer, in terms of reduction of the absorption band and the green fluorescence. However, the marginal benefits are not substantial enough to justify the time increase involved in the polymerization process required for the high molecular weight PS polymer.

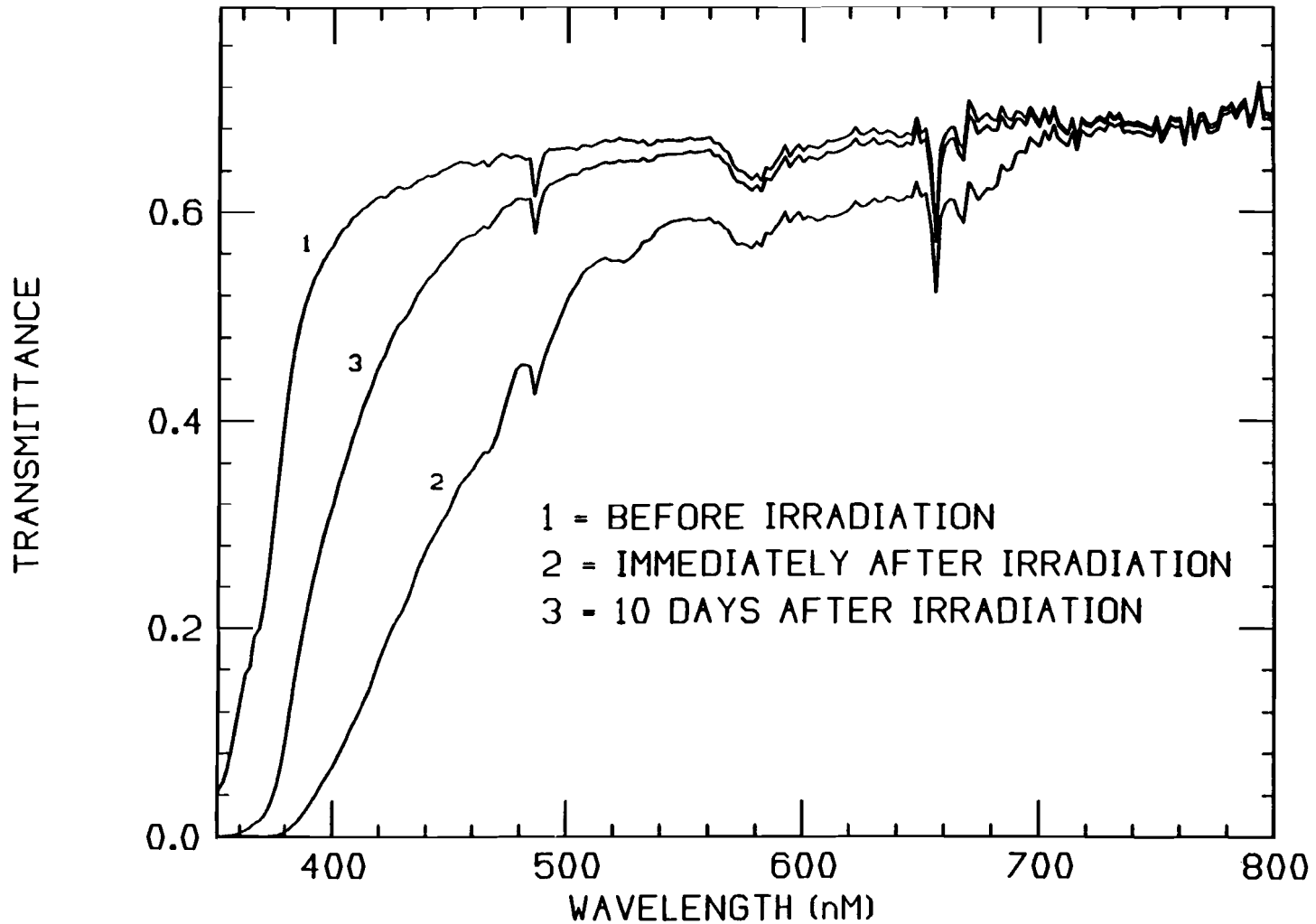

Figure 27. High molecular weight polystyrene irradiated at 10 Mrad.

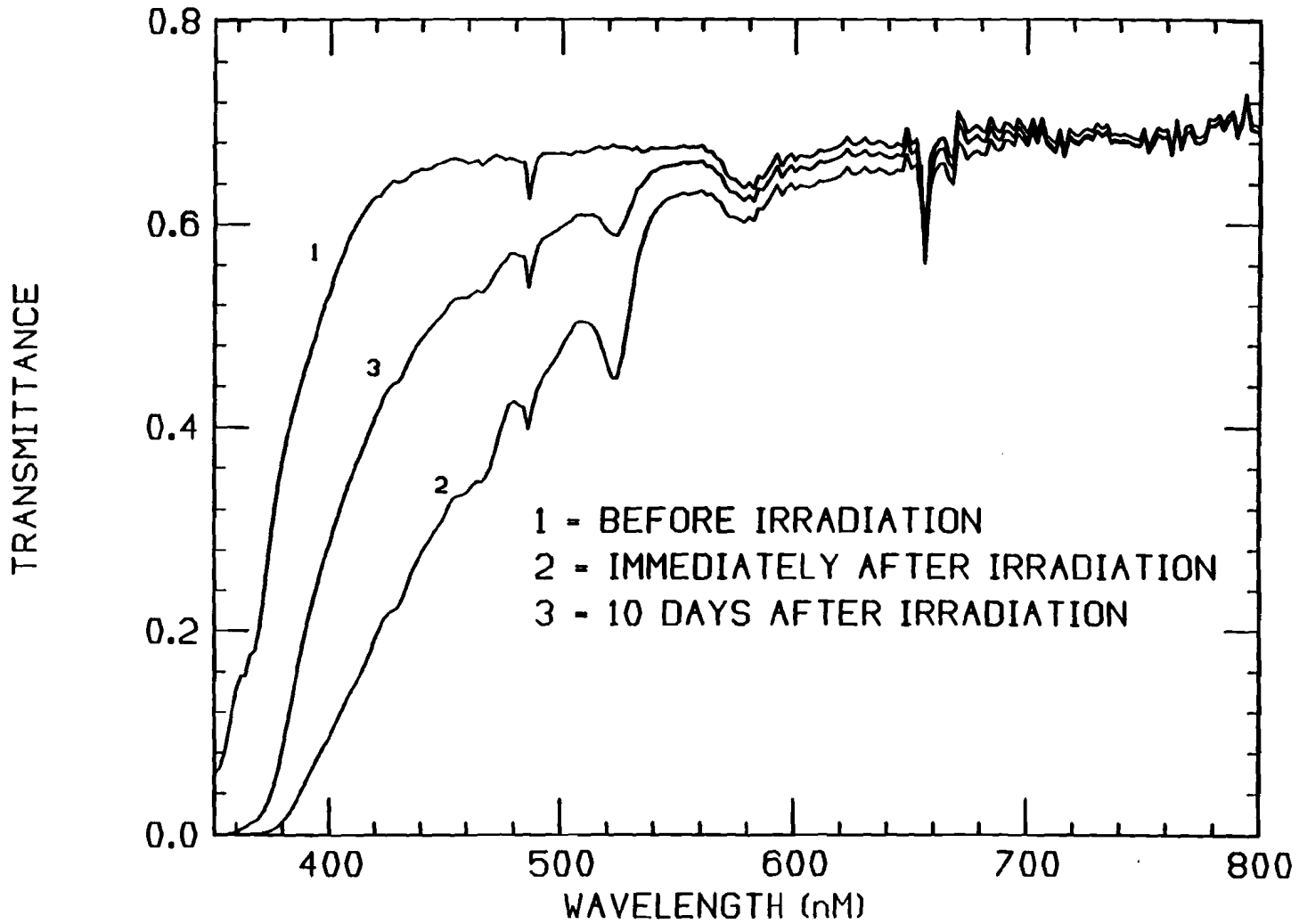

Figure 28. Low molecular weight polystyrene irradiated at 10 Mrad.

3. Irradiation of Samples of Different Monomer Purification Processes

It has been widely reported (17, 80) that, in certain polymers, the discoloration observed after irradiation is caused by the formation of colored radiolysis by-products, mainly from the added stabilizers. Stabilizers are compounds added to the polymerization process to avoid polymers from yellowing under UV exposure from sunlight. Conventional stabilizers are phenolic derivatives which do not have to undergo extensive modification to yield chromophores containing oxidative products which absorb light in the visible part of the spectrum.

The PS samples studied do not contain added UV stabilizers. However, the styrene monomer is stabilized with tert-butylcatechol, a phenolic derivative, to inhibit spontaneous polymerization. Therefore, if the inhibitor has not been completely removed, it could yield colored products under irradiation as mentioned before.

To determine if the coloration caused by irradiation is due to polymer impurities, styrene monomer was more thoroughly purified. After removing tert-butyl-catechol by column filtration, the monomer was distilled under vacuum as usual, then extracted several times with 1M NaOH solution, dried over magnesium hydroxide, and vacuum distilled again.

Several PS samples were made of this purified monomer and irradiated. The absorption spectra recorded immediately after irradiation were no different from those of PS samples using the standard monomer. Therefore, it can be concluded that tert-butylcatechol does not contribute to the discoloration of polystyrene under irradiation.

B. HBT and Its Derivatives

2-(2'-Hydroxyphenyl)benzothiazole (HBT) is known to show a large separation between the absorption and the fluorescence spectra because of its intramolecular proton transfer in the excited state (ESIPT) (see Figure 29). The proton transfer causes a structural rearrangement, which is indicated by the large Stokes shift between the absorption and emission spectra. The proton transfer in the excited state is favored because of an increase in the N basicity and the O acidity in the excited state, and, in addition, it occurs through a pre-existing hydrogen bond.

HBT has been reported to absorb at approximately 350 nm and fluoresce at 525 nm (47, 49). The quantum yield, though, varies considerably from measurements in solution (ϕ = 1.5% ± 0.5% in tetrachloroethylene [51]) to measurements in the solid (ϕ = 31% [47], 38% [49]) and no data are available for its quantum yield in polystyrene. Relative quantum yield measurements, considering the area underneath the fluorescence curve, of HBT in ethanol and in polystyrene indicate that ϕ is higher for HBT/PS than for HBT/ethanol. However, it can be expected that the quantum yield in polystyrene will not be larger than that in the solid phase where, because of the crystalline structure, vibrations and rotations would be expected to be more restricted than in a polymer matrix.

Substitution in the 2-phenyl ring was studied as a possible way to increase the quantum yield of HBT. Electron-withdrawing substituents were considered, since they would mesomerically stabilize the negative charge formed after proton transfer (Figure 30). Large substituents were

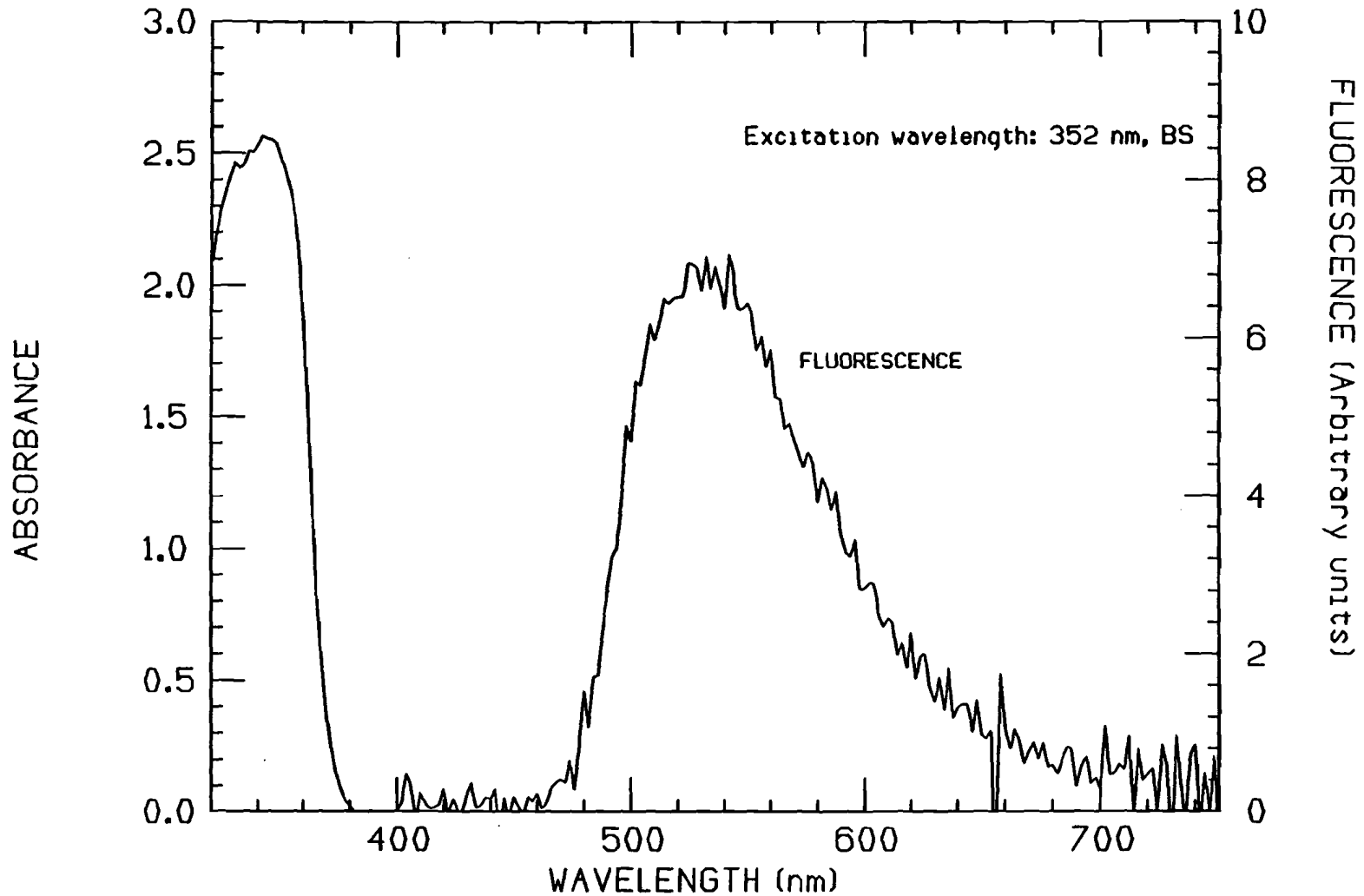

Figure 29. Absorption and fluorescence spectra of HBT in PS.

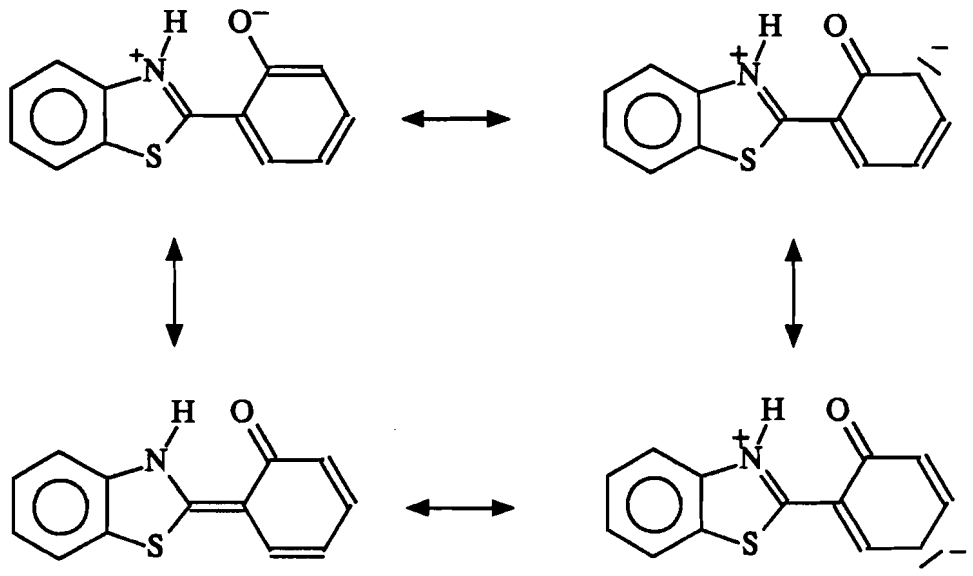

Figure 30. Resonance forms delocalizing the charges created by proton transfer in HBT.

also studied, because they favor certain conformations, and, in so doing, would freeze some of the rotational and vibrational modes, avoiding a non-radiative deexcitation of HBT.

Several HBT derivatives were prepared bearing substituents of different characteristics, from electron-withdrawing (Cl) to resonance delocalization (phenyl), to slightly electron-donating character (methyl).

Various methods for the preparation of HBT derivatives had been described in the literature (66-68). The syntheses for the different derivatives are quite similar, differing mainly in the acid catalyst used. The procedure utilized in most reports involves the condensation of o-aminothiophenol with the corresponding salicylic acid derivative using phosphorous trichloride in refluxing toluene. This method was selected over some possible alternatives because it required lower reaction temperatures and no use of polyphosphoric acid. When the corresponding salicylaldehyde had to be used, then triethylphosphate in acetic acid followed by oxidation with lead tetraacetate were substituted for phosphorous trichloride. Table 1 presents the list of HBT derivatives studied and Table 2 contains their photophysical properties.

It can be observed from Table 2 that substitution does not affect the magnitude of the Stokes shift significantly, which remains at approximately 10,000 cm^{-1} for all substituents. For example, the phenyl group shifts the absorption towards longer wavelengths, but at the same time it also shifts the fluorescence spectrum towards the red, thus maintaining the Stokes shift at approximately the same value. This is in contrast to fluorescent compounds that do not exhibit intramolecular proton transfer, in which, as the absorption shifts to longer wavelengths, the Stokes shift

Table 1. List of HBT derivatives studied.

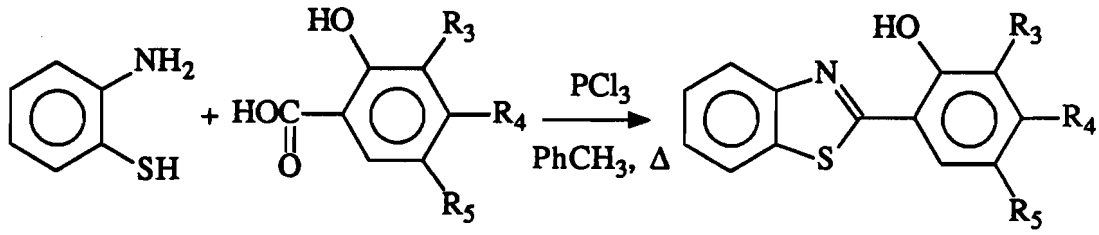

R3	R4	R5	Name	Yield (%)	m.p. (°C)	Ref.
H	H	H	HBT	a	133-134	49
Cl	H	H	3CHBT	45	181-182	49
F	H	H	3FHBT	41	151-152	-
Ph	H	H	3PHBT	55	186-187	-
H	Me	H	4MHBT	a	144-145	49
H	H	NH_2	5AHBT	65[b]	184-186[c]	49
H	H	Cl	5CHBT	49	150-151	49
H	H	Me	5MHBT	a	133-134	49
H	H	Ph	5PHBT	46	141-142	-

[a]Commercially available product.

[b]Prepared from reduction of 2-(2'-hydroxy-5'-nitrophenyl)benzothiazole.

[c]Recrystallized from methylene chloride.

Table 2. Photophysical characteristics of HBT and its derivatives in a polystyrene matrix.

Compound	λ_{max} (nm)	10^{-4} M Threshold (nm)	ε (L $mol^{-1}cm^{-1}$)	λ_{em} (nm)
HBT	340	388	15000	530
3CHBT	344	392	15000	540
3FHBT	340	388	12000	540
3PHBT	350	400	17000	560
4MHBT	340	386	21000	530
5AHBT[a]	350	400	16000	535
5CHBT	350	405	16000	545
5MHBT	346	400	20000	550
5PHBT	355	410	18000	560

[a] Data on 5AHBT was obtained in styrene solution instead of polystyrene.

does not remain constant and a larger overlap between absorption and emission spectra occurs.

Appendix A contains a complete set of absorption and fluorescence spectra for all the HBT derivatives. Another important characteristic of these derivatives is that their absorption does not extend considerably beyond the absorption maximum. Directly related to this characteristic is the color of each compound. The HBT derivatives studied are either white or slightly tinted yellow in color, with the exception of 5'-amino-HBT (5AHBT), which is yellow. Compounds featuring a short absorption tail are preferred because the overlap between absorption and emission will be nearly zero, reducing the self-absorption of the emitted light.

5AHBT was prepared to investigate its emission wavelength because of the disagreement on its value between two different authors: 543 nm in one publication (47) and 640 nm in another (49) (both measured in the solid phase). If the fluorescence maximum in 5AHBT were actually the one at longer wavelength, it would be very interesting to test for scintillators. It would exhibit the largest Stokes shift among the HBT derivatives since it would absorb in the blue region of the spectrum and fluoresce in the red. 5AHBT was synthesized, and fluoresced in the red in the solid phase; however, it fluoresced in the green in styrene solution. Its spectral characteristics were recorded, but further work was not pursued.

The quantum yield determinations were calculated relative to the unsubstituted compound, HBT, by measuring the area underneath the fluorescence distribution. The samples prepared for such purpose were of lower concentration than that required for scintillation detector uses

(1% HBT derivative/PS, or approximately 10^{-3} M). Two sets of samples of different concentrations were prepared in order to verify one set of data against the other. The high concentration (approximately 10^{-4} M) data set did not require any correction for differences in absorbance among them, since the samples absorbed 95% of the excitation light. The low concentration (about 10^{-5} M) samples absorbed approximately 30% of excitation light. Therefore, small differences in absorbance among them will cause differences in the fluorescence distribution area. The data correction involved the normalization of the absorbance values to that of HBT, and the subsequent modification of the areas by the corresponding factor. The calculated relative quantum yields are listed in Table 3. The values obtained for each agree within 10-15%, which is the error expected for this type of determination. However, for two compounds, 4MHBT and 5MHBT, their relative quantum yield values differ by a factor of 20% and 40% respectively.

The relative quantum yield measurements indicate the effect the substituent has on the fluorescence. As illustrated in Figure 30, position C3' and C5' in the 2-phenyl ring have a large electronic density due to their contribution to delocalize the negative charge. Substitution in these positions by an electron-withdrawing group will have a stabilizing effect, thus explaining the experimental results for 3CHBT and 5CHBT, which possess the highest quantum yields. On the other hand, the quantum yield does not increase when a fluorine atom is placed in C3' position (3FHBT). Even though fluorine is a very electro-negative atom, it also possesses a certain electron-donating effect through resonance, which is reflected in the 3FHBT quantum yield. Bromine and iodine substitution is

Table 3. Relative quantum yields of HBT and its derivatives.[a]

Compound	A_1[b]	Rel. Q.Y.[c]	A_2[d]	Rel. Q.Y.[e]
HBT	2.45	1.0	0.75	1.0
3CHBT	2.41	1.64	0.57	1.78
3FHBT	2.42	0.93	0.89	0.91
3PHBT	2.56	1.17	0.71	1.21
4MHBT	2.38	1.03	0.47	1.26
5CHBT	2.51	1.64	0.64	1.65
5MHBT	2.60	0.92	0.64	0.64
5PHBT	2.61	1.52	0.77	1.36

[a]Relative quantum yields measured using a 352 nm excitation wavelength light source directed at the back surface (BS) of the sample and calculating the area underneath the fluorescence distribution.

[b]A_1= absorbance at 352 nm using high concentration (10^{-4} M) samples.

[c]Relative quantum yields using high concentration samples.

[d]A_2 = absorbance at 352 nm using low concentration (10^{-5} M) samples.

[e]Relative quantum yields using low concentration samples.

not recommended due to the negative effect of heavy atoms on the quantum yield (49). At this point, the phenyl group was considered to observe the effect of a large group in that position and also because it would be able to stabilize the negative charge through resonance. 3PHBT has a quantum yield slightly higher than HBT. However, the decrease in quantum yield with respect to 3CHBT can be due to the poor stabilization of the negative charge by the ring because of its lack of planarity. The phenyl ring needs to be coplanar with the rest of the molecule in order to effectively delocalize the negative charge. Since it is a large group next to another group, the phenyl ring is actually positioned at an angle, thereby reducing resonance stabilization. This conclusion is supported by the high relative quantum yield observed in 5PHBT where the phenyl ring, free of any steric hindrance, is coplanar with the rest of the molecule. When a methyl group is placed in the C5' position, the relative quantum yield is similar to HBT. Finally, placing a methyl group in the C4' position does not alter the HBT original quantum yield. In summary, the relative quantum yield in the 3'-substituted HBT derivative decreases from 3CHBT to 3PHBT to 3FHBT, the last two compounds having similar values. For the 5'-substituted HBT derivatives, the relative quantum yield is similar for 5CHBT and 5PHBT, and significantly lower for 5MHBT.

C. 3HF and Its Derivatives

3-Hydroxyflavone (3HF) also exhibits excited state intramolecular proton transfer (ESIPT), which is characterized by the large Stokes shift between the absorption and emission spectra (Figure 31). 3HF in

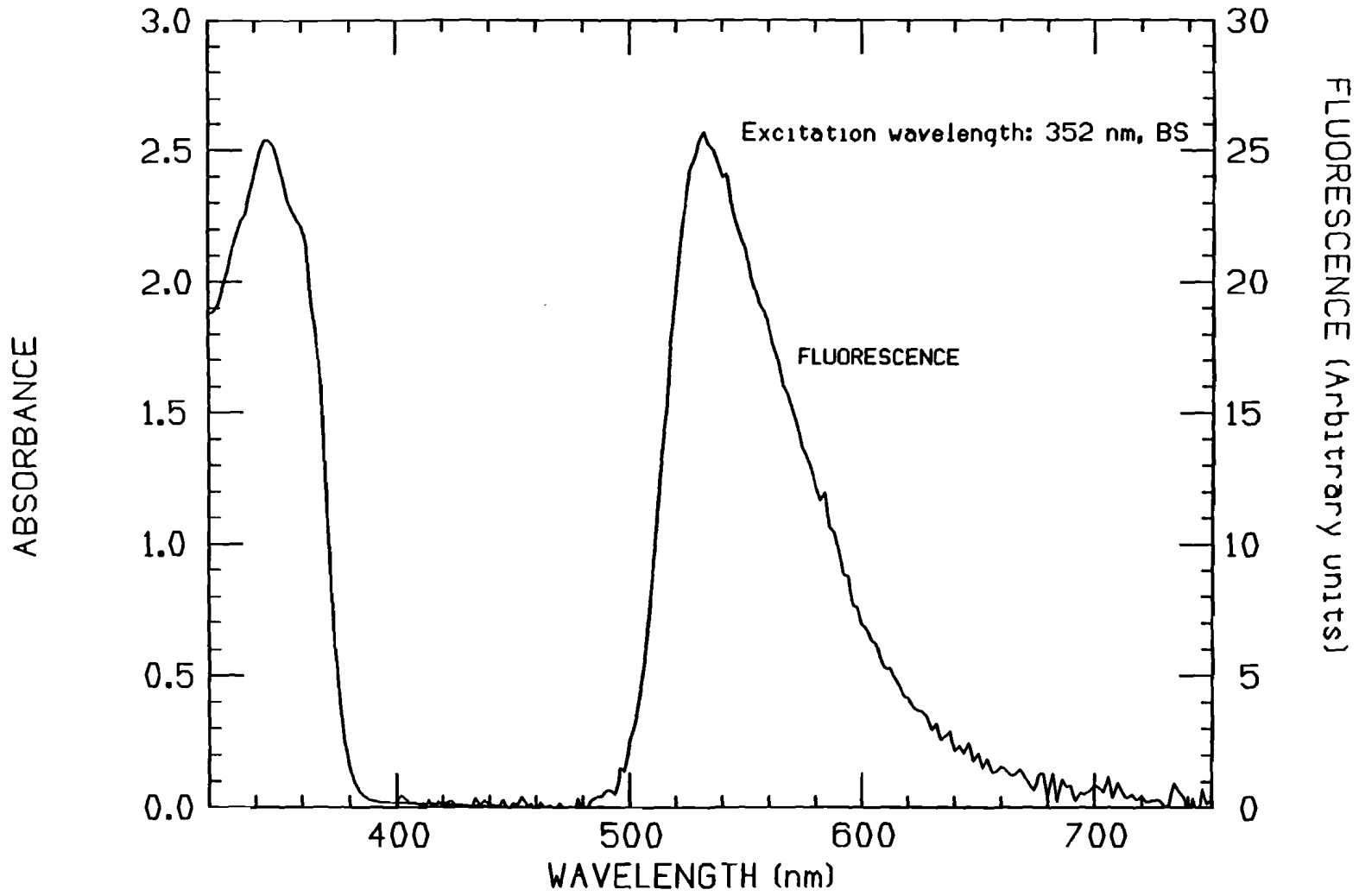

Figure 31. Absorption and fluorescence spectra of 3HF in PS.

polystyrene absorbs at 350 nm and emits at 530 nm (a value slightly shifted to the blue is reported for hydrocarbon solutions [55]). The available information on the quantum yield is reported for 3HF solutions: ϕ = 42% in toluene (35), and 36% in ethanol (81); no data exist for solutions in polystyrene or other polymers.

As mentioned previously, the large spectral separation between absorption and emission spectra is an important feature with respect to the actual use of this product as a dopant in plastic scintillators. 3HF, unlike HBT, has already been considered by the scintillator manufacturing industry as a dopant. Thus, scintillating fibers and sheets containing p-terphenyl, as primary dopant, and 3HF, as wavelength shifter, are commercially available. A plausible explanation for the development of 3HF over HBT doped plastic scintillators is the larger quantum yield.

3HF was first investigated at Fermi National Accelerator Laboratory because of the possibility of using it for intrinsic scintillators, 3HF acting as primary dopant and wavelength shifter in polystyrene. A comparison of a 3HF/PS sample with a standard scintillator proved that 3HF could work as an intrinsic scintillator. However, some difficulty was encountered reproducing 3HF doped samples of the same optical quality. Discrepancies were observed from one polymerization set to another. It was also noted that pure 3HF would discolor in time, turning into a dark yellow solid, indicating that 3HF was slowly decomposing, probably as a result of air oxidation. 3-Hydroxyflavones oxidation has been extensively studied as a model for the oxidative transformation of flavonoids <u>in vivo</u> (82-85). However, most of these studies are carried out in basic solutions

where reaction with oxygen results in the heterocyclic ring being cleaved to release carbon monoxide, forming a dark yellow solution. Nonetheless, this type of reaction also seems to happen in other environments, under milder conditions. In our work, the formation of this colored solution has been observed: (a) on passage of 3HF through a silica gel chromatographic column, and (b) on polymerization of 3HF-doped styrene at 125 °C.

Because of this problem, 3HF is only purified by recrystallization and sublimation. In addition, several tests were performed to determine the reason for 3HF decomposition at the beginning of a polymerization: first, freshly purified 3HF was used; and, second, the polymerization test tubes were covered in aluminum foil, to eliminate photochemically induced decomposition, but the polymerization still failed. A successful polymerization was achieved when the initial polymerization temperature was dropped to 90 °C and slowly increased to 125 °C. There is no sound argument to explain why 3HF decomposed right away when the polymerization was started at 125 °C and did not decompose when the temperature was raised to 125 °C the second day of the polymerization cycle. However, it is known that styrene polymerization is very exothermic at the beginning, and perhaps localized heating effects cause the solution temperature to rise enough to cause the 3HF decomposition.

Preparation of 3HF derivatives substituted in the 2-phenyl ring was undertaken with two goals in mind: (a) to improve in the quantum yield of the compound, and (b) to increase the stability of the molecule. The methodology to synthesize 3HF derivatives is basically described as the Algar-Flynn-Oyamada preparation of flavonols with a few possible modifications. It consists of an aldol condensation of o-hydroxyaceto-

phenone with the corresponding benzaldehyde in basic ethanol followed by hydrogen peroxide oxidation of the isolated chalcone. One modification of this procedure is to avoid the chalcone isolation and have a one-pot two-step reaction (71). The compounds prepared this way are listed in Table 4, and Table 5 presents their photophysical properties.

In Table 5, it can be observed after comparing the derivatives to their parent compound, 3HF, that the ortho-substituted 3HF derivatives have the absorption band slightly blue-shifted (shifted towards shorter wavelengths), by about 20 nm, even though some of them have a long absorption tail (i.e., 2MO3HF) with a threshold similar to 3HF. Another characteristic of the ortho-substituted derivatives is that the emission wavelength is the same as that of 3HF. In other words, the ortho-substituted derivatives have a slightly larger Stokes shift than 3HF, although still in the 10,000 cm^{-1} range, since the absorption spectrum has shifted to shorter wavelengths but the fluorescence spectrum has not changed. This is an important characteristic since it ensures that the overlap between the absorption tail and the fluorescence spectrum is minimized, thus avoiding the self-absorption of the emitted light.

The para-substituted derivatives have an absorption maximum similar to 3HF but with a slightly longer absorption threshold. Their emission spectrum is shifted towards longer wavelengths, except for 4F3HF. Figure 32 shows the absorption and emission spectra of 2M3HF and 4P3HF, presenting the two most extreme differences among the spectra of all the derivatives prepared. Appendix A contains the absorption and fluorescence spectra for the remaining 3HF derivatives.

The quantum yield measurements relative to the unsubstituted

Table 4. List of 3HF derivatives studied.

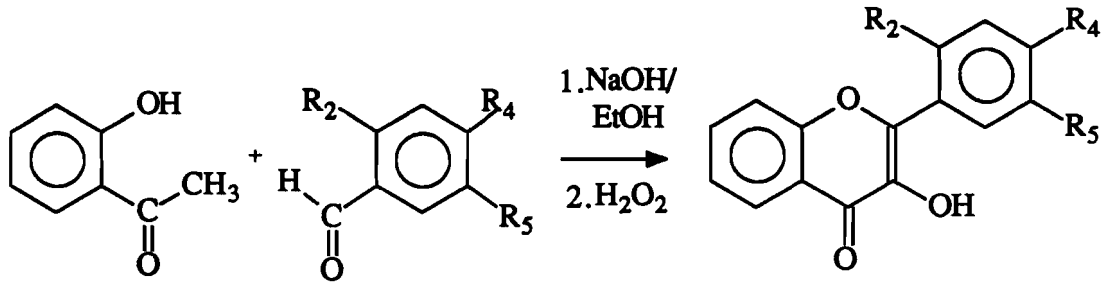

R2	R4	R5	Name	Yield (%)	m.p. (°C)	Ref.
H	H	H	3HF	a	170-172	60
Cl	H	H	2C3HF	42	181-183	-
H	Cl	H	4C3HF	45	202-204	71
F	H	H	2F3HF	66	181-182	86
H	F	H	4F3HF	45	153-154	86
Me	H	H	2M3HF	70	192-193	60
H	Me	H	4M3HF	60	195-197	71
Me	H	Me	25M3HF	67	184-185	60
MeO	H	H	2MO3HF	46	210-212	87
H	MeO	H	4MO3HF	55	230-232	71
H	MeS	H	4MS3HF	55	209-211	-
H	Ph	H	4P3HF	43	220-222	88
H	PhO	H	4PO3HF	40	183-184	-

[a]Commercially available.

Table 5. Photophysical characteristics of 3HF and its derivatives in a polystyrene matrix.

Compound	λ_{max} (nm)	10^{-4} M threshold (nm)	ε (L $mol^{-1}cm^{-1}$)	λ_{em} (nm)
3HF	350	390	14000	530
2C3HF	335	390	6000	532
4C3HF	345	395	23000	536
2F3HF	335	385	10000	532
4F3HF	340	393	11000	532
2M3HF	330	385	11000	530
4M3HF	350	393	16000	534
25M3HF	330	388	15000	534
2MO3HF	335	395	10000	534
4MO3HF	350	403	28000	536
4MS3HF	360	415	20000	545
4P3HF	360	410	35000	548
4PO3HF	350	400	28000	538

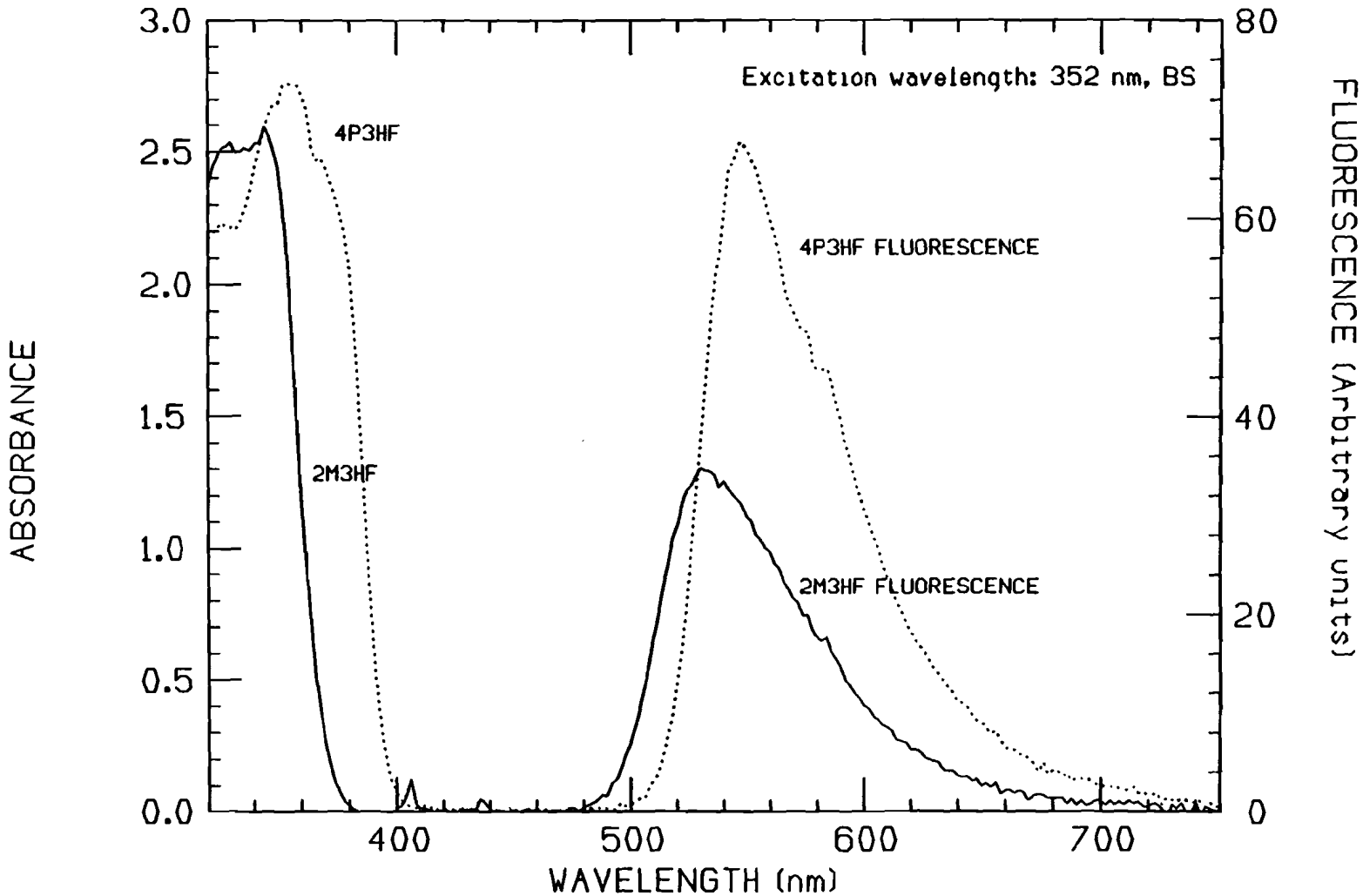

Figure 32. Differences between absorption and fluorescence spectra of 2M3HF and 4P3HF in PS.

compound, 3HF, (Table 6) were performed using a mercury lamp source equipped with a 352 nm bandpass filter as the excitation source. The light was directed at the back surface (BS) of the sample, and relative measurements were determined by calculating the area underneath the fluorescence spectrum. Two sets of samples of different concentrations were prepared with the purpose of correlating the measurements from both sets. A set of samples of approximately 10^{-4} M concentration in PS was prepared and are referred to as the high concentration set (HC). Another set with 10^{-5} M concentrations, also in PS, is the low concentration set (LC). The HC sample set absorbed 95% of the excitation light. Thus, the areas from their fluorescence spectrum were not corrected for the slight difference in absorption among the samples. The LC sample set absorbed approximately 30% of the excitation light. Therefore, the areas calculated from their fluorescence distribution were corrected for the differences in absorption among the samples. This correction in the LC samples was necessary because only a small amount of the excitation light was absorbed, and fluctuations in absorbance among the sample set would cause large differences in the fluorescence distribution area. In the HC sample set, since virtually all the light was absorbed, the small changes in absorbance through the set could not cause large discrepancies in the fluorescence curve area. The two sets of data are presented in Table 6. The results from both sets agree within 10-15%, except for 4MO3HF and 4P3HF, where the discrepancy is about 20%. For 4MS3HF and 4PO3HF, the data obtained for the LC sample was always very inconsistent with the HC sample. New LC samples were prepared and analyzed, but the results did not agree either. The result from the HC

Table 6. Relative quantum yields of 3HF and its derivatives.[a]

Compound	A_1[b]	Rel. Q. Y.[c]	A_2[d]	Rel. Q. Y.[e]
3HF	2.39	1.0	0.36	1.0
2C3HF	2.43	0.74	0.54	0.76
4C3HF	2.56	1.09	0.28	0.94
2F3HF	2.41	0.72	0.49	0.71
4F3HF	2.39	1.12	0.66	1.09
2M3HF	2.29	0.76	0.48	0.72
4M3HF	2.48	1.18	0.51	0.94
25M3HF	2.34	0.78	0.65	0.75
2MO3HF	2.69	0.67	0.29	0.74
4MO3HF	2.50	1.21	0.50	1.01
4MS3HF	2.50	1.20	-	-
4P3HF	2.75	1.40	0.80	1.22
4PO3HF	2.70	1.30	-	-

[a]Relative quantum yields measured using a 352 nm excitation wavelength light source directed at the back surface (BS) of the sample and calculating the area underneath the fluorescence distribution.

[b]A_1= absorbance at 352 nm using high concentration (10^{-4} M) samples.

[c]Relative quantum yields using high concentration samples.

[d]A_2 = absorbance at 352 nm using low concentration (10^{-5} M) samples.

[e]Relative quantum yields using low concentration samples.

sample is listed since the HC sample measurements are more reliable. The relative quantum yield measurements indicate that the ortho-substituted derivatives exhibit lower quantum yields than their parent compound, 3HF. On the other hand, the para-substituted derivatives show higher quantum yields than 3HF. Sengupta and Kasha (55) pointed out the importance of the molecule planarity in order to develop the oxygen basicity to favor the excited-state intramolecular proton transfer. In addition, Brucker and Kelley (65) proved the role of the phenyl torsion as a deactivation mode after proton transfer. The results presented here from the relative quantum yield measurements agree with these two findings. The ortho-substituted derivatives encounter some steric hindrance with the two lone pairs of the oxygen in the heterocyclic ring. Therefore, the substituted phenyl ring will not be coplanar with the rest of the molecule. Nonetheless, in the excited state it will be driven towards planarity, but after proton transfer will return to its original position. This torsion is a non-radiative deactivation pathway to return to the ground state. Therefore, it will be competing with fluorescence (radiative relaxation) to deexcite the molecule. The para-substituted derivatives do not encounter any steric hindrance problem. Thus, the phenyl ring remains on the same plane as the rest of the molecule, and deexcitation after proton transfer does not involve the phenyl ring torsion as a major deactivation mode.

D. Fluorescence as a Function of Temperature

Several 3HF and HBT derivatives have been prepared and their

quantum yield relative to the unsubstituted compounds determined. It has been mentioned in the previous sections how the increase and decrease in the quantum yield correlated with the character of the substituent and its position in the studied compound. For instance, ortho-substituted 3HF derivatives have lower quantum yields than the para-substituted compounds. Furthermore, in the HBT derivatives a phenyl group in the ortho or para position relative to the hydroxyl group will increase or decrease, respectively, the quantum yield relative to HBT.

The fluorescence measurements and the relative quantum yield determinations shed some light on the understanding of the fluorescence mechanism and the deactivation processes generated by vibrations and rotations in the studied compounds. More information can be gathered from experiments carried out below room temperature. In doing this study, other substituent effects could be found. Moreover, the increase in quantum yield due to the freezing of some vibrational and rotational modes could be monitored. These arguments prompted the fluorescence analysis of HBT, 3HF, and their derivatives from liquid helium temperature to room temperature.

The sample under study was placed in a cryostat and the temperature decreased to 5 K. It took approximately 1 h to reach the desired temperature. The temperature was increased in 25 K intervals, and half an hour was allowed between measurements to give the sample time to equilibrate at that temperature. For these measurements, the light source was a deuterium lamp equipped with a broadband filter centered at 300 nm. This system offers less light intensity than that used for the relative quantum yield calculation.

The results for each group of compounds will be presented in separate sections.

1. HBT and Its Derivatives

The results from this study are presented in Figures 33 and 34. In Figure 33, the curves are generated by measuring the area underneath the fluorescence spectrum at each temperature. At room temperature, the trend in fluorescence is similar to that observed previously. 3CHBT, 5CHBT, and 5PHBT have the highest light output; the remaining compounds have approximately the same light output as HBT. In this study, 3FHBT and 5MHBT show poorer fluorescence yield than that measured in other analyses where they fluoresced similarly to HBT. In Figure 34 the area has been normalized to one for each compound relative to its fluorescence yield at room temperature, thus indicating the specific changes undergone for each compound. The relative quantum yield for 5MHBT and 3FHBT at 5 K has increased by a factor of 8 and 9, respectively; 4MHBT and HBT increase it by a factor of 4.

The remaining compounds - 3CHBT, 5CHBT, 3PHBT, and 5PHBT - show a similar increase, up to 3 times their original value. At first glance, it was unexpected to observe 3PHBT following the trend of the compounds that exhibit a large quantum yield at room temperature. This small increase at low temperatures may be caused by the hindered environment in which the phenyl ring is located. By lowering the temperature, some torsion modes can be frozen and thus improve the quantum yield; however, the steric hindrance cannot be changed.

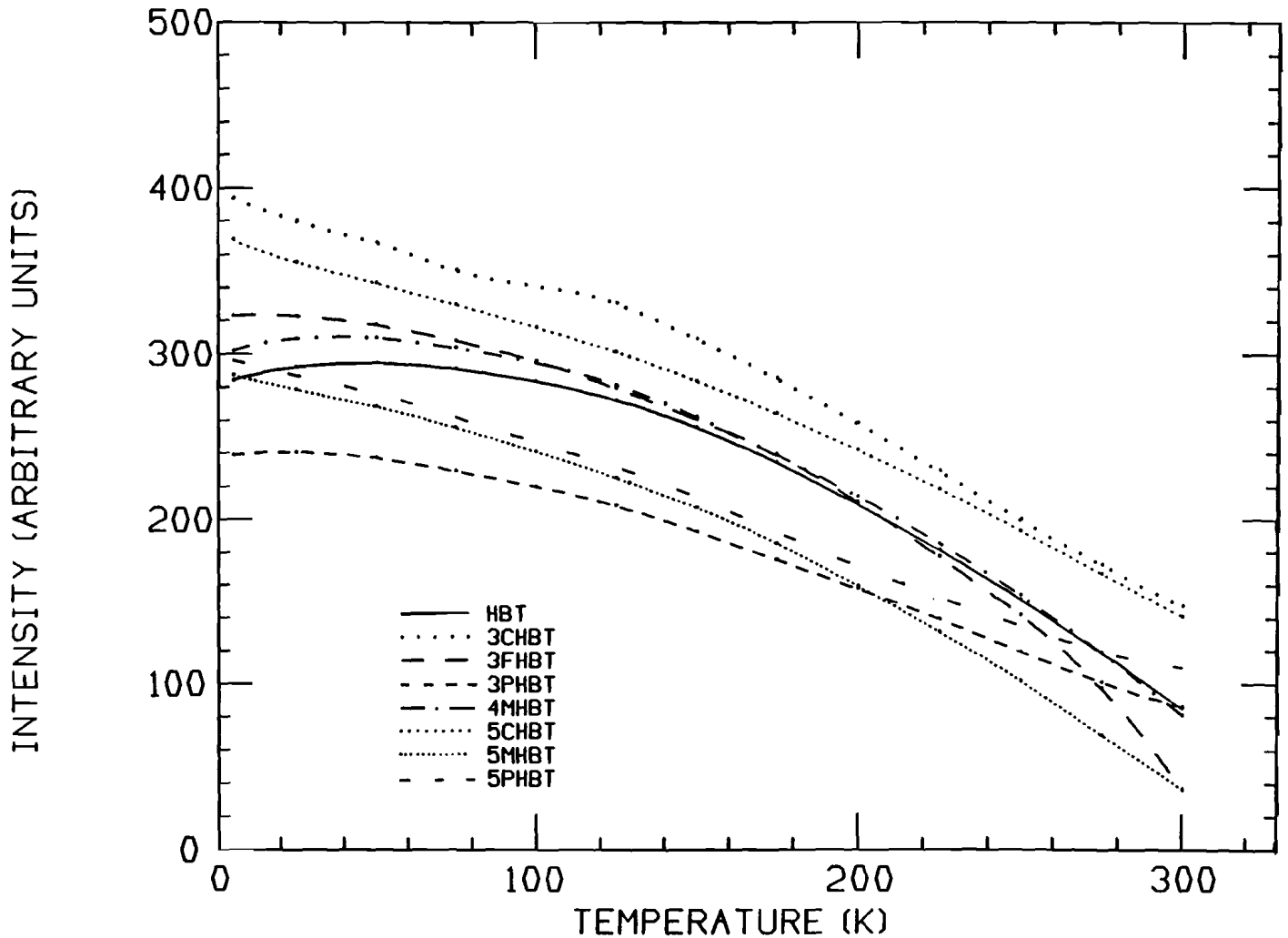

Figure 33. Changes in fluorescence yield of HBT and its derivatives as a function of temperature.

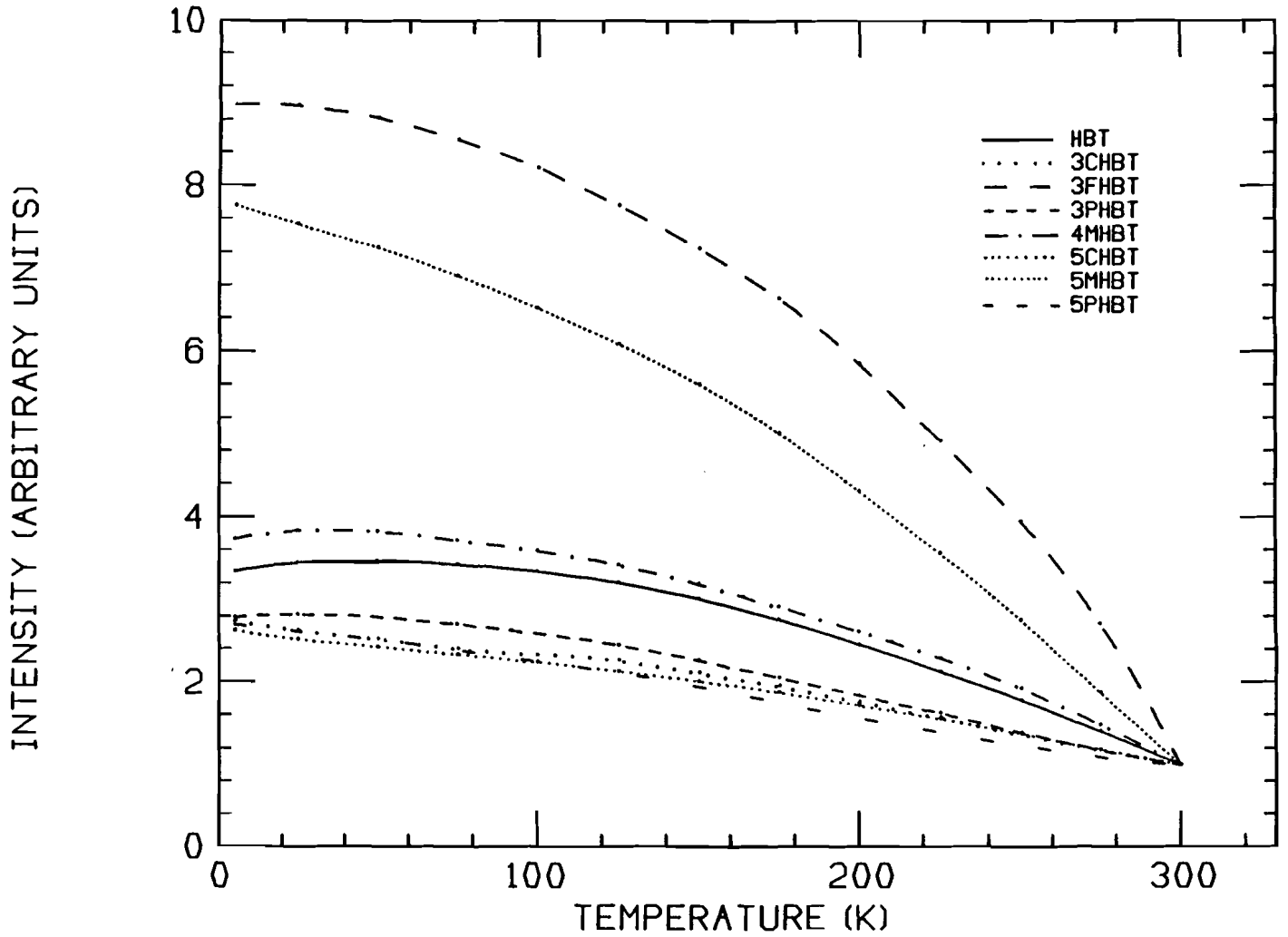

Figure 34. Changes in fluorescence yield as a function of temperature for HBT and its derivatives relative to each value at room temperature.

The major gain in quantum yield occurs for the compounds that have the lowest quantum yield at room temperature, demonstrating that the fluorescence mechanism competes with thermal deactivation processes. These changes in relative quantum yield as a function of temperature indicate an upper limit for the absolute quantum yield of each compound. Based on the relative quantum yield of the derivatives and the data at low temperature, the quantum yield of HBT is approximately 10-12%

2. 3HF and Its Derivatives

The results for 3HF and its derivatives are presented in two sets of plots. The first set represented by Figures 35 and 36 contains the raw data. In the second set, Figures 37 and 38, the experimental data has been normalized to one for each compound relative to its fluorescence yield at room temperature. Figure 35 details the changes in the fluorescence area of the ortho-substituted derivatives relative to 3HF. At room temperature, the trend in the relative quantum yield is the same as that observed in the relative quantum yield determinations presented previously. At 300 K, 3HF has higher light output than any of the ortho-substituted derivatives. Moreover, the difference in fluorescence between the compounds substituted with halogen or methyl groups is small. In contrast, the 2MO3HF compound which is substituted with a strongly electron-donating group, has the lowest quantum yield. As the temperature drops, the yield of the ortho-substituted derivatives increases. This effect is due to the phenyl ring rotation becoming more restricted as the temperature decreases. It has been mentioned

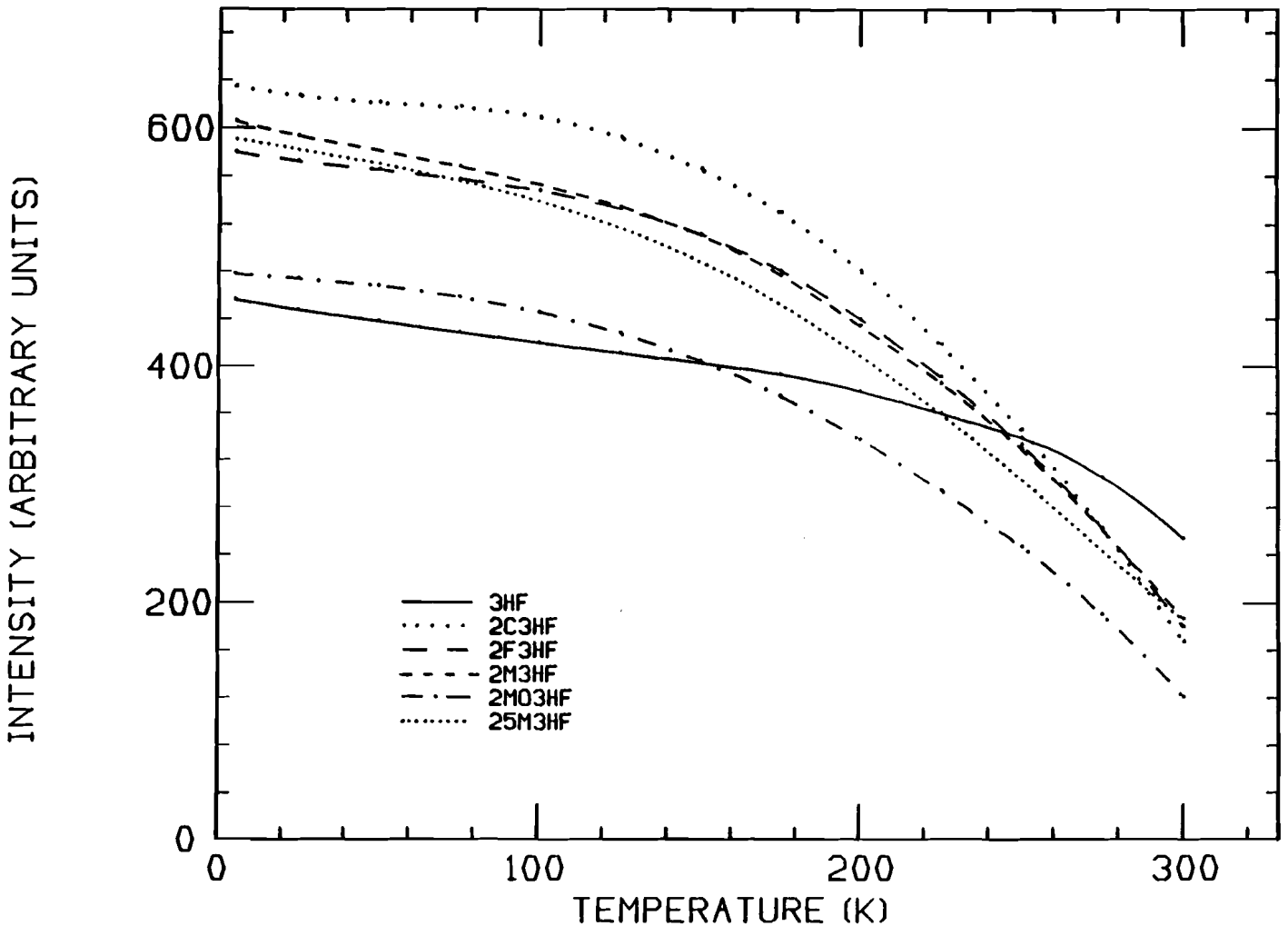

Figure 35. Changes in fluorescence yield of 3HF and its ortho-derivatives as a function of temperature.

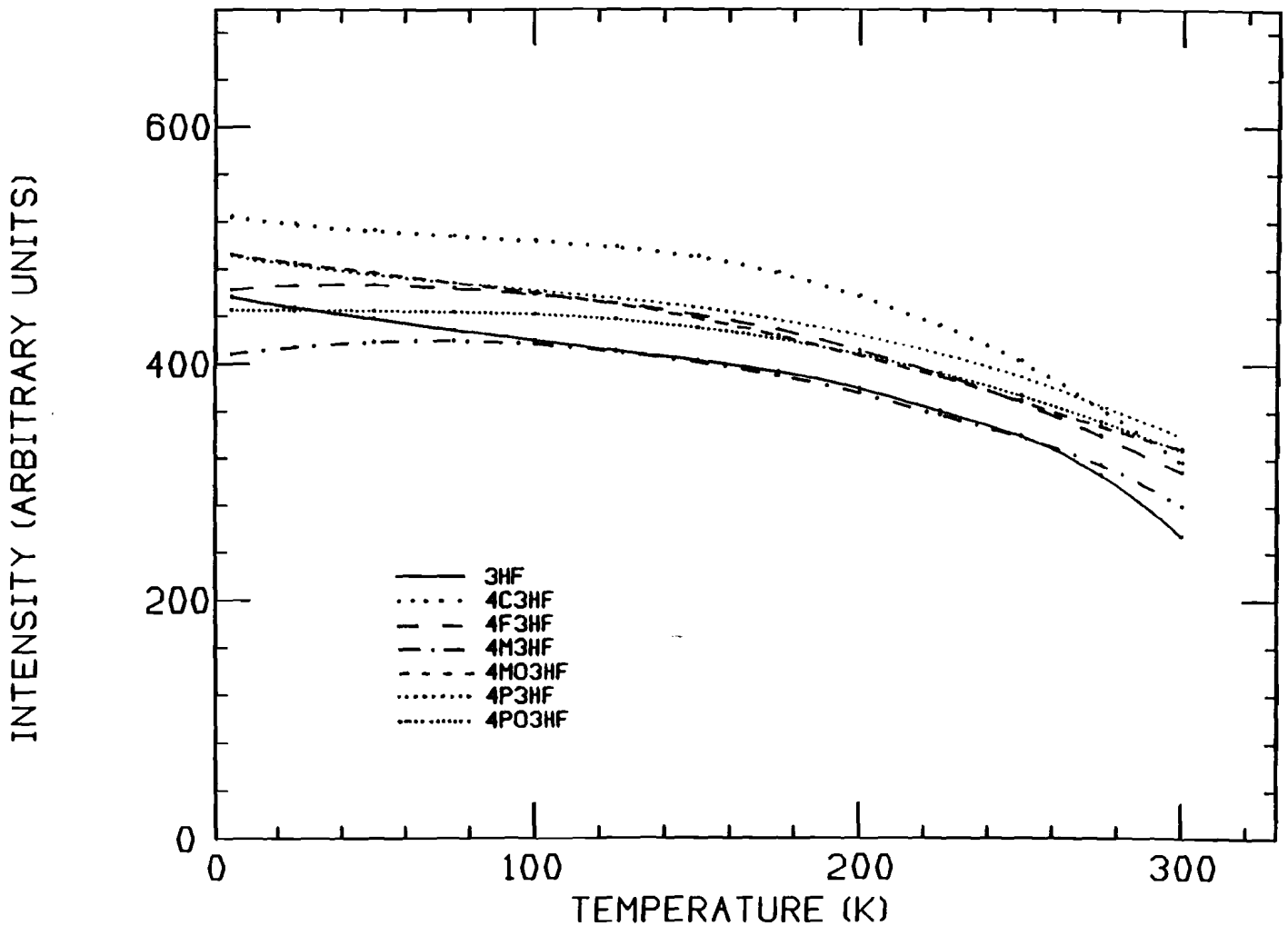

Figure 36. Changes in fluorescence yield of 3HF and its para-derivatives as a function of temperature.

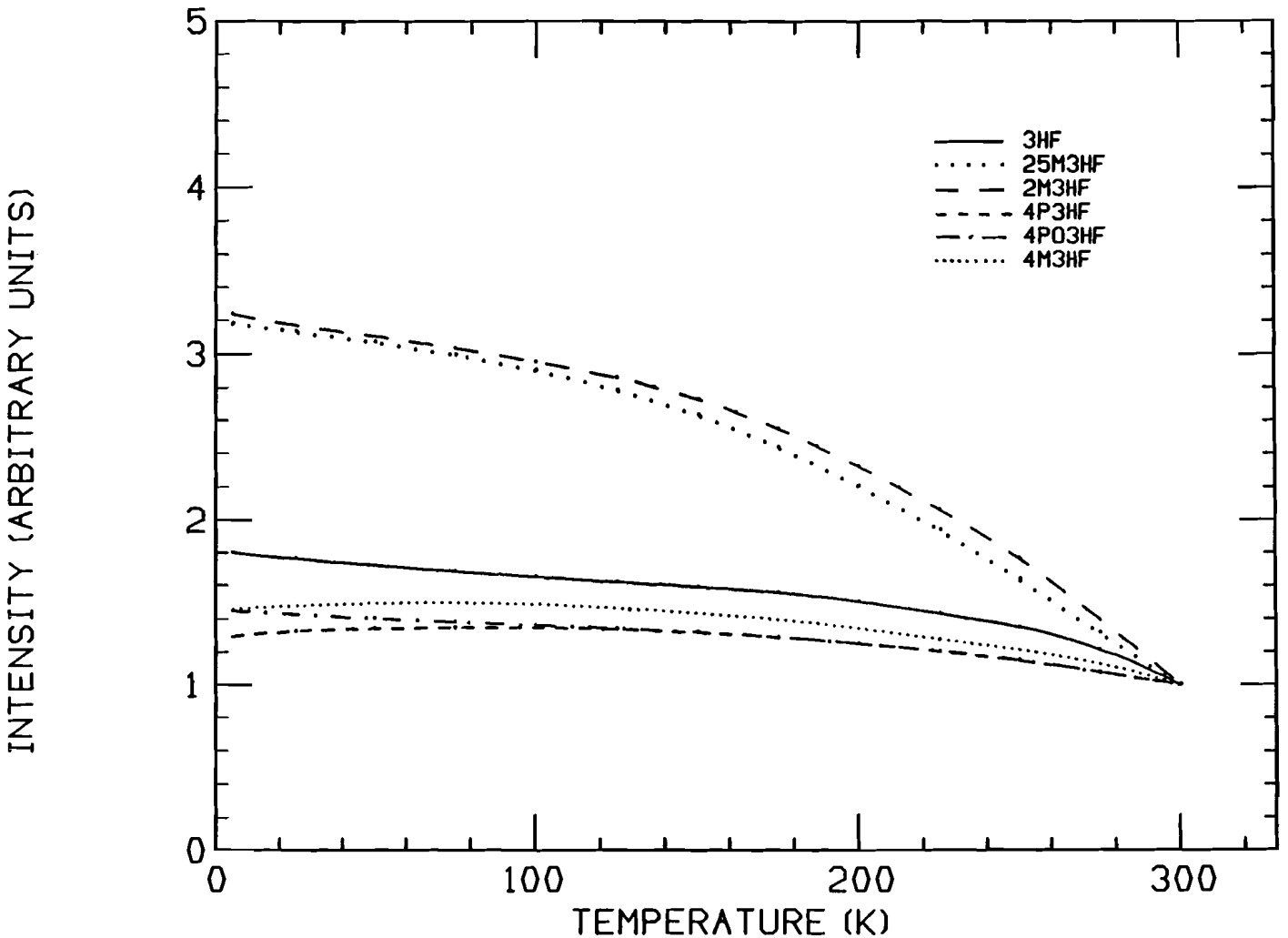

Figure 37. Changes in fluorescence yield as a function of temperature for 3HF and its derivatives relative to each yield at room temperature.

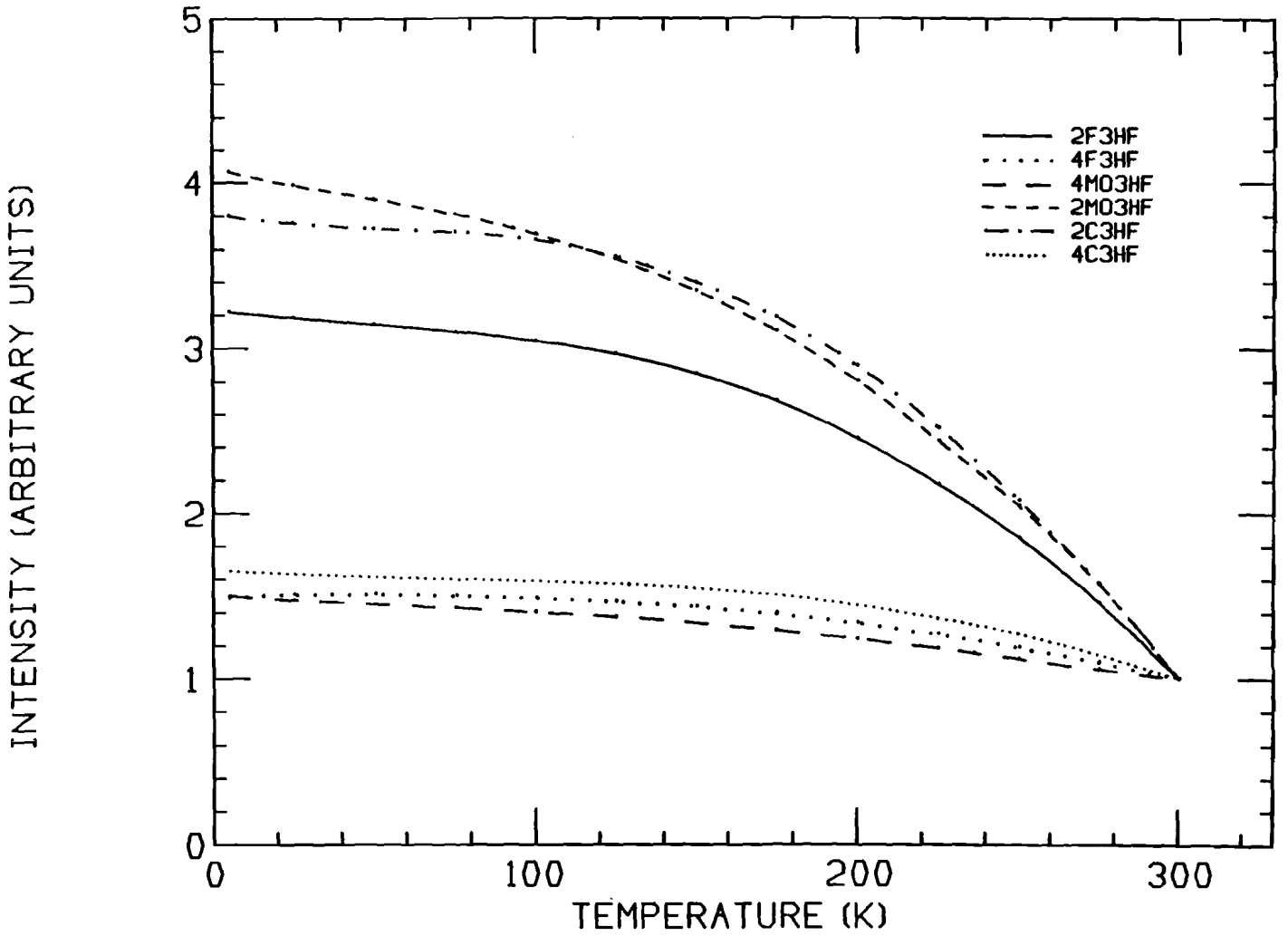

Figure 38. Comparison of changes in fluorescence yield as a function of temperature between ortho- and para-substituted 3HF derivatives relative to each yield at room temperature.

previously that the phenyl torsion competes with fluorescence to deactivate the molecule. In addition, the ortho-substitution forces the phenyl ring to be out of plane, increasing the molecule deactivation through this mode instead of by fluorescence.

Figure 36 presents the fluorescence pattern for the para-substituted relative to 3HF. At room temperature, the para-substituted derivatives have larger quantum yields than 3HF. As reported earlier, 4P3HF exhibits the largest quantum yield. As the temperature decreases, the quantum yield increases moderately. In other words, the fluorescence curves generated as a function of temperature have a small slope compared to those gathered for the ortho-substituted derivatives. In these compounds, the substitution on the ring does not affect its orientation with the rest of the molecule. Therefore, the phenyl torsion is not a major deactivating force as it is in the ortho-substituted compounds.

In Figures 37 and 38, the fluorescence areas have been normalized to one for each compound relative to its value at room temperature. The para-substituted derivatives show a small increase in fluorescence as a function of temperature. In contrast, the ortho-substituted compounds are strongly affected by the temperature, and their quantum yield increased with decreased temperature. These changes in relative quantum yield as a function of temperature indicate an upper limit for the absolute quantum yield of each compound. The absolute quantum yield of 3HF at room temperature cannot be higher than 38-40% to keep within experimental error the data acquired at low temperature. A higher quantum yield value at 25 °C for 3HF would imply quantum yields larger than unity for some of the derivatives at 5 K.

E. Absolute Quantum Yield Measurements for 3HF

The derivatives of both 3HF and HBT groups have been prepared in order to study whether the quantum yield of the unsubstituted compound could be improved. In each group, the fluorescence distribution area was calculated and used to compare the quantum yield relative to the fluorescence area of the parent compound, 3HF and HBT. Relative quantum yields were used because no data were available on the absolute quantum yield in polystyrene of either 3HF or HBT. Moreover, the absolute quantum yields of other fluors in polystyrene (to be used as a standard) were not available either. This lack of information prompted the absolute quantum yield determination of 3HF. 3HF was chosen over HBT because it presented a higher relative quantum yield.

Two sets of measurements were performed using similar methodology but different detection devices: (a) using a silicon photodiode, or (b) using a photomultiplier tube (PMT) modified to operate as a photodiode.

A high concentration (approximately 10^{-4} M) finely polished 3HF sample (0.6 cm cube) was utilized for these determinations. The excitation light was brought to the detector surface by means of a quartz fiber. The excitation wavelength was 352 nm. First, the intensity of the excitation light was measured. Then, the 3HF sample was placed on the detector surface, and the intensity of the emitted light was recorded. The data gathered were corrected for different systematic errors: (a) detector-light-capture efficiency due to the geometry of the sample, (b) quantum yield efficiency of the photodiode or the PMT at the two

wavelengths detected: 352 nm for the excitation light, and 530 nm for the 3HF emission, and (c) amount of excitation light which was not absorbed by the 3HF sample.

The 3HF absolute quantum yield was determined to be approximately 31% ± 5%. The absolute quantum yield for the remaining derivatives was based upon the value estimated for 3HF. The relative and absolute quantum yields of the compounds studied are listed in Table 7.

HBT and its derivatives exhibit lower quantum yields than 3HF and its derivatives. Among the HBT derivatives, 3CHBT, 5CHBT, and 5PHBT present the largest quantum yields. Among the 3HF derivatives, the para-substituted derivatives have larger quantum yields than the ortho-substituted derivatives. 4P3HF has the largest quantum yield.

F. Radiation Damage Studies on HBT- and 3HF-Doped Scintillators

All the HBT and 3HF derivatives have been tested for their radiation hardness because no matter how high their quantum yield is, if they are not resistant to radiation they will not be suitable for scintillation detection applications in high energy physics.

Samples doped with 1% fluorescent compound in polystyrene were prepared. Such is the standard concentration to ensure good energy transfer between the excited polymer and the fluor, even though the optimum concentration may be lower. These samples were placed in an aluminum can and irradiated under nitrogen at 1 and 10 Mrad by gamma/electron radiation. The irradiation results for HBT, 3HF and their derivatives will be presented in two separate sections to better observe

Table 7. Absolute quantum yield values for HBT and 3HF derivatives in polystyrene.

Compound	Relative[a] Quantum Yield	Absolute[b] Quantum Yield (%)
1. HBT Derivatives		
3FHBT	0.9	11
5MHBT	0.9	11
HBT	1.0	12
4MHBT	1.0	12
3PHBT	1.2	15
5PHBT	1.5	19
3CHBT	1.6	20
5CHBT	1.6	20
2. 3HF Derivatives		
2MO3HF	1.7	21
2C3HF	1.8	22
2F3HF	1.8	22
25M3HF	1.9	24
2M3HF	1.9	24
3HF	2.5	31
4C3HF	2.7	34
4F3HF	2.8	35
4M3HF	2.9	36
4MO3HF	3.0	37
4MS3HF	3.0	37
4PO3HF	3.2	40
4P3HF	3.5	43

[a]Quantum yields are relative to the quantum yield of HBT.

[b]These values are based on the estimated absolute quantum yield of 3HF in polystyrene: 31% ± 5%.

their similarities and differences.

1. Irradiation Results for HBT

HBT and the following derivatives were irradiated: 3CHBT, 3PHBT, 4MHBT, 5MHBT, and 5PHBT. Absorption and fluorescence measurements were recorded before, immediately after, and two weeks after irradiation. Figure 39 shows the radiation-induced changes in the HBT absorption. Before irradiation, 1% HBT in polystyrene shows an absorption band with cutoff point at 430 nm. Immediately after irradiation, the absorption area has considerably increased due to the transient absorption from the excited species remaining in the polymer right after irradiation. The absorption band at 530 nm can be seen as in the undoped polymer. After the measurement, the HBT sample is left either exposed to air or placed back into the aluminum can which is then pressurized with oxygen to speed up the annealing process in the polymer. Once the large absorption from the polymer had disappeared, a smaller permanent absorption, such as a longer absorption tail, was expected. After the polymer relaxation, absorbance measurements showed, instead of just a longer tail, a new and very distinctive second band. Fluorescence measurements of this sample using a 313 nm excitation wavelength light, which excites the fluor and not the polymer, showed the typical HBT fluorescence curve. There were no changes in either the emission wavelength maximum or its fluorescence distribution. However, if a longer excitation wavelength light, such as 436 nm, was used, another fluorescence spectrum was recorded. This new spectrum had a fluor-

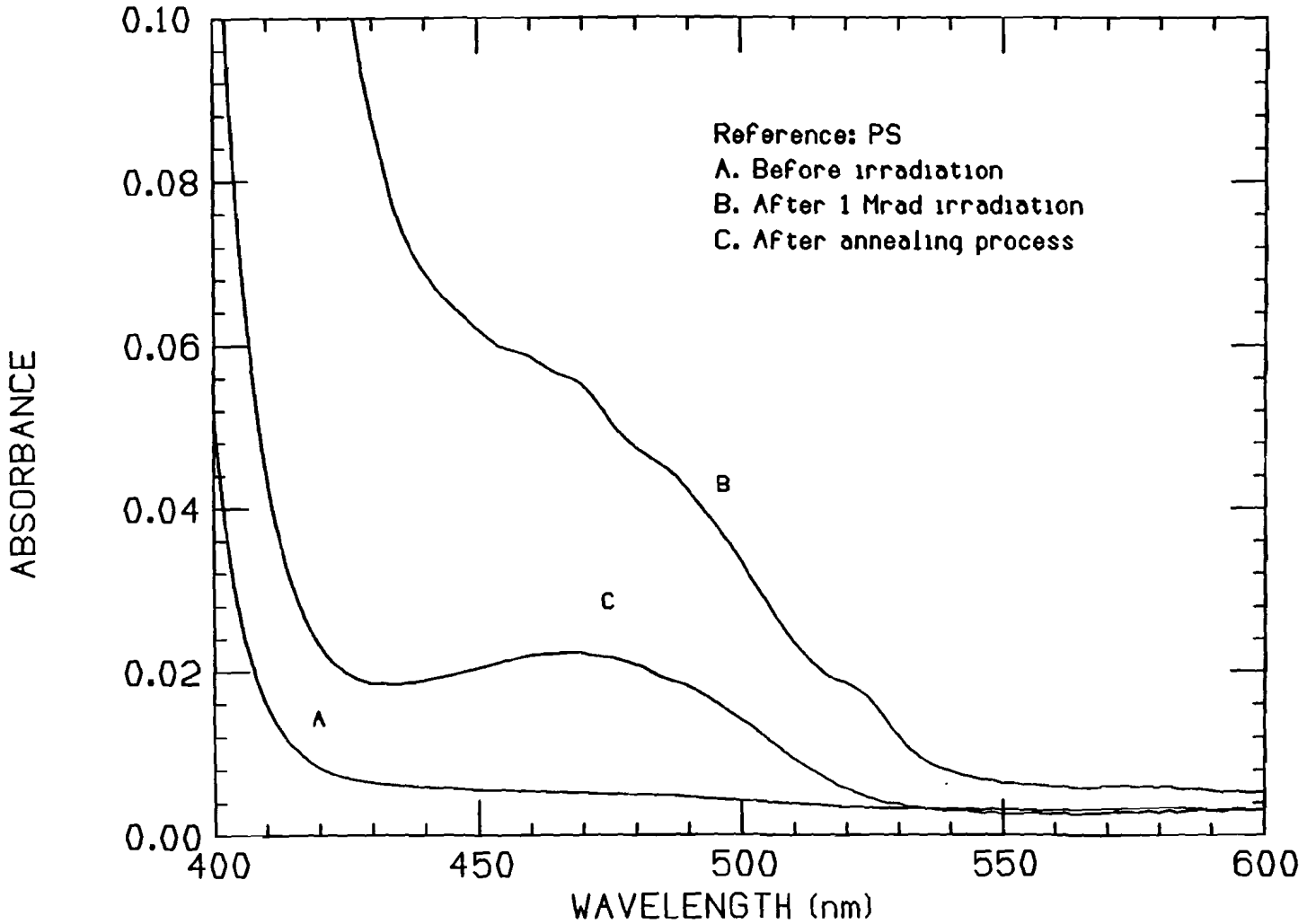

Figure 39. Absorption spectra of irradiated HBT in PS.

escence distribution just like the previous one, but its emission maximum was slightly shifted towards shorter wavelengths (Figure 40). This fluorescence had not been observed earlier. Non-irradiated HBT does not fluoresce when it is excited with a 436 nm light. Therefore, this new fluorescence was due to the formation of a species absorbing at longer wavelengths than HBT. Since the Stokes shift between the absorption and emission spectra of this new species was small, it did not involve excited-state proton transfer. The nature of this new species had to be identified. The irradiated sample contained only HBT and polystyrene. However, this species had not been observed in the undoped PS irradiation studies. Therefore, it was considered to derive from HBT. All the HBT derivatives presented the same characteristics after irradiation. Appendix B contains absorption and fluorescence spectra for the irradiated HBT derivatives.

As mentioned in other sections, HBT can form various conformational isomers such as the keto forms. Williams and Heller (47) had even postulated that the trans-keto form would be more stable than the cis-keto form, which is in a more hindered environment. However, they were not able to observe its formation. Later on, Elsaesser and Kaiser (51) observed the formation of the cis-keto form after proton transfer by picosecond infrared spectroscopy. The trans-keto form was not detected. On the other hand, this new HBT species in the polystyrene sample has only been noted after irradiation. Therefore, it could be postulated that if enough energy is given to the system, the trans-keto form will also be generated in the excited state S_0'' (Figure 41). After relaxation the trans-keto form remains locked in due to the existence of a large energy

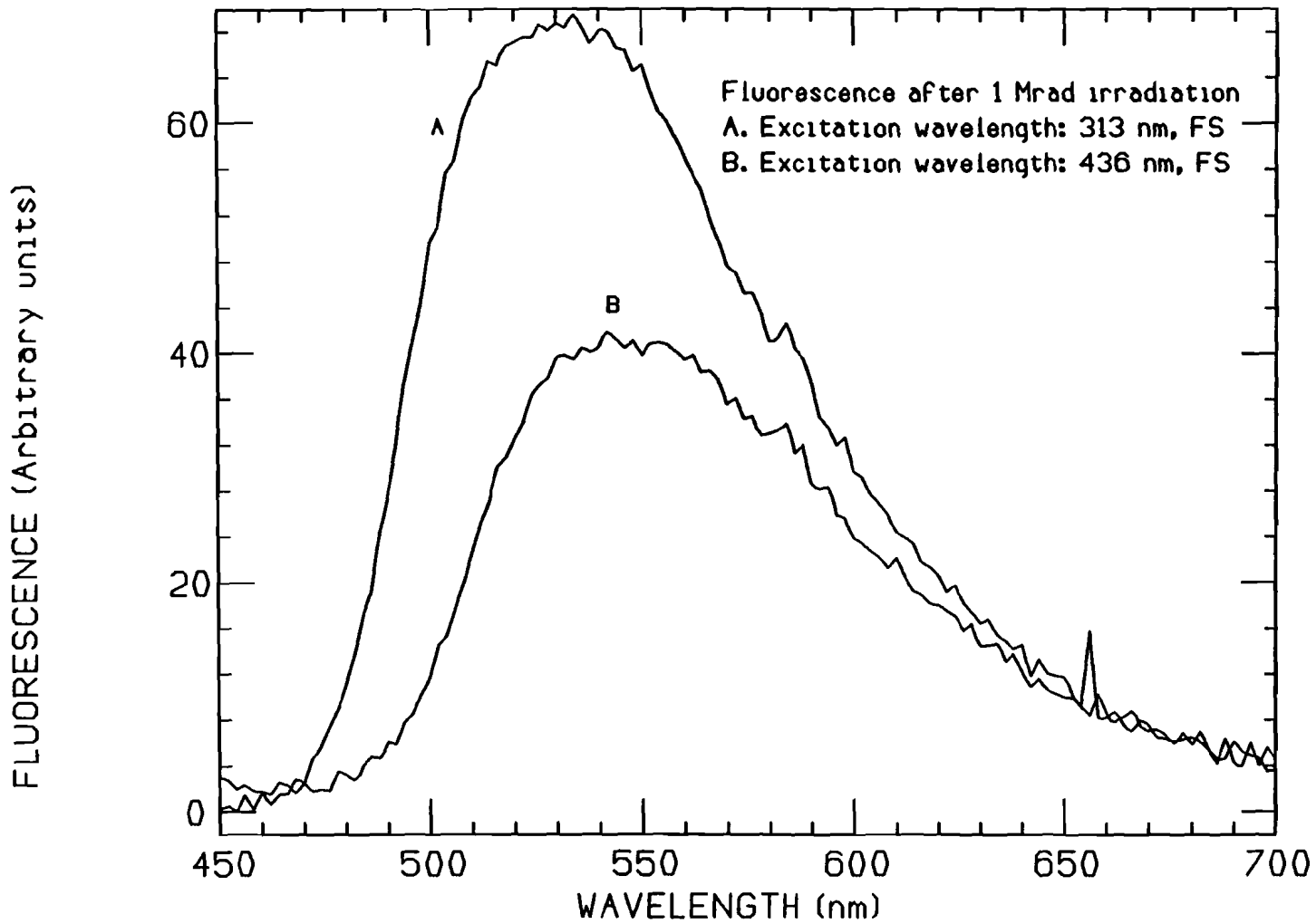

Figure 40. HBT fluorescence immediately after irradiation.

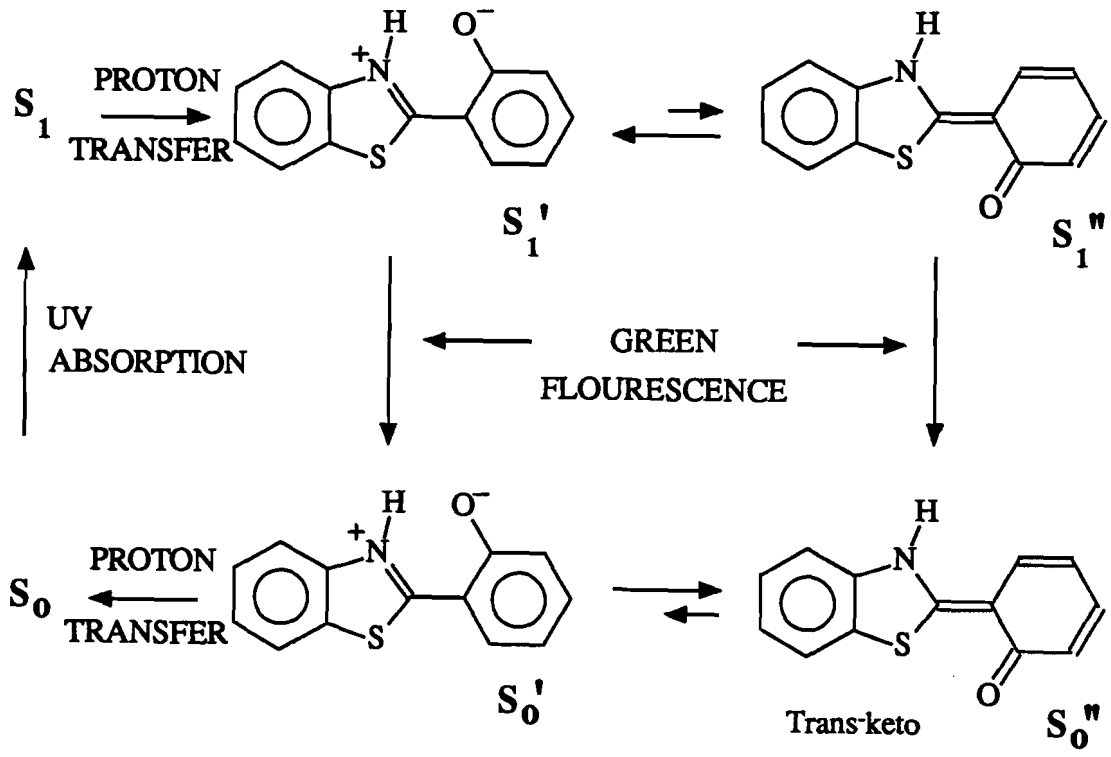

Figure 41. Formation of the trans-keto HBT isomer.

barrier from S_0'' to S_0'. Another explanation could be the formation of the HBT anion which also fluoresces with a small Stokes shift because of the missing proton.

To gain some insight into the nature of this absorption, several tests were carried out in collaboration with Professor Paul Barbara at the University of Minnesota (7). The effort focussed on bleaching this new absorption band from an irradiated HBT sample. Two different processes were considered:

1. A photobleaching process by irradiation of a sample at 488 nm with an Ar-ion laser for 9 hours, and
2. A thermal bleaching process by heating a sample overnight in an oven at 120-130 °C.

In both cases the second absorption disappeared and no fluorescence was observed using a 436 nm excitation wavelength. These two experiments indicated the presence of an energy barrier. Therefore, the hypothesis of a trans-keto isomer formation under irradiation, which was locked in that conformation because of a large energy barrier, was possible. When more energy was given to the system, the trans-keto form would return to the cis ionic form (S_0' in Figure 41) which would transfer the proton back to the oxygen to yield S_0, the stable HBT form in the ground state.

In collaboration with Professor Steven Bachrach at Northern Illinois University, various semi-empirical molecular orbital calculations were performed to estimate the magnitude of this energy barrier. These calculations were performed using the computer code MOPAC written by J. J. P. Stewart (89). The input data file contains the Z-matrix which is

created using the bond lengths, bond angles, and dihedral angles of the atoms in the studied molecular geometry. This program can use different semi-empirical Hamiltonians to perform the calculation: MNDO, MINDO3, or AM1. These semi-empirical Hamiltonians are used in the electronic part of the calculation to obtain molecular orbitals, the heat of formation, and the energy gradient with respect to molecular geometry. AM1 is the set that best represents hydrogen bonding but contains no parameters for sulfur, so it cannot be used for HBT calculations. MINDO3 failed to represent the existing hydrogen bond in HBT. Using MNDO, an energy barrier of approximately 20 kcal/mol was calculated for the rotation from the cis to the trans form (from S_0' to S_0'' in Figure 41). Figure 42 represents the relative energies for the different isomers involved in the HBT excitation and deactivation. This stability trend was found using MNDO parameters, but the energy separation between the excited and the ground states was very large, which could be caused if the parameter set used was not properly representing the system. To verify the energy barrier and the relative stability found, a parallel analysis was carried on 2-(2'-hydroxyphenyl)benzoxazole (HBO). The analogy between HBO and HBT is sufficient to expect similar results. Now, without the presence of the S atom, the AM1 parameter set could be used, which would afford more accurate results. For HBO, an energy barrier for the rotation from the cis-ionic/keto form to the trans-ionic/ keto form of approximately 30 kcal/mol was calculated, and the relative energy for the different isomers exhibited the same trend as seen for HBT. A 20-30 kcal/mol energy barrier for the rotation of the single bond in the ionic form is larger than expected a priori. This supports, together with the bleaching experi-

ments, the formation of the trans-keto isomer which remains locked by this large energy barrier, until enough energy is available to surpass it.

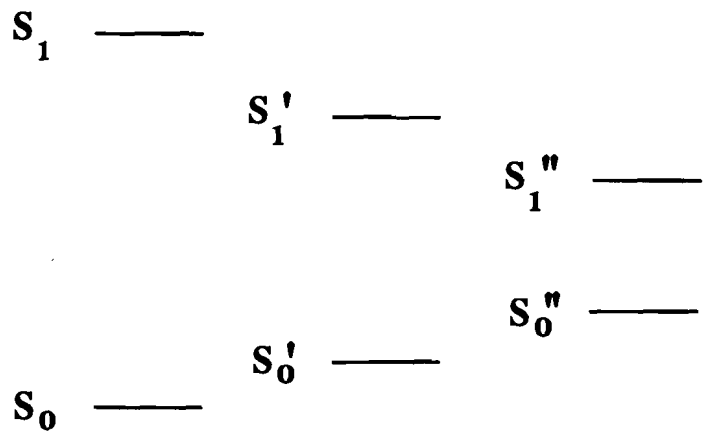

Figure 42. Relative energy diagram for HBT isomers.

2. Irradiation Results for 3HF

Polystyrene samples doped with 1% 3HF, or its derivatives - 2C3HF, 4C3HF, 2M3HF, 4M3HF, 25M3HF - were irradiated at 10 Mrad by a gamma/electron radiation. Only a fraction of the 3HF derivatives have been irradiated. Figure 43 shows the radiation-induced changes in absorption for 1% 3HF in PS. Before irradiation, 3HF absorbed at 350 nm with an absorption cutoff at 450 nm. Immediately after irradiation, a large absorption was observed due to the transient excited species from the polymer. The samples were returned to the aluminum cans and pressurized with oxygen in order to increase the polystyrene annealing

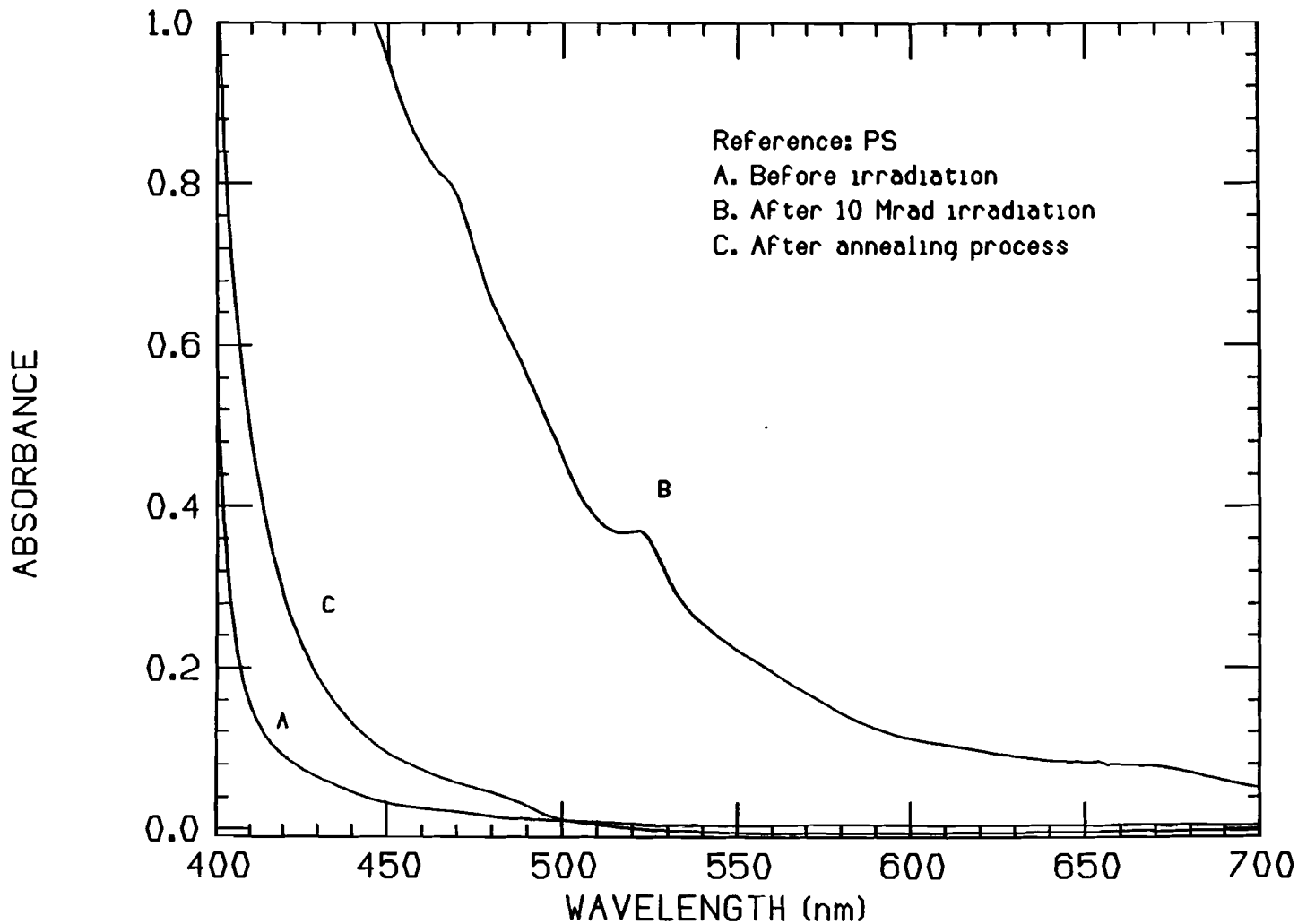

Figure 43. Absorption spectra of irradiated 3HF in PS.

rate. After the oxygen annealing process, the absorption spectrum showed a small absorbance increase in the 400-500 nm region, similar to that observed for undoped polystyrene and other commercial scintillator samples. No effect similar to that noted for HBT and its derivatives is detected when 3HF and the mentioned 3HF derivatives are irradiated. On the other hand, 3HF cannot form any other isomers as HBT does. The resonance form that can be written for 3HF after proton transfer is the pyrillium cation (mentioned in Figure 23) which does not lead to the formation of other conformational isomers.

Fluorescence measurements were recorded before and after irradiation. These spectra show no appreciable changes other than differences caused by the fluctuation in the intensity of the excitation light source. Absorbance and fluorescence measurements indicate that 3HF is not damaged by radiation at least to the extent detectable by our instruments.

Another set of measurements can be carried out using ^{207}Bi, which emits a β-particle. When this electron strikes the scintillator sample, the fluor emits light which is collected and transformed into an electric signal by means of a photomultiplier tube. Under the same conditions the pulse height of this signal can be used to compare the light output of different scintillators. This technique was utilized to support the absorption and fluorescence data, which indicated that no actual damage was caused in the 3HF molecule. These new measurements pointed out that a considerable light loss occurred immediately after irradiation. However, after the annealing period in oxygen, there was a large light output recovery, up to 95% of its initial value. These results agree with the previous

absorption and fluorescence measurements in that 3HF does not undergo substantial damage under radiation.

These findings contradict those by other authors who report that 3HF decomposition under irradiation is up to 25% (90) or 50% (91). However, in both cases the 3HF is irradiated in solution (e.g., in toluene). The information gathered in irradiation of plastic samples and solutions cannot always be compared. Fluors that were known to be radiation hard in liquid scintillators have proved to be seriously damaged in plastic samples, and vice versa (92).

From the data collected, the 3HF derivatives behave under radiation in the same manner as the parent compound. Appendix B has the absorption spectra for the irradiated 3HF derivatives. These spectra show the formation of a long absorption tail or shoulder after the annealing process for the irradiated derivatives. Impurities in the dopant before polymerization can generate this absorption under irradiation. This effect has been observed for 3HF samples that decomposed slightly during the polymerization cycle. However, when the 3HF/PS sample was pure, the absorption after the annealing process is similar to the original. A similar behavior is expected of 3HF derivatives.

III. CONCLUSIONS

The design of new fluorescent materials for scintillation detection in high energy physics is required to meet the demands set by the new generation of particle accelerators. Plastic scintillation detectors exhibit two characteristics that indicate their suitability for the future experiments: short response time and versatility. A key issue in the development of plastic scintillation detectors to comply with the new requirements is their radiation hardness, since radiation doses of 1 Mrad/year or higher, depending upon the detector location are expected.

Most commercially available plastic scintillators are based on a polymer matrix doped with two fluorescing compounds, a primary and a wavelength shifter that emits light in the blue region of the spectrum. However, the light output of these scintillators seems to be significantly affected by radiation-induced damage in the polymer, such as the formation of color centers. Therefore, a new kind of scintillator emitting at longer wavelengths would be preferred. Another type of plastic scintillator has recently been developed: the intrinsic scintillator. These scintillators consist of a polymeric base containing one single dopant which exhibits a large spectral separation between absorption and emission spectrum. Fluorescent compounds having an excited state intramolecular proton transfer have been suggested as intrinsic scintillators since their main characteristic is the large Stokes shift between absorption and fluorescence.

Polystyrene-based scintillators doped with 2-(2'-hydroxyphenyl)benzothiazole (HBT) or 3-hydroxyflavone (3HF) or their respective derivatives have been studied. The polymer, polystyrene, was tested for its radiation hardness. The dopants were investigated to learn about their absorption and fluorescence spectra, their quantum yield and also radiation resistance.

Radiation damage tests on the polymer (in inert atmosphere) indicate the formation of a large transient absorption immediately after irradiation. At this stage, the presence of a novel fluorescence in the green region of the visible spectrum is detected. The nature of this green fluorescence (at 550 nm) is credited to the formation of an excited species absorbing at 530 nm. By comparison to published data on a different type of polystyrene irradiation, this absorption is probably caused by the generation of singlet excimers of polystyrene. This fluorescence decays as the irradiated polystyrene sample anneals. In other words, as the excited species created in the polymer under irradiation deactivate, the green fluorescence disappears. This annealing process is accelerated by oxygen. Oxygen diffuses into the sample and quenches the excited species. This annealing process occurs at a much slower rate if the samples are kept under nitrogen or argon atmosphere after irradiation. Two weeks after irradiation the absorption area has considerably decreased. However, the irradiated sample presents an absorption area larger than that observed before irradiation. This absorption is not reduced in size with longer exposure to oxygen. Permanent damage to the polymer in the 350-400 nm region occurs during irradiation.

The nature of the radiation-induced permanent damage in the polymer has also been studied relative to the average molecular weight. No change in the absorption area due to different average molecular weight was found.

2-(2'-Hydroxyphenyl)benzothiazole (HBT) was studied because of the large Stokes shift presented (absorption at 340 nm, emission at 525 nm). HBT derivatives with substituents in the 2-phenyl ring were prepared to improve the fluorescence quantum yield. The relative quantum yield increased with substitution on the ring by chlorine atoms in position ortho- or para- to the hydroxyl group, or by a phenyl group in the para-position to the hydroxyl group. The remaining derivatives showed no change in relative quantum yield.

Radiation damage studies on HBT and its derivatives show the formation of an isomer under irradiation. The absorption of this isomer is at long wavelength (360-450 nm) relative to the absorption of the original compound, and its fluorescence is shifted towards the blue by 20 nm. This isomer is suggested to be the trans-keto form S_0'' (Figure 41) which has to overcome a large energy barrier to afford the cis-keto isomer S_0' (Figure 41), which by proton transfer gives the most stable form, the cis-enol S_0 (Figure 41). The magnitude of the energy barrier to this rotation is estimated, by semi-empirical calculations, to be approximately 20-30 kcal/mol.

HBT and its derivatives are not eligible for scintillation detection uses because they present both low quantum yields and the formation under irradiation of the corresponding trans-keto form. The formation of this conformational isomer extends the absorption threshold to longer

wavelengths, reducing considerably the Stokes shift exhibited originally by the compound.

3-Hydroxyflavone (3HF) was studied because it also presents a large Stokes shift (absorption at 350 nm, emission at 530 nm) and has a higher quantum yield than HBT. 3HF has been noted to slowly oxidize at room temperature. The 3HF-doped scintillator samples are very sensitive to these oxidation-induced impurities. Various 3HF derivatives were prepared with the objective of improving the compound stability and quantum yield. The derivatives tested were either ortho- or para-substituted.

The compound stability has increased with substitution in the phenyl ring, except for the para-chloro derivative (4C3HF). A disadvantage of these derivatives is that the absorption threshold has shifted towards longer wavelengths, increasing the possibility of an overlap between absorption and fluorescence. The one exception is 2M3HF which is white, indicating its blue-shifted absorption.

The quantum yield at room temperature for all the para-substituted compounds is larger than that of the unsubstituted compound, 3HF, with 4P3HF presenting the highest value. However, the quantum yield relative to 3HF for all the ortho-substituted derivatives is smaller, with 2MO3HF having the poorest yield. As the temperature decreases, the relative quantum yield in both sets of compounds increases reaching their maximum at liquid helium temperature. At 5K, the relative quantum yield for the ortho-substituted derivatives increases by a bigger factor than the para-substituted derivatives. These studies at low temperature set an upper limit for the absolute quantum yield of the

unsubstituted compound, 3HF, at room temperature. The quantum yield for 3HF cannot be higher than 38%. The experimental absolute quantum yield of 3HF has been measured to be 31% ± 5%. The changes in the quantum yield as a function of temperature between the ortho- and the para-substituted 3HF derivatives are due to the phenyl torsion, which has been recognized as a major deactivation mode. The phenyl torsion plays a more important role in the ortho-compounds due to the steric hindrance caused by the substituent.

The radiation damage tests performed on 3HF and a few of its derivatives indicated that they were resistant to radiation within the accuracy given by the instrumentation used.

3HF and its derivatives are suitable for scintillation detection purposes. However, special attention has to be directed towards their tendency to oxidize. Among the derivatives prepared, 2M3HF and 4P3HF present the most advantages, even though they also have some drawbacks. 2M3HF exhibits the largest Stokes shift, however, its quantum yield is low (24% ± 5%). 4P3HF shows the largest quantum yield (43% ± 5%). Nevertheless, it has a long absorption tail which could cause a large self-absorption effect in long fibers.

The quantum yield of HBT and 3HF has been modified by substitution in the phenyl ring. The relationship between structure and property (quantum yield) has been proved. The results presented verify the possibility of designing a compound with high quantum yield. However, these compounds must also be resistant to radiation. The radiation damage studies performed indicate the formation of isomers as a reactive pathway under irradiation. This formation must be avoided in the

development of new fluorescent compounds. Currently, 3HF and some of its derivatives are the best candidates for scintillation detectors emitting in the green region of the visible spectrum. Polystyrene samples doped with 3HF performed better under irradiation than the standard commercially available scintillator emitting in the blue spectral region.

IV. EXPERIMENTAL SECTION

A. General Considerations

1. Instrumentation

All melting points were determined on a Fisher-Johns melting point apparatus and are uncorrected. UV-Visible and fluorescence spectra were recorded on a HP8451A Diode Array Spectrophotometer. The ^{1}H NMR and ^{13}C NMR (200 MHz) spectra were determined on a Bruker WP200SY spectrometer. CHN analyses were performed on a Perkin-Elmer 240 Analyzer by Paulanne Ryder.

2. Fluorescence Measurements

Fluorescence measurements were performed using the diode array spectrophotometer as a fluorimeter, which was possible using a computer program (93) developed at Fermilab by A. D. Bross to collect and correct the raw data. These measurements could be carried out in two different ways:

1. Using the spectrophotometer light source with a broadband filter (Melles Griot SB-300) to select the excitation wavelength at approximately 300 nm, or
2. Bringing the light of an external Hg lamp (Oriel 66002) into the instrument by means of a quartz fiber, and selecting the excitation

wavelength at 254 nm, 313 nm, or 352 nm with the use of bandpass filters, Oriel models 56500, 56510, or 52936, respectively.

In turn, two different types of measurements were possible when the external light source was utilized:

1. Front surface (FS) excitation measurement, in which the quartz fiber was positioned at an angle 45° with respect to the plane of the sample surface that was closest to the detector (front surface).
2. Back surface (BS) excitation measurements, in which the quartz fiber was exciting the back surface (sample surface farthest away from the detector) at an angle of 45° with respect to the surface plane.

Studies of fluorescence at low temperatures were performed using an Oxford Instruments CF1204 Cryostat placed in the spectrophotometer sample cavity.

3. Polymerizations

Styrene purchased from Aldrich Chemical Co. was purified using a tert-butylcatechol removal column also supplied by Aldrich. Styrene was distilled under vacuum conditions using a rotary-evaporator and could be stored in a freezer between one week and two months.

Styrene doped with a given amount of the organic flour was polymerized in 250 by 25 mm silylated test tubes in a silicone bath with the following temperature profile: 2 h at 90 °C, 24 h at 110 °C, 48 h at 125 °C, 12 h at 140 °C, and ramp down 10 °C/h back to 90 °C. Before the test tubes were placed in the bath, they underwent three freeze-thaw-pump cycles to degas the solutions. When the bath temperature

was raised to 125 °C, the solutions were backfilled with nitrogen to prevent them from boiling. At the end of the polymerization cycle, the test tubes were quenched in liquid nitrogen to accelerate the release of the polymer and avoid the formation of vacuum bubbles. Afterwards each sample was cut into the shape of a cuvette of dimensions 4 x 1.24 x 1.24 cm and polished using diamond paste of 15, 6, and 1 μm particle size, and finally 0.05 μm particle size alumina to achieve a glossy finish.

Silylation procedure. The test tubes were first washed with both concentrated nitric acid and sulfuric acid, rinsed with distilled water, and dried using compressed air. Then they were filled with a solution of 30% dichlorodimethylsilane/chloroform and soaked for four to five hours. After this period, they were rinsed in turn with chloroform, methanol, and distilled water, and were finally dried.

4. Radiation Damage Studies

Irradiation of doped and undoped polystyrene samples was done at the Department of Energy's Idaho National Engineering Laboratory (INEL) in Idaho Falls. The samples were irradiated with electrons and γ-rays at 1 and 10 Mrad. The dose received was calculated using a thermoluminiscent dosimeter (TLD-700). The samples were irradiated in sealed aluminum cans which had been purged with nitrogen. Absorption and fluorescence spectra were recorded for each sample before they were exposed, immediately after they were returned from Idaho, and two weeks later. Between the last two sets of measurements, the samples

were returned to the cans which were then backfilled with oxygen to accelerate the annealing process.

5. Quantum Yield Determinations

A high concentration (approximately 10^{-4} M), finely polished 3HF cubic sample (0.6 cm) was utilized for the determinations. Two different sets of measurements were performed using different detectors:

1. A silicon photodiode (UDT 247).
2. A photomultiplier tube (PMT) (Hamamatsu R669) used as a photodiode.

The excitation light was brought to the detector surface by means of a quartz fiber. The excitation wavelength (352 nm) was selected using a bandpass filter (Oriel 52936). The intensity of the light detected was measured with a pico-ammeter (Keithley 480).

First, the intensity directly from the light source was determined. Then, the 3HF sample was placed on the detector surface and the quartz fiber was positioned on top of the sample. The intensity of the emitted light was recorded. Several measurements were taken at different excitation light intensities. The data acquired from both methods was corrected for the following systematic effects:

1. For the detector light capture efficiency due to the geometry of the sample.
2. For the quantum yield efficiency of the photodiode or the PMT at the two wavelengths detected: 352 nm for the excitation light, and 530 nm for the emitted light.

3. For the amount of excitation light which was not absorbed by the 3HF sample. Five percent of the excitation light was not absorbed.

6. Molecular Orbital Calculations

The energy barrier for the rotation between the cis and trans ionic forms of HBT in the ground state was estimated using a semi-empirical molecular orbital program MOPAC (89). The semi-empirical Hamiltonian MNDO was used in these calculations. A parallel analysis was carried out for 2-(2'-hydroxyphenyl)benzoxazole (HBO), using AM1 as the semi-empirical Hamiltonian for the calculations. All structures were fully optimized using gradient techniques. Calculations were performed on a MicroVAX-II at Fermi National Accelerator Laboratory.

B. Starting Materials

The 3-hydroxyflavone derivatives were prepared from 2-hydroxy-acetophenone and the corresponding benzaldehyde derivatives, all of which were available from Aldrich Chemical Co. For the synthesis of the derivatives of 2-(2'-hydroxyphenyl)benzothiazole, the starting materials were o-aminothiophenol and the corresponding salicylic acid derivative, which were purchased from Aldrich, except 5-phenylsalicylic acid which was prepared at Georgia Institute of Technology by Suzanne Fitzwater, and 3-fluorosalicylic acid, whose synthesis is described below.

1. Preparation of 3-Fluorosalicylic Acid

3-Fluorosalicylic acid was prepared by a modification of the procedures described by Ferguson et al. (94) and Cameron et al. (95). Lithium o-fluorophenoxide was obtained by the addition of an equimolar amount of Li (0.62 g, 0.089 mol) and o-fluorophenol (10 g, 0.089 mol) to dry methanol (25 mL), with stirring. Small fractions of each were added alternatively, keeping the methanol solution below its boiling point. The reaction mixture was stirred for 2 h, and refluxed for 15 min. After cooling down to ca. 25 °C, the solvent was removed and the residue, a thick oil, was kept under vacuum (0.01 mm) overnight, to yield a white solid that was ground to a powder and used in the next step without further purification.

The lithium salt was placed in a pressure vessel and backfilled with carbon dioxide (600 psi) at 150 °C for 7 h. The thick crust at the bottom of the flask was dissolved in hot water. Unreacted o-fluorophenol was removed by extraction with ether (2 x 100 mL). The aqueous solution was acidified with 2M HCl, whereupon a precipitate formed, and was extracted with ether (3 x 100 mL). The combined ether extracts were washed with distilled water, and dried over magnesium sulfate. Evaporation of the solvent left an off-white solid. Recrystallization from toluene yielded 13 g (20%) of 3-fluorosalicylic acid as a white solid (m.p. 147-148 °C, lit. [90] 145-147 °C).

^{1}H NMR (d_6-acetone, δ) 1H (d, J_H = 7.5 Hz) 7.7, 1H (dd, J_H = 7.5 Hz, JF = 10 Hz) 7.4, 1H (m) 6.95, 1H (s) 3.50.

C. Products: Fluorescent Compounds

Two different families of compounds were prepared: derivatives of 2-(2'-hydroxyphenyl)benzothiazole (HBT) and derivatives of 3-hydroxyflavone (3HF).

1. 2-(2'-Hydroxyphenyl)benzothiazole Derivatives

The parent compound 2-(2'-hydroxyphenyl)benzothiazole and two derivatives, 2-(2'-hydroxy-4'-methylphenyl)benzothiazole (4MHBT) and 2-(2'-hydroxy-5-methylphenyl)benzothiazole (5MHBT), were purchased from Frinton and further purified by sublimation (twice). The remaining derivatives were prepared in our laboratory using a modification of the procedure described by Williams and Heller (47) and Anthony et al. (49).

General Procedure for the preparation of HBT derivatives: Preparation of 2-(2'-hydroxy-3'-chlorophenyl)benzothiazole (3CHBT). 3-Chlorosalicylic acid (12 g, 0.07 mol) was added to dry toluene (180 mL) placed in a 500 mL three-neck flask provided with a reflux condenser, addition funnel, thermometer and magnetic stirrer. The solution was warmed to 40 °C and o-aminothiophenol (9.64 g, 0.077 mol) was added dropwise to the reaction mixture. After the addition was complete, the solution was heated at 100 °C for 6 to 8 hours, and then cooled to room temperature. The solution was neutralized by extracting several times with a 20% sodium carbonate solution (5 x 100 mL), washed with distilled water, and dried over magnesium sulfate. Evaporation of the solvent produced a yellowish solid (8.3 g, 45%). Crude benzothiazole

derivative was purified by flash column chromatography through silica gel (hexane/methylene chloride 1:1) and by sublimation, yielding pure 2-(2'-hydroxy-3'-chloro-phenyl)benzothiazole (m.p. 181-182 °C, lit. [49] 183-184 °C).

^{1}H NMR ($CDCl_3$, δ) 1H (s) 13.3, 1H (d, J_H = 8 Hz) 7.94, 1H (d, J_H = 8 Hz) 7.86, 4H (m) 7.6-7.4, 1H (t, J_H = 8 Hz) 6.86.

UV/VIS (Polystyrene, λ_{max} [ε]) 344 nm (15000 L mol^{-1} cm^{-1}).

Fluorescence (Polystyrene, λ_{em}) 540 nm.

Preparation of 2-(2'-hydroxy-3'-fluorophenyl)benzothiazole (3FHBT). Following the HBT General Procedure described above, 3-fluorosalicylic acid (6.24 g, 0.04 mol) was added to dry toluene (75 mL). The solution was warmed to 40 °C, and o-aminothiophenol (5.51 g, 0.044 mol) was added. Keeping the temperature below 45 °C, phosphorous trichloride (5.49 g, 0.04 mol) was added dropwise. After the solvent had been evaporated, the solid residue (4.02 g, 41%) was purified by flash column chromatography through silica gel (hexane/methylene chloride, 3:1) and by sublimation, to yield pure 2-(2'-hydroxy-3'-fluoro-phenyl)benzothiazole (m.p. 151-152 °C).

^{1}H NMR ($CDCl_3$, δ) 1H (s) 12.7, 1H (d, J_H = 8 Hz) 8.0, 1H (d, J_H = 8 Hz) 7.9, 3H (m) 7.6-7.4, 1H (dd, J_H = 8 Hz, J_F = 10 Hz) 7.17, 1H (dt, J_H = 8 Hz, J_F = 5 Hz), 6.84.

^{13}C NMR ($CDCl_3$, δ) 168.5, 154.4, 151.5, 149.5, 146.9, 132.5, 126.8, 125.8, 123.1, 122.3, 121.5, 118.7, 118.4.

UV/VIS (Polystyrene, λ_{max} (ε)) 340 nm (12000 mol^{-1} cm^{-1}).

Fluorescence (Polystyrene, λ_{em}) 540 nm.

C H N Analysis Found: C, 63.68; H, 3.15; N, 5.59. Calc. for $C_{13}H_8FNOS$: C, 63.66; H, 3.29; N, 5.71%.

Preparation of 2-(2'-hydroxy-3'-biphenyl)benzothiazole (3PHBT). As already described in the HBT General Procedure, 3-phenylsalicylic acid (12.84 g, 0.06 mol) was added to dry toluene (150 mL). The solution was warmed up to 40 °C and o-aminothiophenol (6.26 g, 0.066 mol) was added. Phosphorous trichloride (8.24 g, 0.06 mol) was added at a rate such that the reaction temperature would not exceed 45 °C. After the usual work-up, solvent evaporation yielded a pale yellow solid (10.0 g, 55%). The crude 2-(2'-hydroxy-3'-biphenyl)benzothiazole product was further purified by flash column chromatography through silica gel using hexane/methylene chloride (4:1) and by sublimation (m.p. 186-187 °C).

^{1}H NMR ($CDCl_3$, δ) 1H (s) 13.13, 2H (dd, J_H = 7.5 Hz) 7.90, 2H (m) 7.75-7.65, 7H (m) 7.55-7.3, 1H (t, J_H = 7.5 Hz) 7.01.

^{13}C NMR ($CDCl_3$, δ) 169.6, 155.2, 151.6, 137.8, 133.7, 132.6, 130.7, 129.4, 128.1, 127.7, 127.2, 126.6, 125.5, 122.0, 121.4, 119.4, 116.9.

UV/VIS (Polystyrene, λ_{max} [ε]) 350 nm (17000 L mol^{-1} cm^{-1}).

Fluorescence (Polystyrene, λ_{em}) 560 nm.

CHN Analysis Found: C, 75.06; H, 4.31; N, 4.54. Calc. for $C_{19}H_{13}NOS$: C, 75.22; H, 4.32; N, 4.64%.

Preparation of 2-(2'-hydroxy-5'-chlorophenyl)benzothiazole (5CHBT). As described in the HBT General Procedure, 5-chlorosalicylic acid (10.36 g, 0.06 mol) was dissolved in dry toluene (150 mL). The solution was warmed up to 40 °C before o-aminothiophenol (8.26 g, 0.066 mol) was

added. Keeping the reaction temperature below 45 °C, phosphorous trichloride (8.24 g, 0.06 mol) was added dropwise. After the reaction work-up and solvent evaporation, a yellow solid (7.65 g, 49%) was obtained. Further purification was performed by flash column chromatography through silica gel using hexane/methylene chloride (3:1) and by sublimation (m.p. 150-151 °C, lit. [49] 149-150 °C).

^{1}H NMR ($CDCL_3$, δ) 1H (s) 12.50, 1H (d, J_H = 8 Hz) 7.96, 1H (d, J_H = 8 Hz) 7.88, 1H (d, J_H = 2 Hz) 7.60, 2H (m) 7.55-7.35, 1H (dd, J_H = 10 Hz, J_H =2 Hz) 7.28, 1H (d, J_H = 10 Hz) 6.01.

UV/VIS (Polystyrene, λ_{max} [ε]) 350 nm (21741 L mol^{-1} cm^{-1}).

Fluorescence (Polystyrene, λ_{em}) 545 nm.

Preparation of 2-(4'-hydroxy-3'-biphenyl)benzothiazole (5PHBT). As outlined in the HBT General Procedure, 5-phenylsalicylic acid (7.06 g, 0.036 mol) was added to dry toluene (75 mL). The solution was warmed up to 40 °C and o-aminothiophenol (4.51 g, 0.036 mol) added to the reaction flask. Phosphorous trichloride (4.53 g, 0.033 mol) was added dropwise to the reaction mixture while the reaction temperature was maintained below 45 °C. After the usual work-up, solvent evaporation yielded a yellow solid (5 g, 46%), which was purified by flash column chromatography through silica gel (hexane/methylene chloride, 3:1) and by sublimation (m.p. 141-142 °C).

^{1}H NMR ($CDCl_3$, δ) 1H (s) 12.59, 1H (d, J_H = 8 Hz) 8.02, 1H (d, J_H = 8 Hz) 7.92, 1H (d, J_H = 2 Hz) 7.89, 3H (m) 7.6-7.5, 5H (m) 7.5-7.3, 1H (d, J_H = 8 Hz) 7.19.

^{13}C NMR ($CDCl_3$, δ) 169.1, 157.4, 151.8, 140.0, 132.8, 132.5, 131.5, 128.8, 127.0, 126.6, 125.5, 122.1, 121.4, 118.2, 116.8.

UV/VIS (Polystyrene, λ_{max} [ε]) 360 nm (18000 L mol^{-1} cm^{-1}).

Fluorescence (Polystyrene, λ_{em}) 560 nm.

CHN Analysis Found: C, 75.4; H, 4.58; N, 4.38. Calc. for $C_{19}H_{13}NOS$: C, 75.22; H, 4.32; N, 4.62%.

Preparation of 2-(2'-hydroxy-5'-aminophenyl)benzothiazole (5AHBT). This compound was prepared from the reduction of 2-(2'-hydroxy-5'-nitrophenyl)benzothiazole by a modification of the method suggested by Anthony et al. (49) and McCafferty (67). The reduction of the nitro group is accomplished using Sn/HCl instead of Zn/Acetic acid, as recommended by those authors.

2-(2'-hydroxy-5'-nitrophenyl)benzothiazole was obtained from the condensation reaction of 5-nitrosalicylaldehyde (8 g, 0.05 mol) with o-aminothiophenol (4 g, 0.03 mol) in triethyl phosphate (40 mL). The reaction mixture was stirred for 15 min, and glacial acetic acid (40 mL) was added. After 15 min, lead tetraacetate (24 g, 0.05 mol) was added at small fractions to maintain the reaction temperature below 60 °C. The reaction mixture was stirred for 30 min after the addition was complete. Ethylene glycol (4 mL) was added, and the reaction mixture was cooled to room temperature, whereupon crystals formed. The product was filtered and washed with ethanol and water sequentially. The residue (5 g, 75%) was dried in a desiccator. Recrystallization from aqueous ethanol

afforded 2-(2'-hydroxy-5'-nitrophenyl)benzothiazole (m.p. 211-212 °C, lit. [49] 212-214 °C).

2-(2'-hydroxy-5'-nitrophenyl)benzothiazole (5 g, 0.020 mol) was added to concentrated HCl (45 mL); Sn (12 g, 0.1 mol) was added at small portions over 30 min to the stirred acidic solution while the temperature of the reaction was kept below 80 °C. The reaction was allowed to stir for an additional hour, after which time water (50 mL) was added, followed by activated charcoal (1 g) and celite 545 (1.2 g). This mixture was stirred and allowed to cool to about 35 °C, and then filtered. The resulting filter cake was washed with 50% hydrochloric acid. The filtrate was cooled to 10 °C or below and neutralized with ammonium hydroxide. The reduced product precipitated as a brownish solid that fluoresced red. The solid (3.2 g, 65%) was filtered and purified by recrystallization from methylene chloride to afford pure 2-(2'-hydroxy-5'-aminophenyl)benzothiazole (m.p. 184-186 °C, lit. [49] 185-186 °C).

^{1}H NMR (d_6-DMSO, δ) 1H (s) 10.7, 2H (dd, J_H = 8 Hz) 8.1, 2H (m) 7.5, 2H (dd, J_H = 8 Hz) 6.9, 1H (s) 6.8, 2H (s) 4.9.

2. 3-Hydroxyflavone Derivatives

3-Hydroxyflavone was purchased from Kodak, recrystallized as needed from a mixture of methylene chloride and hexane, and kept under vacuum in the desiccator. The rest of the derivatives were synthesized following the procedure outlined by Smith et al. (71), which is a modification of the Algar-Flynn-Oyamada method for preparation of flavonols (69).

General Procedure for the synthesis of flavonols: Preparation of 2',5'-dimethyl-3-hydroxyflavone (25M3HF). o-Hydroxyacetophenone (6.0 g, 0.04 mol) and 2,5-dimethylbenzaldehyde (5.94 g, 0.04 mol) in 95% ethanol (60 mL) were mixed in a 250 mL three-necked flask provided with magnetic stirring. A NaOH (6 g) solution in water (12 mL) was added to the mixture, and a yellow precipitate formed, although it redissolved in a few minutes. In rapid order, the reaction mixture color changed from yellow to orange to red, and was let stand overnight. An aqueous NaOH solution (3 g/15 mL) was prepared, added to 300 mL 95% ethanol, and the resulting solution poured into the reaction flask. The reaction mixture was then cooled to approximately 15 °C, the ice bath was removed, and a 30% hydrogen peroxide solution (36 mL, 0.35 mol) was added all at once. A precipitate formed instantly, and the solution color slowly changed to yellow. The reaction mixture was stirred for 6 h, neutralized with 1M H_2SO_4 solution, and poured into ice cold water (400 mL). A yellow precipitate (8.1 g, 67%) was collected by filtration, and was purified by recrystallization from hexane followed by sublimation (m.p. 184-185 °C, lit. [60] 184-186 °C).

^{1}H NMR ($CDCl_3$, δ) 1H (d, J_H = 8 Hz) 8.20, 2H (m) 7.9-7.7, 1H (d, J_H = 8 Hz) 7.62, 3H (m) 7.55-7.4, 3H (s) 2.37, 3H (s) 2.34.

UV/VIS (Polystyrene, λ_{max} [ε]) 330 nm (15000 L mol^{-1} cm^{-1}).

Fluorescence (Polystyrene, λ_{em}) 534 nm.

Preparation of 2'-methyl-3-hydroxyflavone (2M3HF). A solution was prepared from o-hydroxyacetophenone (6 g, 0.04 mol) and o-methylbenzaldehyde (5.4 g, 0.04 mol) in 95% ethanol (60 mL). An aqueous

solution of NaOH (6 g/12 mL) was poured into the flask and let stand overnight. The reaction mixture was diluted with aqueous NaOH/ethanol mixture (3 g, 15 mL/ 300 mL), cooled to 15 °C, and a 30% hydrogen peroxide solution (36 mL, 0.35 mol) was added. The 3HF General Procedure described above was followed. A yellow solid (7.8 g, 70%) was obtained in the last precipitation, filtered, and dried in a desiccator. Recrystallization from methylene chloride/hexane yielded 2'-methyl-3-hydroxyflavone as a white powder (m.p. 192-193 °C, lit. [60] 191-192 °C).

^{1}H NMR ($CDCl_3$, δ) 1H (d, J_H = 8 Hz) 8.30, 7H (m) 7.8-7.28, 1H (s) 6.64, 3H (s) 2.41.

UV/VIS (Polystyrene, λ_{max} [ε]) 330 nm (11000 L mol^{-1} cm^{-1}).

Fluorescence (Polystyrene, λ_{em}) 530 nm.

Preparation of 4'-methyl-3-hydroxyflavone (4M3HF). In a flask provided with mechanical stirring, o-hydroxyacetophenone (6 g, 0.04 mol) and p-methylbenzaldehyde (5.3 g, 0.04 mol) were dissolved in 95% ethanol (60 mL), and an aqueous solution of NaOH (6 g/12 mL) was added to the solution. The reaction mixture turned into a paste which was let stand overnight, and was later dissolved in an aqueous NaOH/ ethanol mixture (3 g, 15 mL/300 mL). 30% Hydrogen peroxide (36 mL, 0.35 mol) was added at 15 °C. The reaction was carried out following the 3HF General Procedure described above. A yellow solid (6.8 g, 60%) was collected by filtration as the final product. The crude product was recrystallized from methylene chloride/hexane to yield pure 4'-methyl-3-hydroxyflavone (m.p. 195-197 °C, lit. [71] 196-198 °C).

^{1}H NMR ($CDCL_3$, δ) 1H (d, J_H = 8 Hz) 8.25, 4H (AB system, J_H = 8 Hz) 8.16, 7.34; 1H (m) 7.8-7.65, 1H (d, J_H = 8 Hz) 7.58, 1H (m) 7.5-7.3, 1H (s) 7.05, 3H (s) 2.43.

UV/VIS (Polystyrene, λ_{max} [ε]) 350 nm (16000 L mol^{-1} cm^{-1}).

Fluorescence (Polystyrene, λ_{em}) 530 nm.

Preparation of 2'-chloro-3-hydroxyflavone (2C3HF). As mentioned in the description of the 3HF General Procedure, o-hydroxy-acetophenone (6 g, 0.04 mol) and o-chlorobenzaldehyde (6.2 g, 0.04 mol) were dissolved in 95% ethanol (60 mL). The aldol condensation was carried out using a concentrated aqueous NaOH solution (6 g/12 mL), followed by oxidation with hydrogen peroxide (36 mL, 0.35 mol). The final product was a yellowish solid (5 g, 42%). Recrystallization from cyclohexane/methylene chloride yielded pure 2'-chloro-hydroxyflavone as a powder with a slight yellow tint (m.p. 181-183 °C).

^{1}H NMR ($CDCl_3$, δ) 1H (d, J_H = 8 Hz) 8.30, 7H (m) 7.8-7.3, 1H (s) 6.77.

^{13}C NMR ($CDCl_3$, δ) 173.4, 156.0, 145.0, 139.0, 134.0, 133.7, 131.6, 131.5, 130.3, 129.7, 126.7, 125.6, 124.6, 121.3, 118.4.

UV/VIS (Polystyrene, λ_{max} [ε]) 335 nm (6000 L mol^{-1} cm^{-1})

Fluorescence (Polystyrene, λ_{em}) 532 nm.

C H N Analysis Found: C, 66.07; H, 3.18. Calc. for $C_{15}H_9ClO_3$: C, 66.07; H, 3.33%.

Preparation of 4'-chloro-3-hydroxyflavone (4C3HF). A solution was prepared from o-hydroxyacetophenone (6 g, 0.04 mol) and p-chloro-benzaldehyde (6.24 g, 0.04 mol) in 95% ethanol (60 mL). The solution

was stirred mechanically, and an aqueous NaOH solution (6 g/12 mL) was added all at once. In 30 min the reaction mixture set into a thick paste, which was dissolved in an aqueous NaOH/ethanol mixture (3 g, 15 mL/ 300 mL) prior to oxidation with 30% hydrogen peroxide (36 mL, 0.35 mol) at 15 °C. The work-up was carried out as outlined in the 3HF General Procedure. A yellow solid (5.6 g, 45%) was collected by filtration and was recrystallized from methylene chloride to yield pure 4'-chloro-3-hydroxyflavone as yellow needles (m.p. 202-204 °C, lit. [71] 203-205 °C).

^{1}H NMR (d_6-DMSO)1H (s) 9.85, 4H (AB system, J_H = 8 Hz) 8.24, 7.63; 1H (d, J_H = 8 Hz) 8.10, 2H (m) 7.88-7.70, 1H (m) 7.51-7.39.

UV/VIS (Polystyrene, λ_{max} [ε]) 345 nm (23000 L mol^{-1} cm^{-1}).

Fluorescence (Polystyrene, λ_{em}) 536 nm.

Preparation of 2'-fluoro-3-hydroxyflavone (2F3HF). As it has been described in the 3HF General Procedure, o-hydroxyacetophenone (6 g, 0.04 mol) and o-fluorobenzaldehyde (5.5 g, 0.04 mol) were dissolved in 95% ethanol (60 mL). Addition of an aqueous NaOH solution (6 g/12 mL) formed the aldol adduct which, when treated with 30% hydrogen peroxide (36 mL, 0.35 mol) at 15 °C, yielded the final product. The reaction residue (7.5 g, 66%) was recrystallized from methylene chloride and hexane. The pure 2'-fluoro-3-hydroxyflavone precipitated as pale yellow crystals (m.p. 181-182 °C, lit. [86] 178-179 °C).

^{1}H NMR ($CDCl_3$, δ) 1H (d, J_H = 8 Hz) 8.28, 2H (m) 7.88-7.65, 5H (m) 7.6-7.23, 1H (s) 6.73.

UV/VIS (Polystyrene, λ_{max} (ε)) 335 nm (10000 L mol^{-1} cm^{-1}).

Fluorescence (Polystyrene, λ_{em}) 532 nm.

Preparation of 4'-fluoro-3-hydroxyflavone (4F3HF). In a flask provided with mechanical stirring, o-hydroxyacetophenone (6 g, 0.4 mol) and p-fluorobenzaldehyde (5.5 g, 0.04 mol) were added to 95% ethanol (60 mL). Once the NaOH solution (6 g in 12 mL of water) was added, a large precipitate formed which redissolved but finally turned into a paste. The reaction mixture was diluted with an aqueous NaOH/ethanol mixture (3 g, 15 mL/300 mL), and 30% hydrogen peroxide (36 mL, 0.35 mol) was added as detailed in the General Procedure for 3HF compounds. A yellow solid (5 g, 45%) was filtered off and recrystallized from methylene chloride and hexane. The final product, pure 4'-fluoro-3-hydroxyflavone, was obtained as pale yellow needles (m.p. 153-154 °C, lit. [86] 150-151 °C).

^{1}H NMR ($CDCl_3$, δ) 2H (t, J_H = 8 Hz, J_F = 10 Hz) 8.26, 1H (d, J_H = 8 Hz) 8.29, 1H (dt, J_H = 8 Hz, J_H = 2 Hz) 7.70, 1H (d, J_H = 8 Hz) 7.56, 1H (dt, J_H = 8 Hz, J_H = 2 Hz) 7.41, 2H (d, J_H = 8 Hz).

UV/VIS (Polystyrene, λ_{max} [ε]) 340 nm (11000 L mol^{-1} cm^{-1}).

Fluorescence (Polystyrene, λ_{em}) 532 nm.

Preparation of 2'-methoxy-3-hydroxyflavone (2MO3HF). This compound was prepared as described in the 3HF General Procedure outlined above. A solution was prepared with o-hydroxyacetophenone (6 g, 0.04 mol) and o-methoxybenzaldehyde (6.1 g, 0.04 mol) in 95% ethanol (60 mL). A NaOH solution (6 g in 12 mL of water) was added to

the mixture. The reaction mixture was diluted with an aqueous NaOH/ethanol mixture (3 g, 15 mL/300 mL) and oxidized with 30% hydrogen peroxide (36 mL, 0.35 mol) at 15 °C. The reaction proceeded as described before. A yellow solid (5 g, 46%) was collected after filtration, which was recrystallized from methylene chloride and ethyl acetate. Pure 2'-methoxy-3-hydroxyflavone was obtained in the form of a yellow powder (m.p. 210-212 °C, lit. [87] 213-215 °C).

^{1}H NMR ($CDCl_3$, δ) 1H (dd, J_H = 8 Hz, J_H = 2 Hz) 8.26, 5H (m) 7.76-7.35, 2H (m) 7.18-7.0, 1H (s) 6.45, 3H (s) 3.86.

UV/VIS (Polystyrene, λ_{max} [ε]) 335 nm (10000 L mol^{-1} cm^{-1}).

Fluorescence (Polystyrene, λ_{em}) 534 nm.

Preparation of 4'-methoxy-3-hydroxyflavone (4MO3HF). A solution in 95% ethanol (60 mL) of o-hydroxyacetophenone (6 g, 0.04 mol) and p-methoxybenzaldehyde (6 g, 0.04 mol) was prepared. An aqueous NaOH solution (6 g/12 mL) was added all at once and a yellow precipitate formed and turned into an orange thick paste within 15 min. The reaction mixture was let stand overnight, treated with basic ethanol, and 30% hydrogen peroxide (36 mL, 0.35 mol) was added, controlling the bath temperature to around 15 °C. The reaction mixture was stirred for 6 h at room temperature. The reaction work-up followed the 3HF General Procedure. A yellow residue (6.5 g, 55%) was filtered off and dried. Purification by recrystallization from methylene chloride/hexane afforded pure 4'-methoxy-3-hydroxyflavone as a yellow fibrous solid (m.p. 230-232 °C, lit. [71] 231-232 °C).

^{1}H NMR ($CDCl_3$ + d_6-DMSO) 4H (AB system, J_H = 8 Hz) 8.27, 7.05; 1H (d, J_H = 8 Hz) 8.18, 1H (dt, J_H = 8 Hz, J_H = 2 Hz) 7.72, 1H (d, J_H = 8 Hz) 7.60, 1H (s) 7.48, 1H (dt, J_H = 8 Hz, J_H = 2 Hz) 7.40.

UV/VIS (Polystyrene, λ_{max} [ε]) 350 nm (28000 L mol^{-1} cm^{-1}).

Fluorescence (Polystyrene, λ_{em}) 536 nm.

Preparation of 4'-phenyl-3-hydroxyflavone (4P3HF). Following the steps indicated in the General Procedure for the preparation of flavonols, a solution was prepared of o-hydroxyacetophenone (6 g, 0.04 mol) and 1,1'-biphenylyl-4'-carboxaldehyde (8.1 g, 0.04 mol) in 95% ethanol (60 mL). A 12.5M aqueous NaOH solution (15 mL) was poured into the reaction flask. A thick precipitate formed within a few minutes. The mixture was allowed to react overnight. The reaction mixture was dissolved in basic ethanol and cooled to 15 °C. A 30% hydrogen peroxide solution (36 mL, 0.35 mol) was added all at once to the reaction mixture. The reaction work-up followed 6 h later. The yellow residue collected (5 g, 43%) was recrystallized from methylene chloride/hexane to yield pure 4'-phenyl-3-hydroxyflavone as bright yellow needles (m.p. 220-222 °C, lit. [88] 222-223 °C).

^{1}H NMR ($CDCl_3$, δ) 4H (AB system, J_H = 8 Hz) 8.35, 7.78; 1H (d, J_H = 8 Hz) 8.28, 5H (m) 7.85-7.60, 3H (m) 7.55-7.35.

UV/VIS (Polystyrene, λ_{max} [ε]) 360 nm (35000 L mol^{-1} cm^{-1}).

Fluorescence (Polystyrene, λ_{em}) 548 nm.

Preparation of 4'-phenoxy-3-hydroxyflavone (4PO3HF). A solution of o-hydroxyacetophenone (6 g, 0.04 mol) and 4-phenoxy-benzaldehyde

(8.8 g, 0.04 mol)in 95% ethanol (60 mL) was prepared. A 12.5M aqueous NaOH solution (15 mL) was added to the reaction mixture. An orange precipitate formed within 20 min. The reaction was allowed to stand overnight. The reaction mixture was diluted with basic ethanol, followed by oxidation with 30% hydrogen peroxide (36 mL, 0.35 mol) at 15 °C. The reaction work-up followed the General Procedure and yielded a yellow residue (6 g, 40%) which was purified by recrystallization from methylene chloride to afford pure 4'-phenoxy-3-hydroxy-flavone (m.p. 183-184 °C).

^{1}H NMR ($CDCl_3$, δ) 1H (s) 9.9, 4H (AB system, J_H = 8 Hz) 8.25, 7.12; 1H (d, J_H = 8 Hz) 8.08.

^{13}C NMR (d_6 - DMSO, δ) 172.8, 158.1, 155.7, 154.5, 145.0, 138.6, 133.6 130.2, 129.8, 126.1, 124.8, 124.5, 124.2, 121.3, 119.3, 118.3, 118.0.

UV/VIS (Polystyrene, λ_{max} [ε]) 350 nm (28000 L mol^{-1} cm^{-1}).

Fluorescence (Polystyrene, λ_{em}) 538 nm.

CHN Analysis Found: C, 76.19; H, 4.12. Calc. for $C_{21}H_{14}O_4$: C, 76.36; H, 4.27%.

Preparation of 4'-thiomethyl-3-hydroxyflavone (4MS3HF). A solution was prepared from o-hydroxyacetophenone (6 g, 0.04 mol) and 4-thiomethylbenzaldehyde (6.75 g, 0.04 mol) in 95% ethanol (60 mL). An aqueous NaOH solution (6 g/12 mL) was poured into the reaction flask. The reaction was let stand overnight. As outlined in the General Procedure, the reaction mixture was dissolved in basic ethanol, cooled down to 15 °C and oxidized with 30% hydrogen peroxide (36 mL, 0.35

mol). The reaction was allowed to proceed for 6 h. The reaction work-up afforded a yellow residue (7 g, 55%). Purification by recrystallization from methylene chloride/ethyl acetate yielded pure 4'-thiomethyl-3-hydroxyflavone (m.p. 209-211 °C).

^{1}H NMR (d_6 - DMSO, δ) 1H (s) 9.52, 4H (AB system, J_H = 8 Hz) 8.12, 7.35; 1H (d, J_H = 8 Hz) 8.07, 2H (m) 7.8-7.65, 1H (t, J_H = 8 Hz) 7.4, 3H (s) 2.45.

^{13}C NMR (d_6 - DMSO, δ) 173.2, 154.5, 140.5, 138.8, 133.0, 130.2, 128.0, 127.9, 127.4, 125.2, 124.7, 120.5, 117.2, 12.2.

UV/VIS (Polystyrene, λ_{max} [ε]) 360 nm (20000 L mol^{-1} cm^{-1}).

Fluorescence (Polystyrene, λ_{em}) 545 nm.

CHN Analysis Found: C, 67.21; H, 4.13. Calc. for $C_{16}H_{12}O_3S$: C, 67.59; H, 4.25%.

REFERENCES

1. Birks, J. B. The Theory and Practice of Scintillation Counting; Pergamon Press, The McMillan Co.: New York, 1964.

2. Leo, W. R. Techniques for Nuclear and Particle Physics Experiments; Springer-Verlag: Berlin, 1987.

3. Förster, Th. Ann. Phys. **1948**, 2, 55.

4. Förster, Th. Discussions Faraday Soc. **1959**, 27, 7.

5. Robinson, G. W.; Frosch, R. P. J. Chem. Phys. **1963**, 38, 1187.

6. Frederickson, G. H.; Frank, C. W. Macromolecules **1983**, 16, 1198.

7. Kang, T. C. Ph.D. Dissertation, University of Minnesota, 1989 (unpublished).

8. Berlman, I. B. Handbook of Fluorescence Spectra of Aromatic Molecules, 2nd ed.; Academic Press, Inc.: New York, 1971.

9. Schorr, M. G.; Torney, F. L. Phys. Rev. **1950**, 80, 474.

10. Swank, R. K.; Buck, W. L. Phys. Rev. **1953**, 91, 927.

11. Sandler, S. R.; Loshack, S. J. Chem. Phys. **1961**, 34, 438.

12. Bezuglii, V. D.; Nagornaya, L. L. J. Nuc. Eng. **1965**, 19, 490.

13. Andreeschev, E. A.; Baroni, E. E. Bull. Acad. Sci. USSR, Phys. Ser. **1958**, 22, 64.

14. Carlson, T.; Koski, W. S. Phys. Rev. **1952**, 85, 697.

15. Medvedev, M. N.; Matveeva, E. N. Bull. Acad. Sci. USSR, Phys. Ser. **1958**, 22, 42.

16. Basile, L. J. J. Chem. Phys. **1957**, 27, 801.

17. Clough, R. L. "Radiation Resistant Polymers", Encyclopedia of Polymer Science and Engineering; John Wiley and Sons, Inc.: New York, 1988.

18. Bowen, M. K. M.S. Thesis, University of Florida, 1988 (unpublished).

19. Linssen, L. Proceedings of the Workshop on Scintillator Fiber Detector Development for the SSC, Fermi National Accelerator Laboratory, Batavia, IL, Nov. 14-16, 1988, pp. 3-34.

20 Pichat, L.; Koechlin, Y. J. Chim. Phys. **1951**, 48, 225.

21. Hayes, F. N.; Rodgers, B. S.; Sanders, P.; Schuch, R. L.; Williams, D. L. Los Alamos Sci. Lab. Rpt. LA-1639, 1953.

22. Hayes, F. N.; Gould, R.G. Science **1953**, 117, 480.

23. Kerr, V. N.; Hayes, F. N.; Ott, D. G.; Hansbury, E. J. Org. Chem. **1959**, 24, 1861.

24. Barnett, M. D.; Daub, G. H.; Hayes, F. N.; Ott, D. G. J. Am. Chem. Soc. **1960**, 82, 2282.

25. Wiley, R. H.; Jarboe, C. H. Hayes, F. N. J. Am. Chem. Soc. **1957**, 79, 2602.

26. Wirth, H. O. Molecular Crystals **1968**, 4, 321.

27. Kauffman, J. M.; Kelley, C. J.; Ghiorghis, A.; Neister, E.; Armstrong, L.; Prause, P. Laser Chem. **1987**, 7, 343.

28. Kauffman, J. M. Proceedings of the Workshop on Scintillator Fiber Detector Development for the SSC, Fermi National Accelerator Laboratory, Batavia, IL, Nov. 14-16, 1988, pp. 675-740.

29. Kauffman, J. M.; Kelley, C. J.; Ghiorghis, A.; Neister, E.; Armstrong, L. Laser Chem. **1988**, 8, 335.

30. Bross, A. D. Technical Report TM-1587, 1990; Fermi National Accelerator Laboratory, Batavia, IL.

31. Güsten, H.; Schuster, P.; Seitz, W. J. Phys. Chem. **1978**, 82, 459.

32. Destruel, P.; Taufer, M.; D'Ambrosio, C.; Da Via, C.; Fabre, J. P.; Kirby, J.; Lentz, H. Technical Report CERN/EF 88-9, 1988; CERN, Geneve, Switzerland.

33. Langhals, H.; Pust, S. Chem. Ber. **1985**, 118, 4674.

34. Sepiol, J.; Bulska, H.; Grabowska, A. Chem. Phys. Lett. **1987**, 140, 607.

35. Renschler, C. L.; Harrah, L. A. Nuc. Inst. Meth. **1985**, A235, 41.

36. Pla-Dalmau, A.; Bross, A. D.; Spangler, C. W. Abstracts of Papers, 199th National Meeting of the American Chemical Society, Boston, MA, American Chemical Society; Washington, DC, 1990; PHYS242.

37. Zorn, C.; Majewski, S. Nuc. Inst. Meth. **1988**, A273, 108.

38. Kang, T. J.; Barbara, P. F.; Pla-Dalmau, A.; Bross, A. D. Proceedings of the Workshop on Scintillator Fiber Detector Development for the SSC, Fermi National Accelerator Laboratory, Batavia, IL, Nov. 14-16, 1988, pp. 769-782.

39. Bross, A. D. Proceedings of the Workshop on Scintillator Fiber Detector Development for the SSC, Fermi National Accelerator Laboratory, Batavia, IL, Nov. 14-16, 1988, pp. 741-768.

40. Para, A. Proceedings of the Workshop on Radiation Hardness of Plastic Scintillators, University of Florida, Tallahassee, FL, March 19-21, 1990, in press.

41. Barbara, P. F.; Jarzeba, W. Acc. Chem. Res. **1988**, 21, 195.

42. Kasha, M. J. Chem. Soc. Faraday Trans. 2 **1986**, 82, 2379.

43. Cohen, M. D.; Flavian, S. J. Chem. Soc. (B) **1967**, 317.

44. Klopffer, W. Adv. Photochem. **1977**, 10, 311.

45. Nakagaki, R.; Kobayashi, T.; Nakamura, J.; Nagakura, S. Bull. Chem. Soc. Japan **1977**, 50, 1909.

46. Huppert, D.; Gutman, M.; Kaufmann, K. J. Adv. Chem. Phys. **1981**, 47, 643.

47. Williams, D. L.; Heller, A. J. Phys. Chem. **1970**, 74, 4473.

48. Barbara, P. F.; Brus, L. E.; Rentzepis, P. M. J. Am. Chem. Soc. **1980**, 102, 5631.

49. Anthony, K.; Brown, R. G.; Hepworth, J. D.; Hodgson, K. W.; May, B. J. Chem. Soc. Perkin Trans. 2 **1984**, 2111.

50. Ding, K.; Courtney, S. J.; Strandjord, A. J. G.; Flom, S.; Friedrich, D.; Barbara, P. F. J. Phys. Chem. **1983**, 87, 1184.

51. Elsaesser, T.; Kaiser, W. Chem. Phys. Lett. **1986**, 128, 231.

52. Elsaesser, T.; Schmetzer, B. Chem. Phys. Lett. **1987**, 140, 293.

53. Becker, R. S.; Lenoble, C.; Zein, A. J. Phys. Chem. **1987**, 91, 3509.

54. Elsaesser, T.; Schmetzer, B.; Lipp, M.; Bauerle, R. J. Chem. Phys. Lett. **1988**, 148, 112.

55. Sengupta, P. K.; Kasha, M. Chem. Phys. Lett. **1979**, 68, 382.

56. McMorrow, D.; Kasha, M. J. Phys. Chem. **1984**, 88, 2235.

57. Strandjord, A. J. G.; Courtney, S. H.; Friedrich, D. M.; Barbara, P. F. J. Phys. Chem. **1983**, 87, 1125.

58. Strandjord, A. J. G.; Barbara, P. F. Chem. Phys. Lett. **1983**, 98, 21.

59. Strandjord, A. J. G.; Barbara, P. F. J. Chem. Phys. **1985**, 89, 2355.

60. Strandjord, A. J. G.; Smith, D. E.; Barbara, P. F. J. Phys. Chem. **1985**, 89, 2362.

61. Etter, M. C.; Urbanczyk-Lipkowska, Z.; Baer, S.; Barbara, P. F. J. Mol. Struc. **1986**, 144, 155.

62. Salman, O. A.; Drickamer, H. G. J. Chem. Phys. **1982**, 77, 3329.

63. Dick, B.; Ernsting, N. P. J. Phys. Chem. **1987**, 91, 4261.

64. Brucker, G. A.; Kelley, D. F. J. Phys. Chem. **1987**, 91, 2856.

65. Brucker, G. A.; Kelley, D. F. J. Phys. Chem. **1988**, 92, 3805.

66. Hein, D. W.; Alheim, R. J.; Leavitt, J. J. U.S. Patent 2 985 661, 1961.

67. McCafferty, E. A. U.S. Patent 3 162 642, 1964.

68. Freyermuth, H. B. U.S. Patent 3 669 979, 1972.

69. Seshadri, T. R. In The Chemistry of Flavonoid Compounds; Geissman, T. A., Ed.; Pergamon Press: Oxford, 1962.

70. Adams, J. H. J. Org. Chem. **1967**, 32, 3992.

71. Smith, M. A.; Newmann, R. M.; Webb, R. A. J. Heterocycl. Chem. **1968**, 5, 425.

72. Rao, T. S.; Singh, A. K.; Trivedi, G. K. Heterocycles **1984**, 22, 1377.

73. Ramakrishna Murthy, M.; Radakrishna, S. Indian J. Pure Appl. Phys. **1963**, 582.

74. Washio, M.; Tagawa, S.; Tabata, Y. Radiat. Phys. Chem. **1983**, 21, 239.

75. Tagawa, S.; Schnabel, W.; Washio, M.; Tabata, Y. Radiat. Phys. Chem. **1981**, 18, 1087.

76. Irie, S.; Horii, H.; Irie, M. Macromolecules **1980**, 13, 1355.

77. Thomas, J. K.;, Mani, I. J. Chem. Phys. **1969**, 51, 1834.

78. Smith, W. R., II; Kiefer, R. L.; Orwoll, R. A.; Long, S. A. T. Polymer Preprints **1990**, 1, 609.

79. Platt, A. E. "Styrene Polymers", Encyclopedia of Polymer Science and Technology; Mark, H. F., Ed.; John Wiley and Sons, Inc.,Wiley-Interscience: New York, 1970.

80. Williams, J. L.; Dunn, T. S. Radiat. Phys. Chem. **1980**, 15, 59.

81. Chou, P.; McMorrow, D.; Aartsma, T. J.; Kasha, M. J. Phys. Chem, **1984**, 88, 4596.

82. Nishinaga, A.; Matsuura, T. J. Chem. Soc. Chem. Comm. **1973**, 1, 9.

83. Nishinaga, A.; Togo, T.; Tomita, H. J. Chem. Soc. Perkin I **1979**, 2511.

84. El-Sukkary, M. M. A.; Speier, G. J. Chem. Soc. Chem. Comm. **1981**, 15, 745.

85. Matsuura, T.; Takemoto, T.; Nakashima, R. Tetrahedron **1973**, 29, 3337.

86. Chen, F. C.; Chen, T. S.; Ueng, T. J. Chinese Chem. Soc. **1962**, 9, 308.

87. Simpson, T. H.; Whalley, W. B. J. Chem. Soc. **1955**, 166.

88. Hsu, K. K.; Shi, J. Y. J. Chinese Chem. Soc. **1973**, 20, 51.

89. Stewart, J. J. P. "MOPAC 4.0 Compouter Code" QCPE #455.

90. Clough, R.; Cahill, P.; Renschler, C. Proceedings of the Workshop on Radiation Hardness of Plastic Scintillators, University of Florida, Tallahassee, FL, March 19-21, 1990, in press.

91. Shimizu, T., Kyowa Gas, Japan, personal communication, 1989.

92. Bross, A. D., Fermi National Accelerator Laboratory, Batavia, IL, personal communication, 1990.

93. Bross, A. D. "FLUOR8 Computer Code", Fermi National Accelerator Laboratory, Batavia, IL, 1986 (unpublished).

94. Fergusson, L. N.; Holmes, R. R.; Calvin, M. J. Am. Chem. Soc. **1950**, 72, 5315.

95. Cameron, D.; Jeskey, H.; Baine, O. J. Org. Chem. **1950**, 15, 233.

APPENDIX A

ABSORPTION AND EMISSION SPECTRA OF HBT AND 3HF DERIVATIVES IN POLYSTYRENE

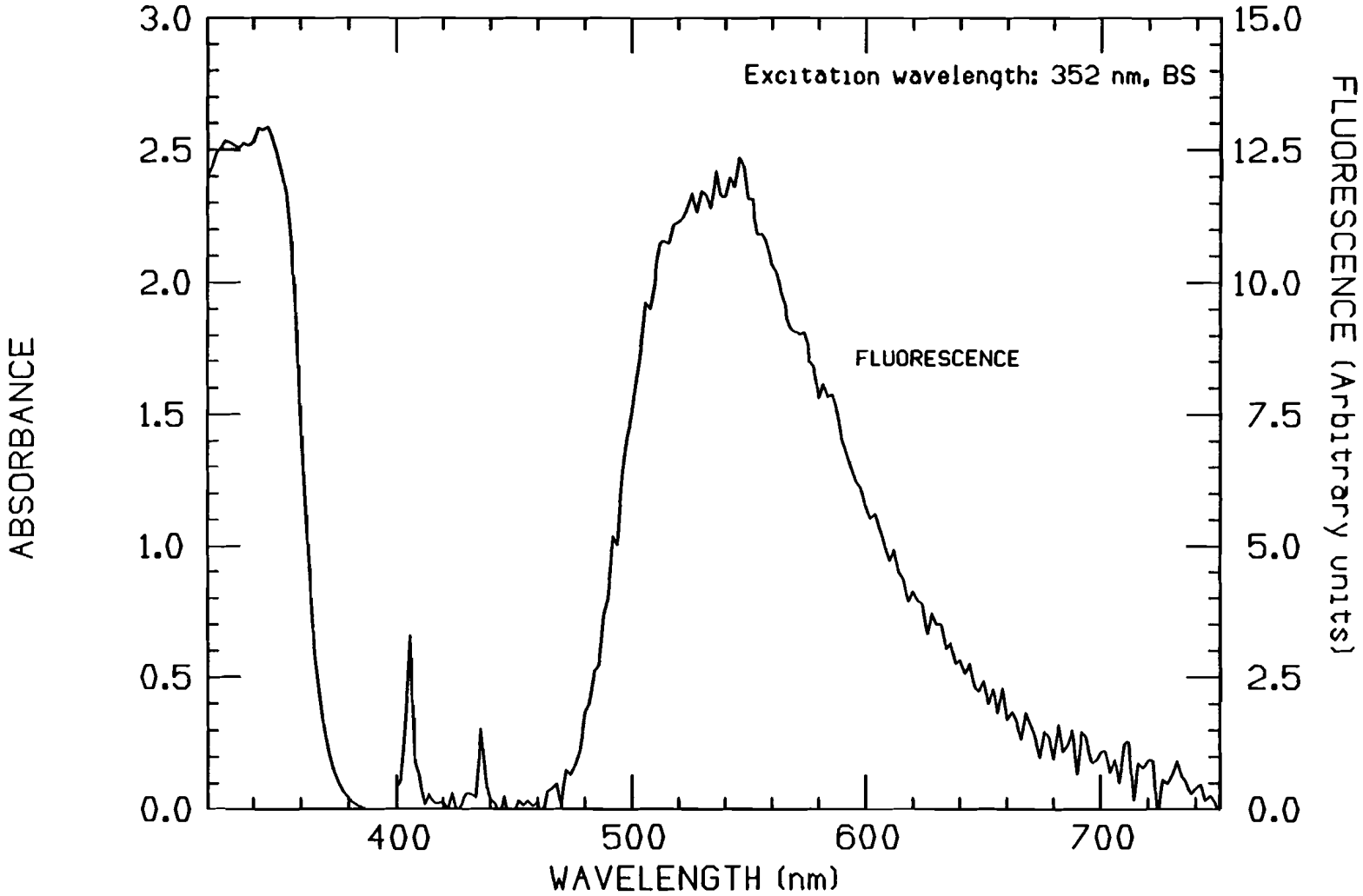

Figure 44. Absorption and emission spectra of 3FHBT in PS.

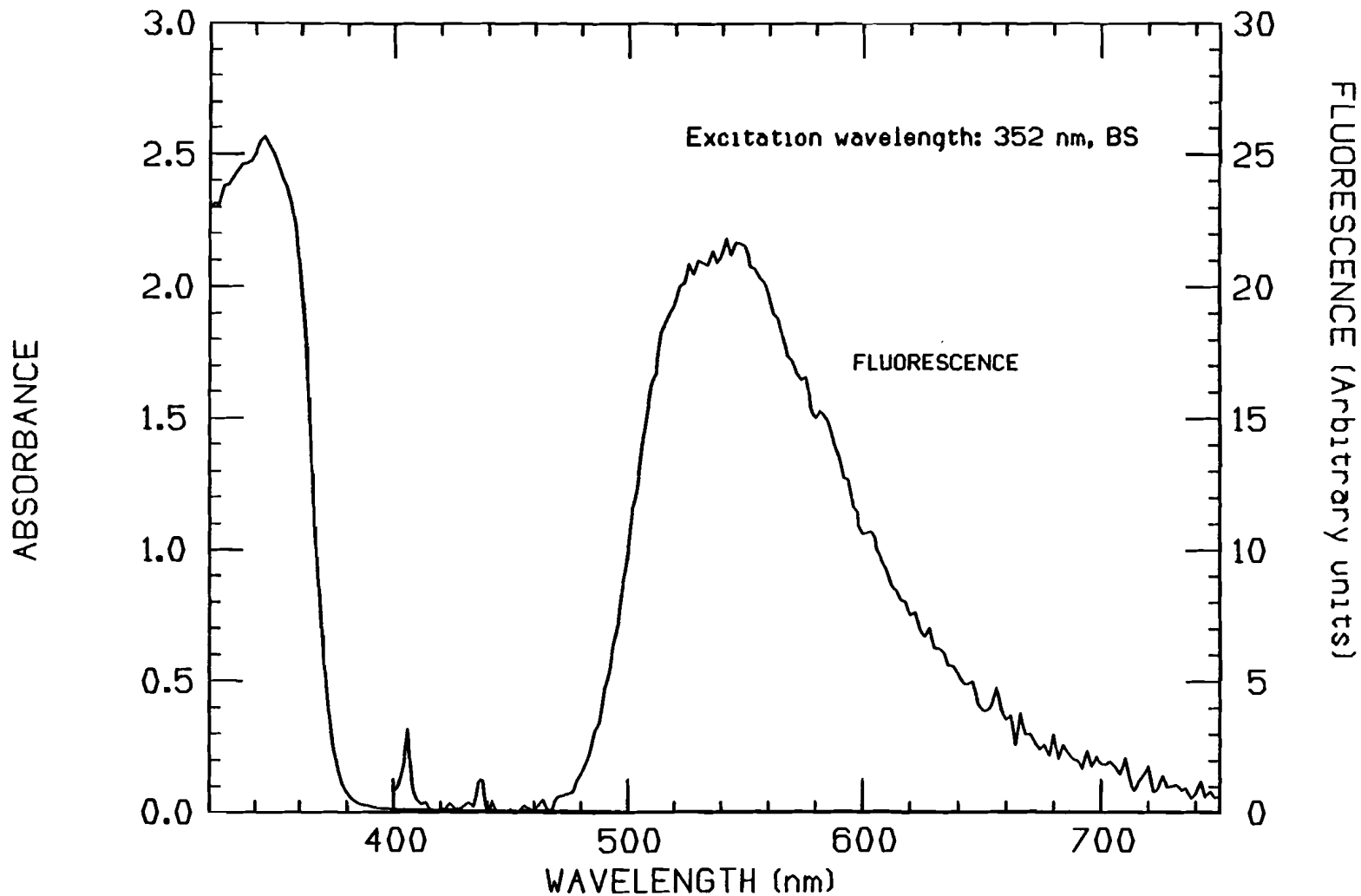

Figure 45. Absorption and emission spectra of 3CHBT in PS.

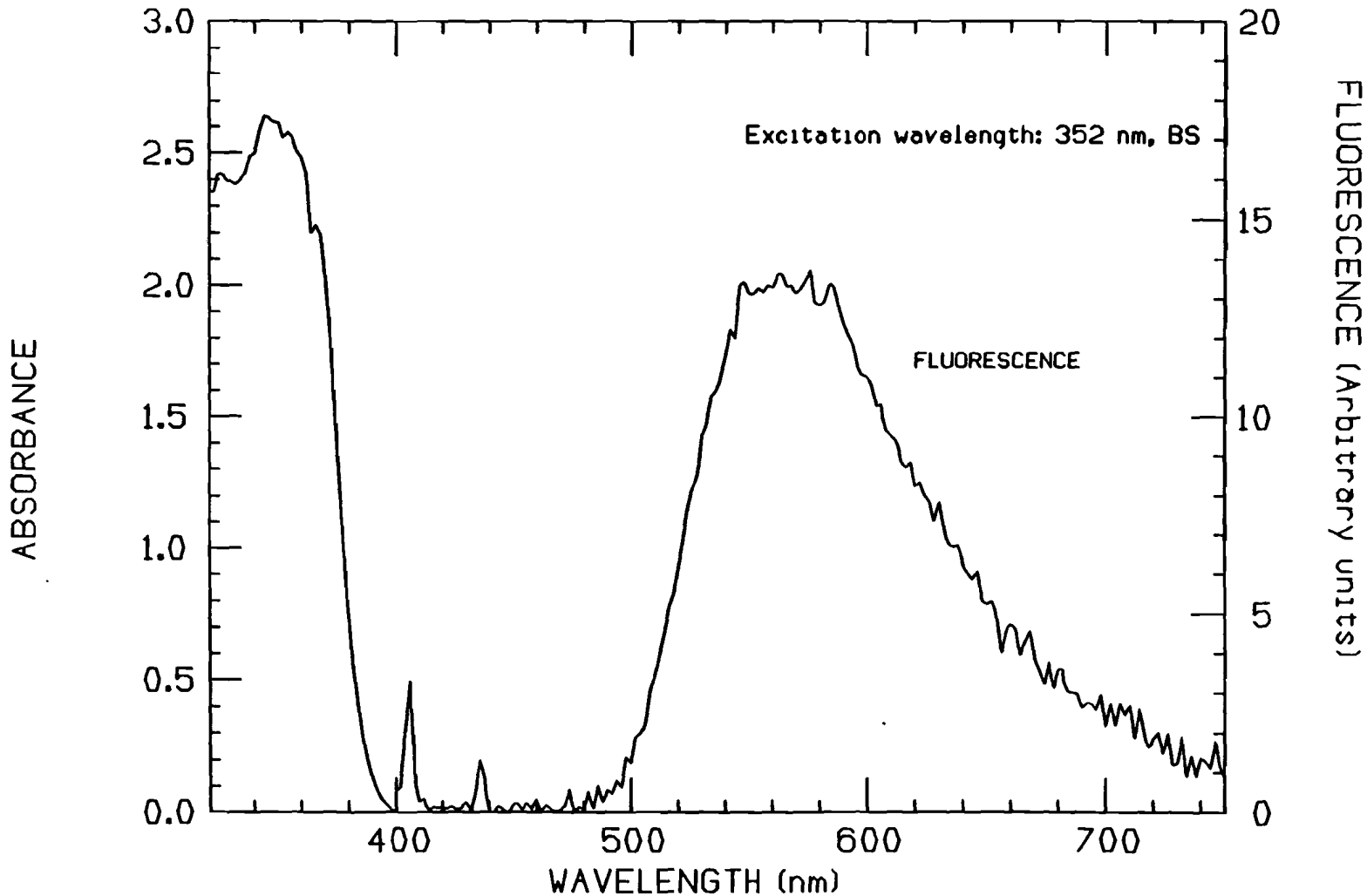

Figure 46. Absorption and emission spectra of 3PHBT in PS.

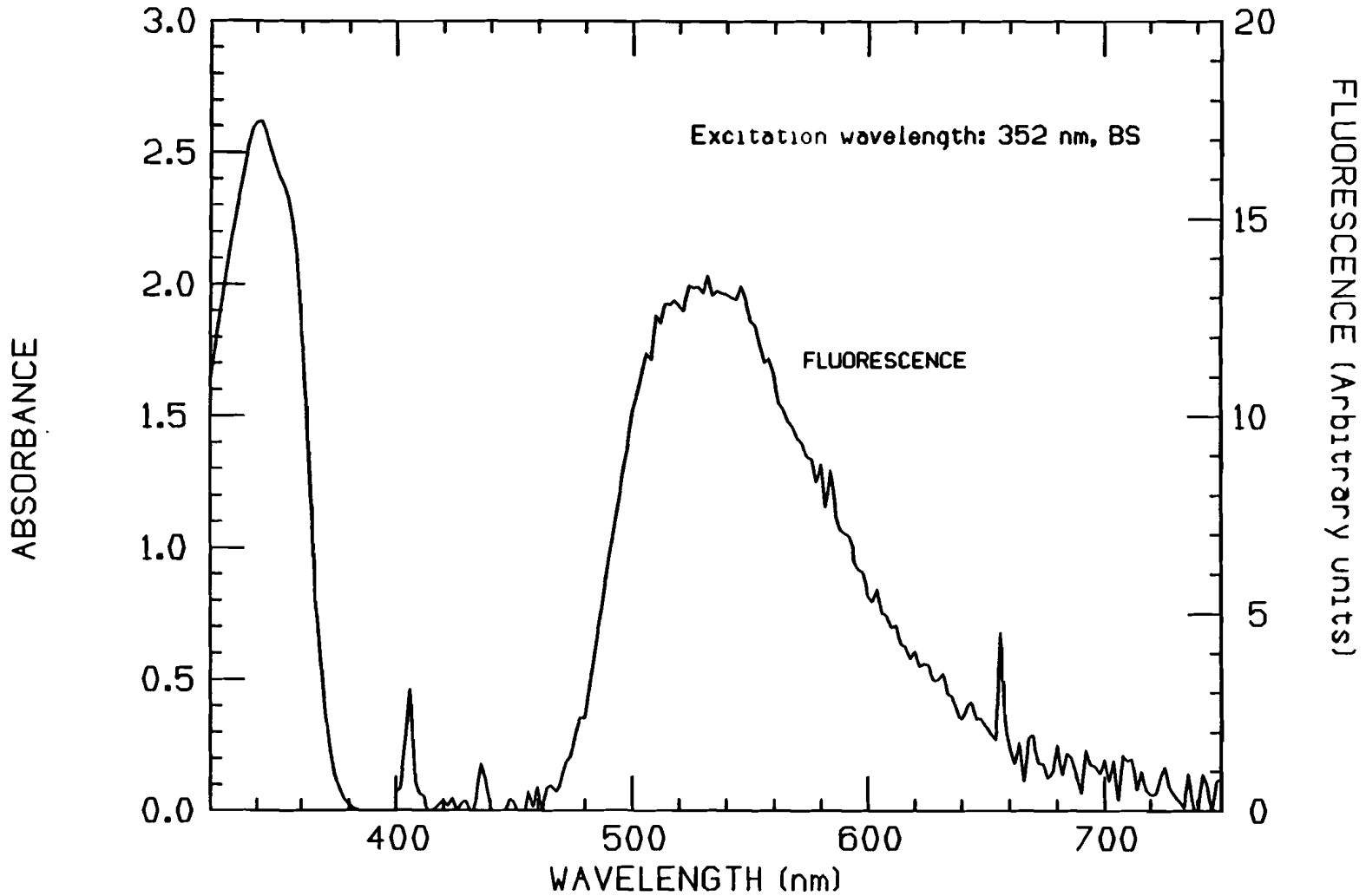

Figure 47. Absorption and emission spectra of 4MHBT in PS.

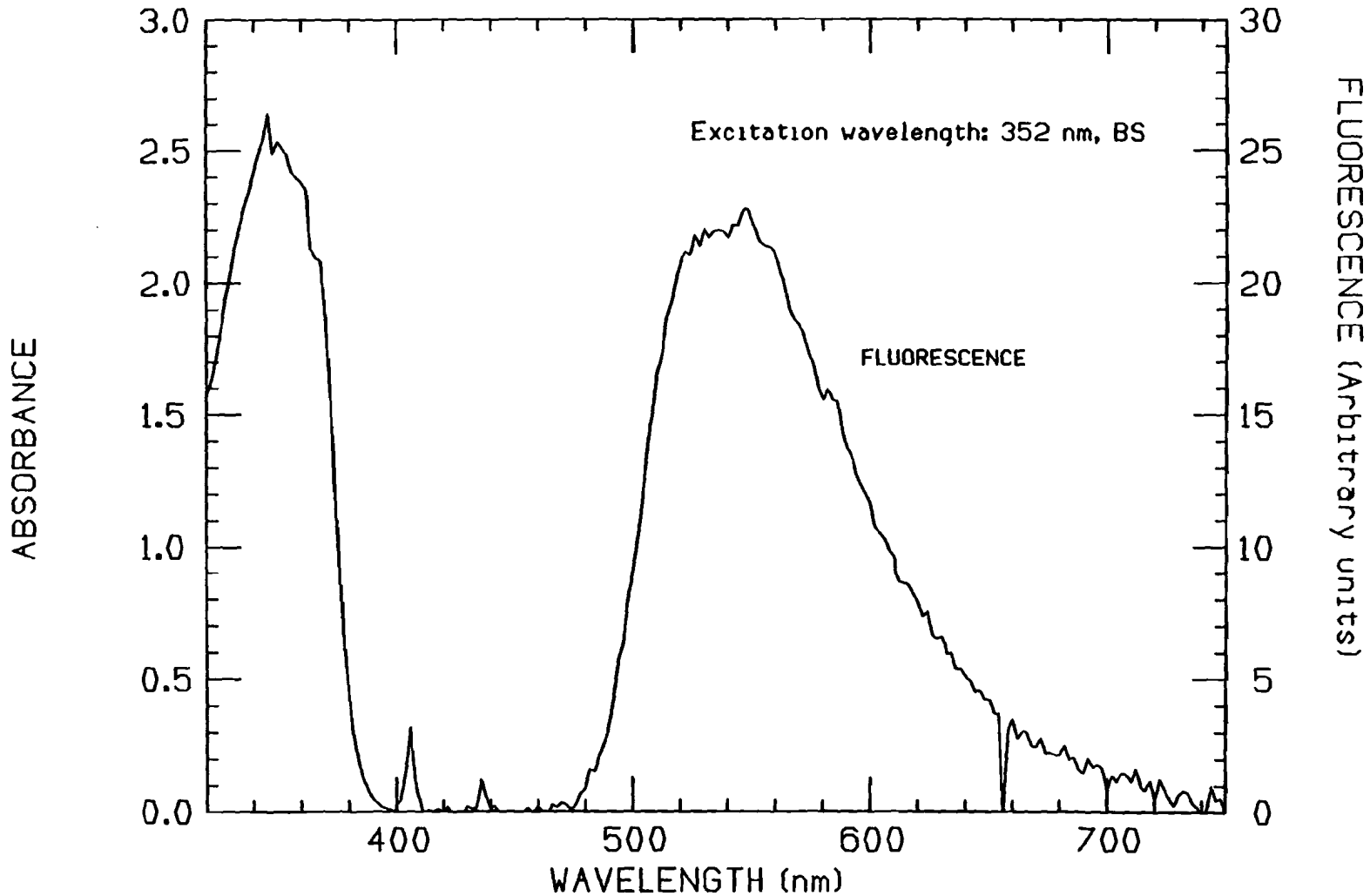

Figure 48. Absorption and emission spectra of 5CHBT in PS.

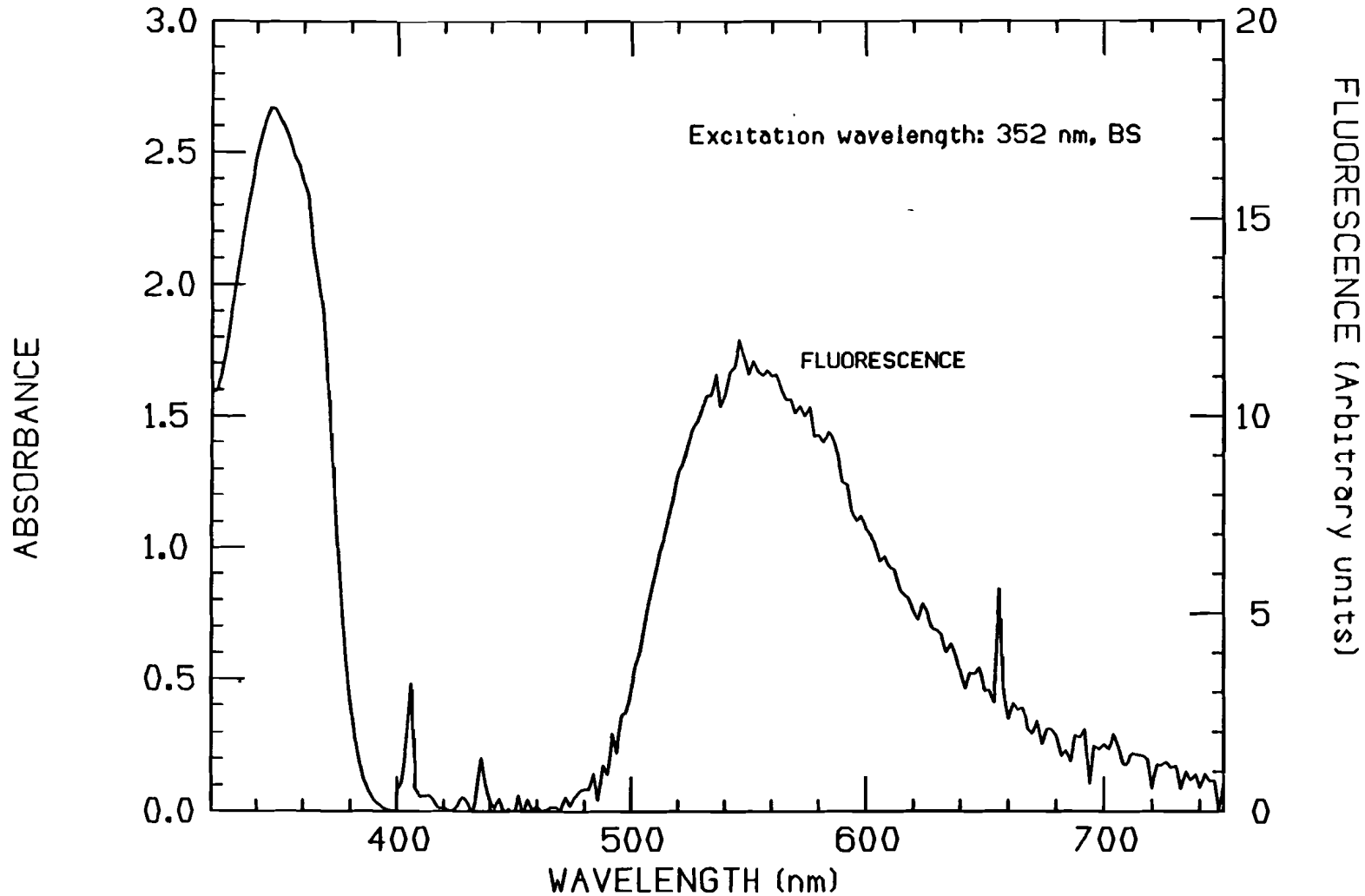

Figure 49. Absorption and emission spectra of 5MHBT in PS.

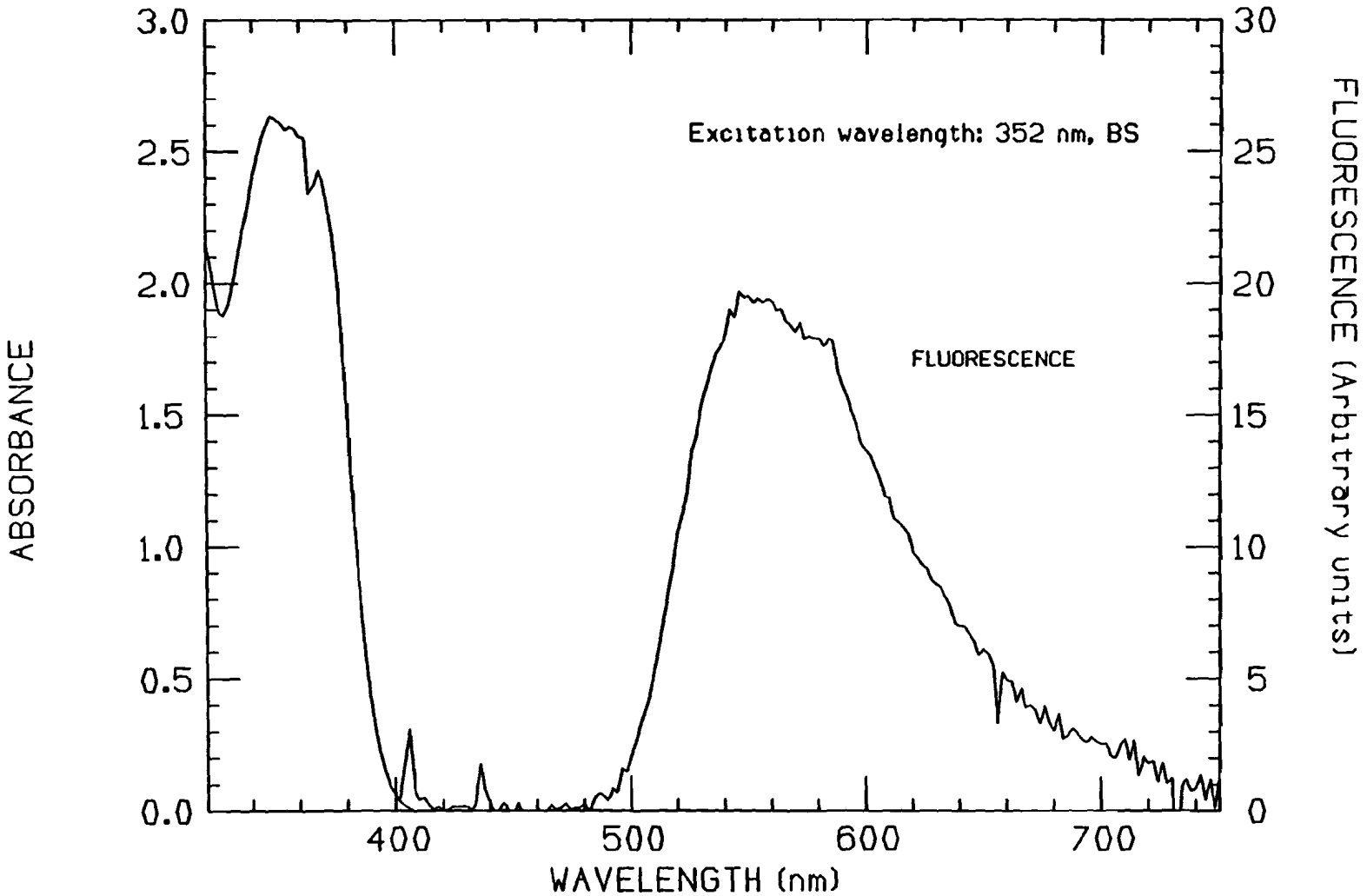

Figure 50. Absorption and emission spectra of 5PHBT in PS.

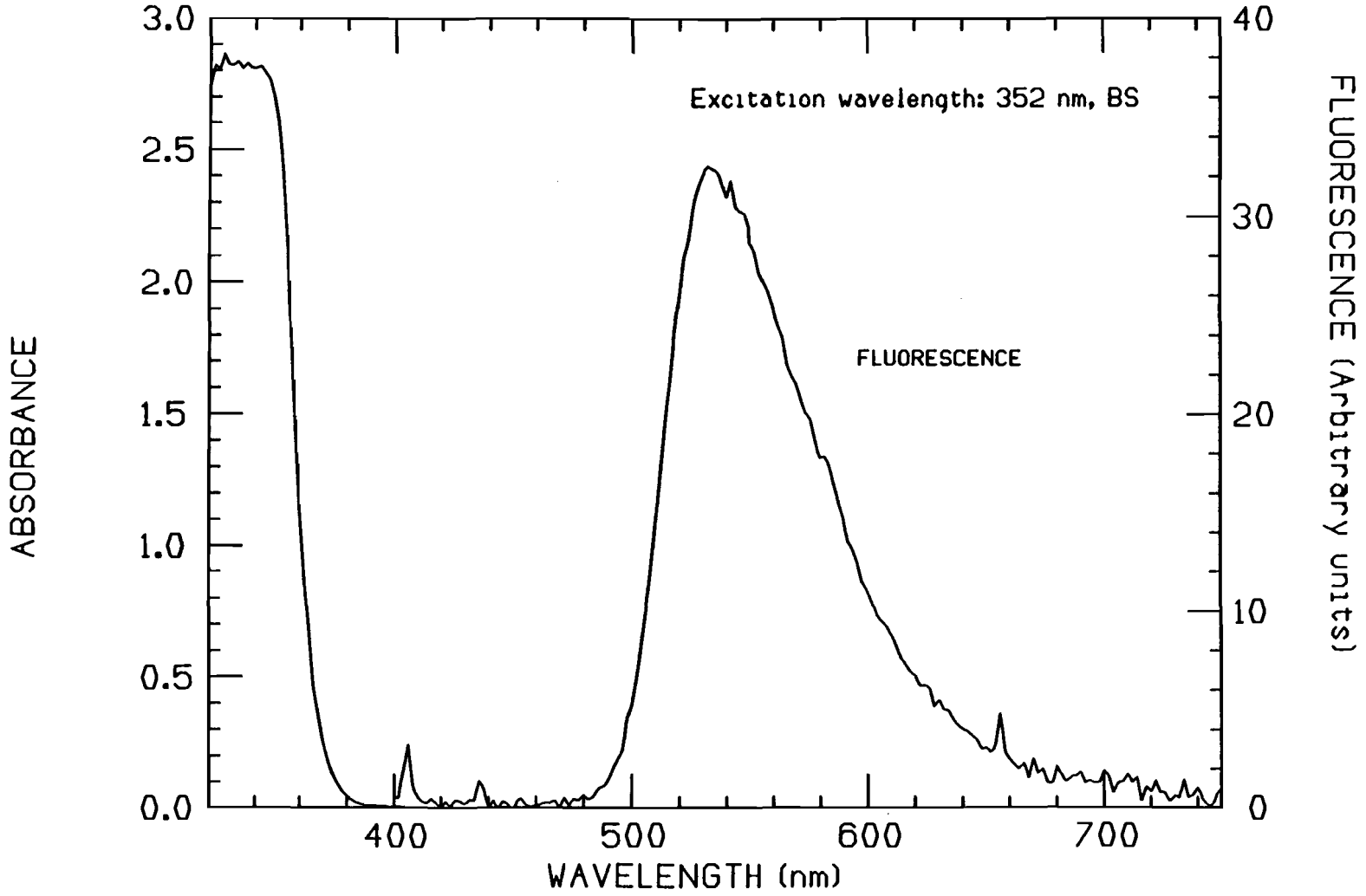

Figure 51. Absorption and emission spectra of 2C3HF in PS.

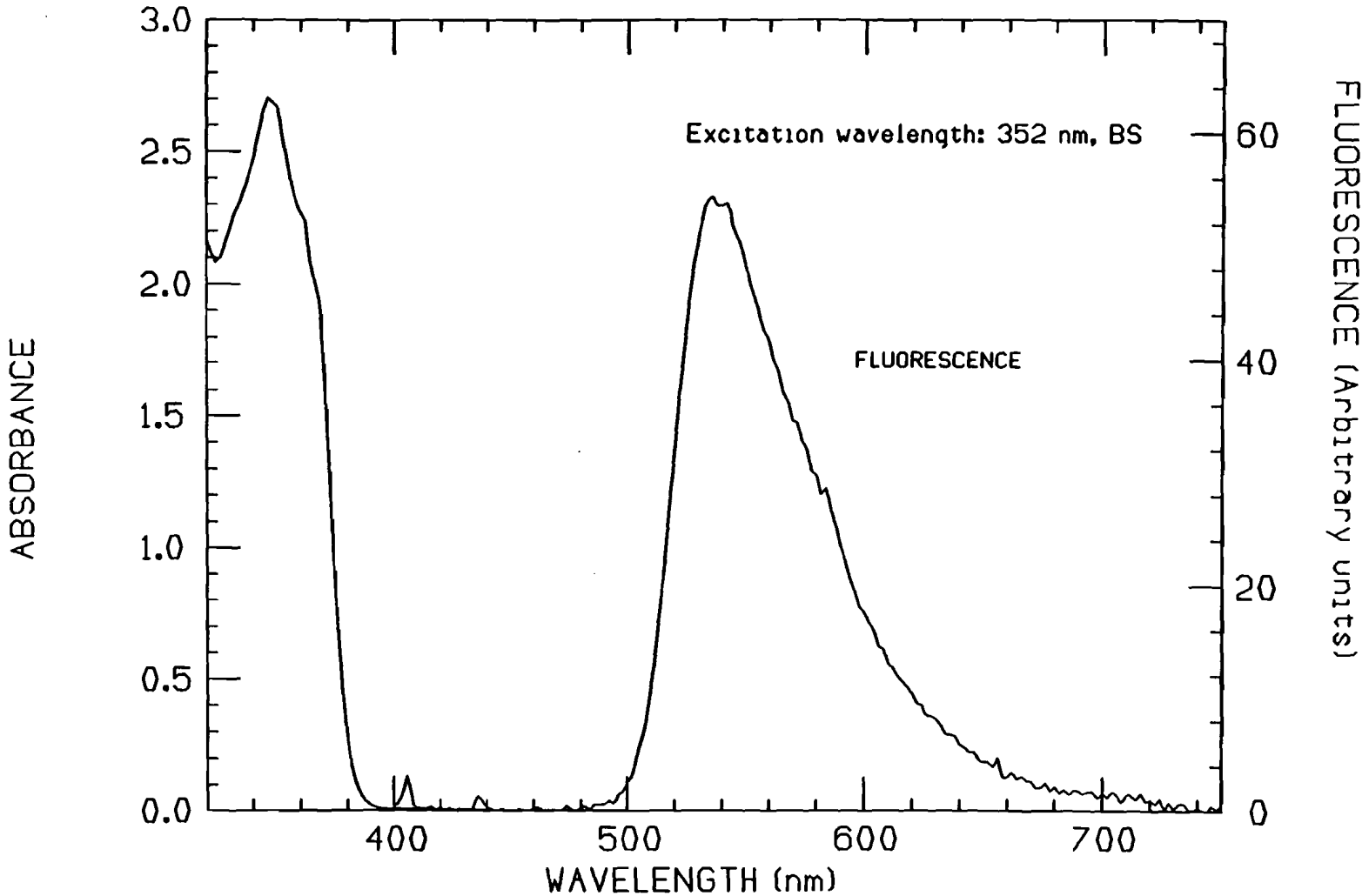

Figure 52. Absorption and emission spectra of 4C3HF in PS.

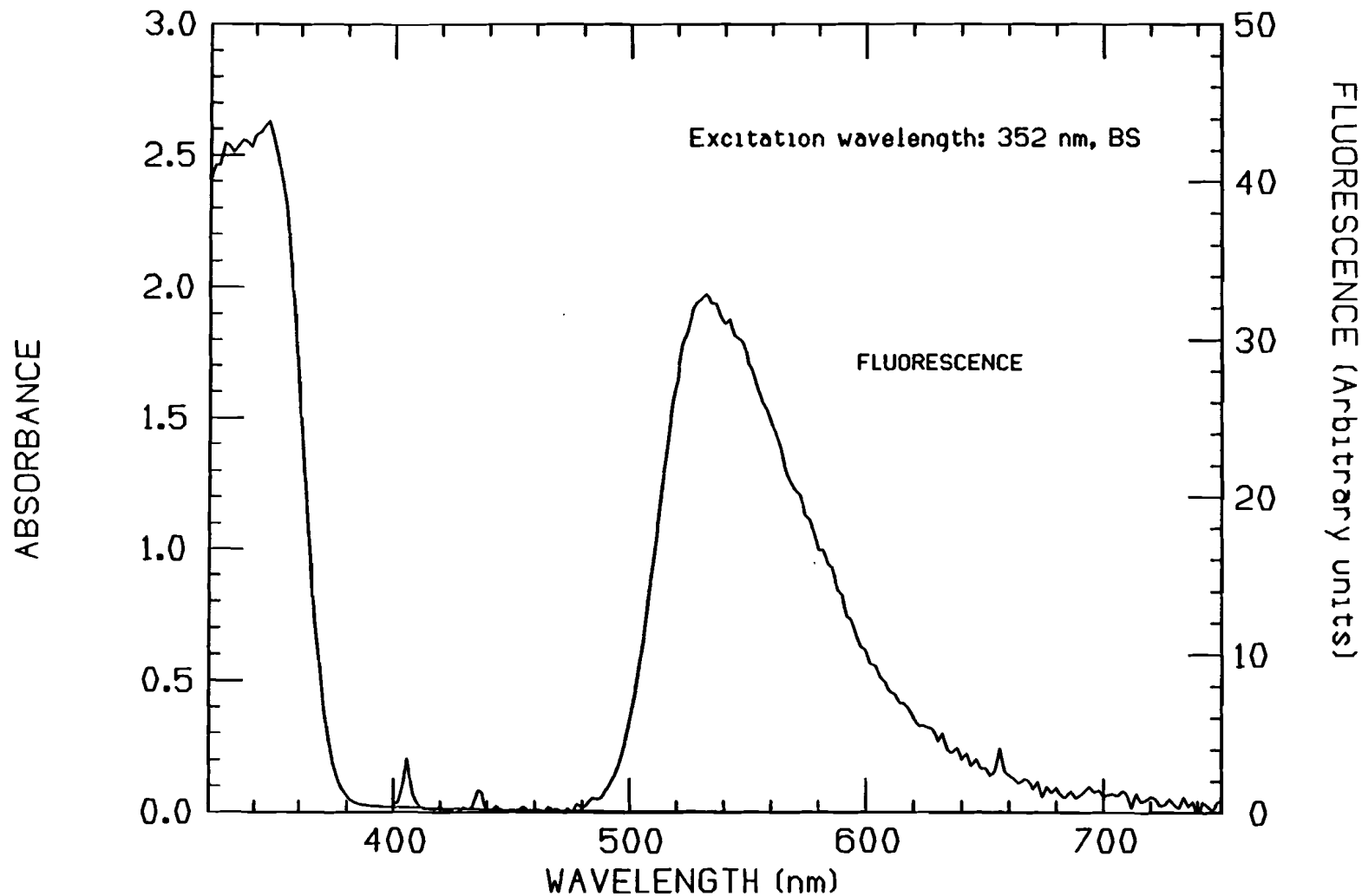

Figure 53. Absorption and emission spectra of 2F3HF in PS.

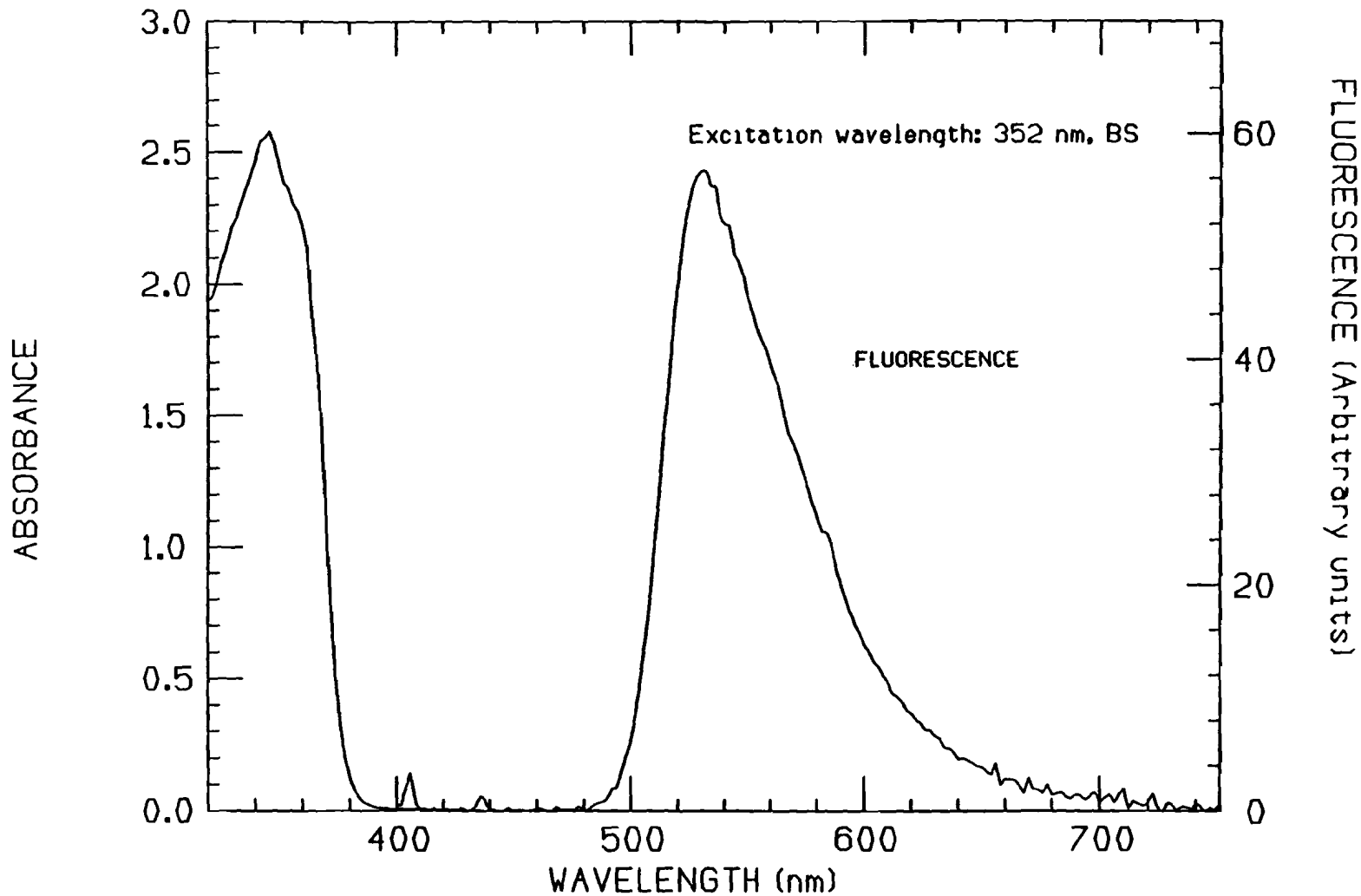

Figure 54. Absorption and emission spectra of 4F3HF in PS.

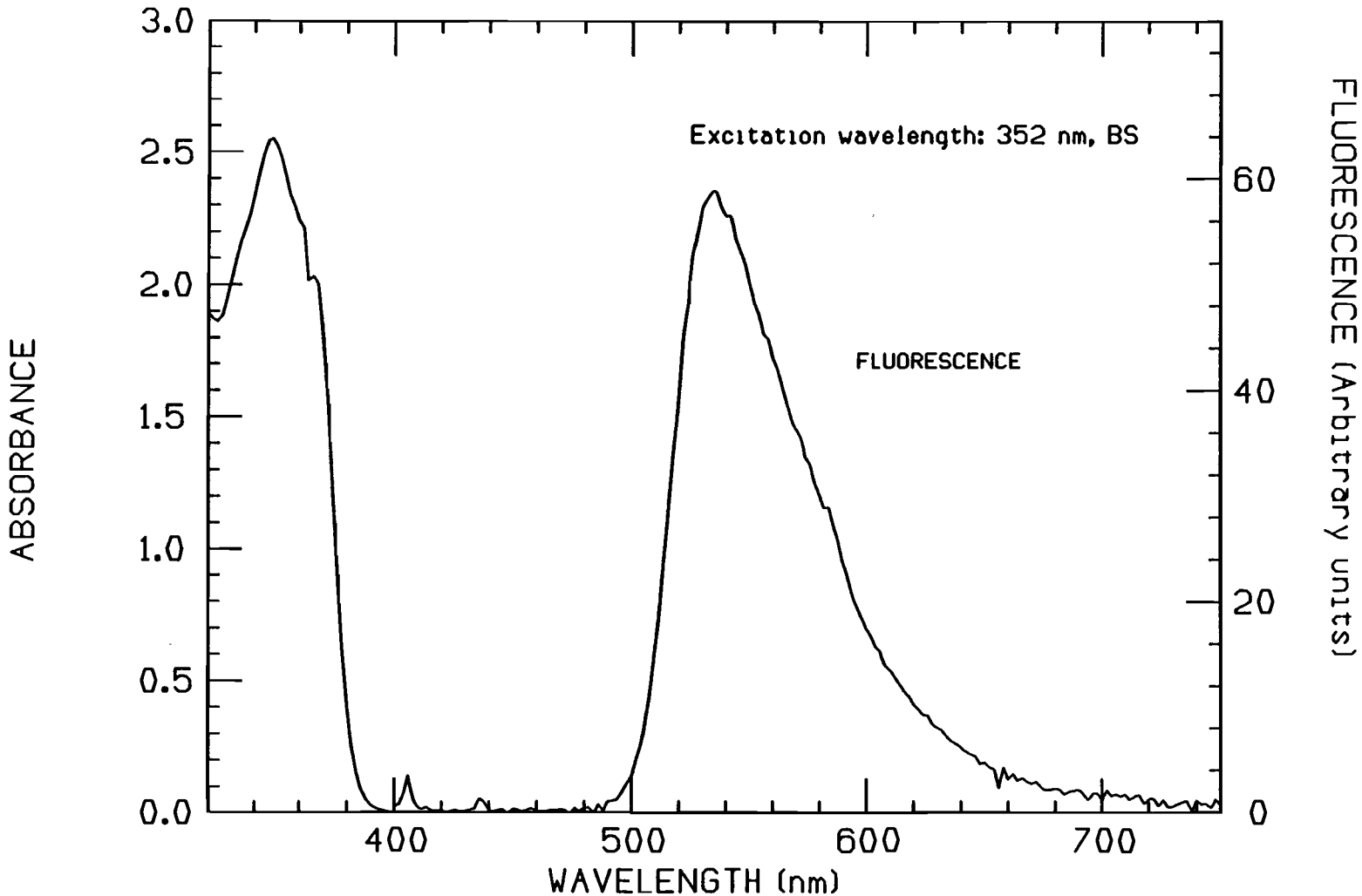

Figure 55. Absorption and emission spectra of 4M3HF in PS.

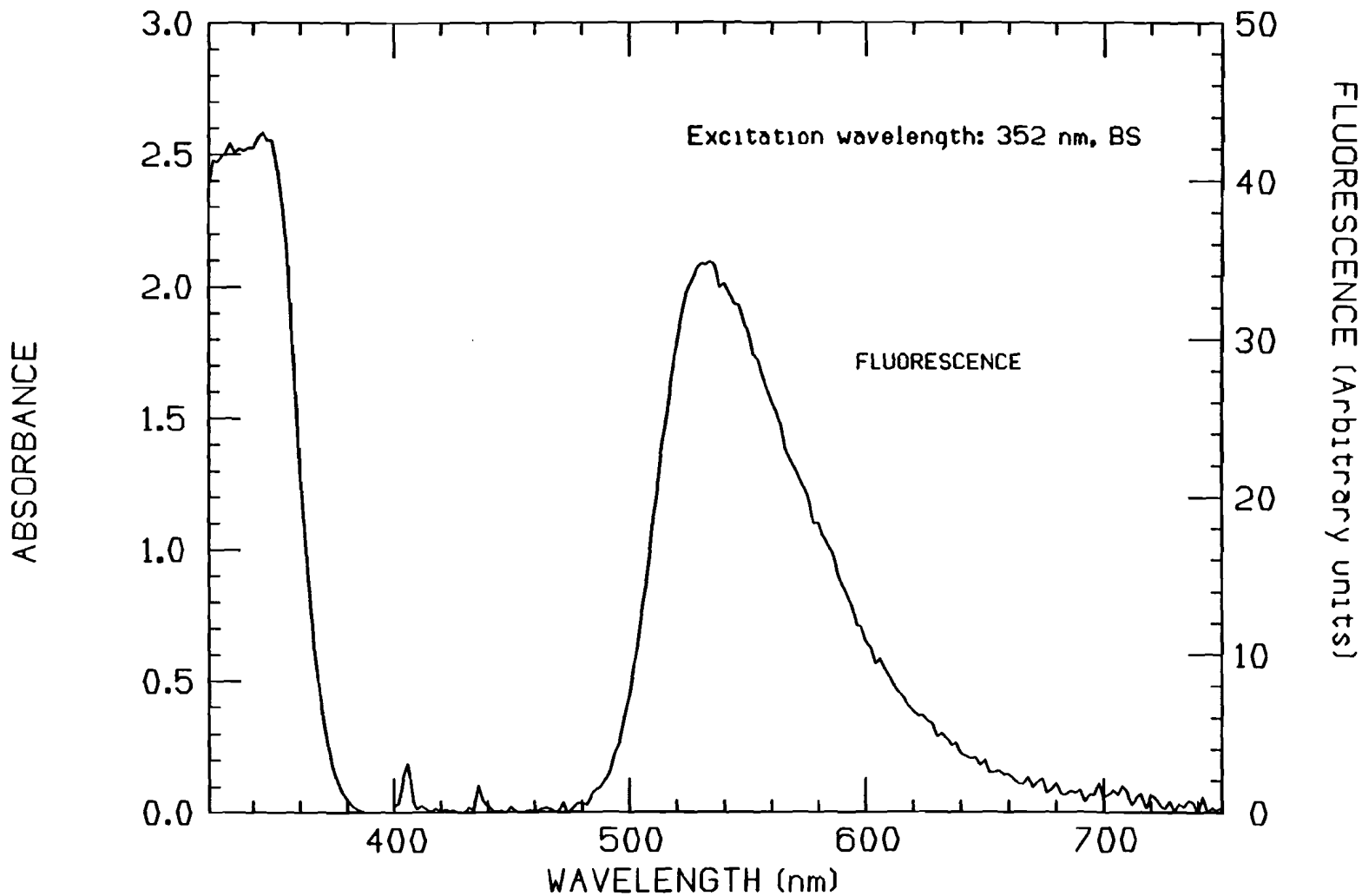

Figure 56. Absorption and emission spectra of 25M3HF in PS.

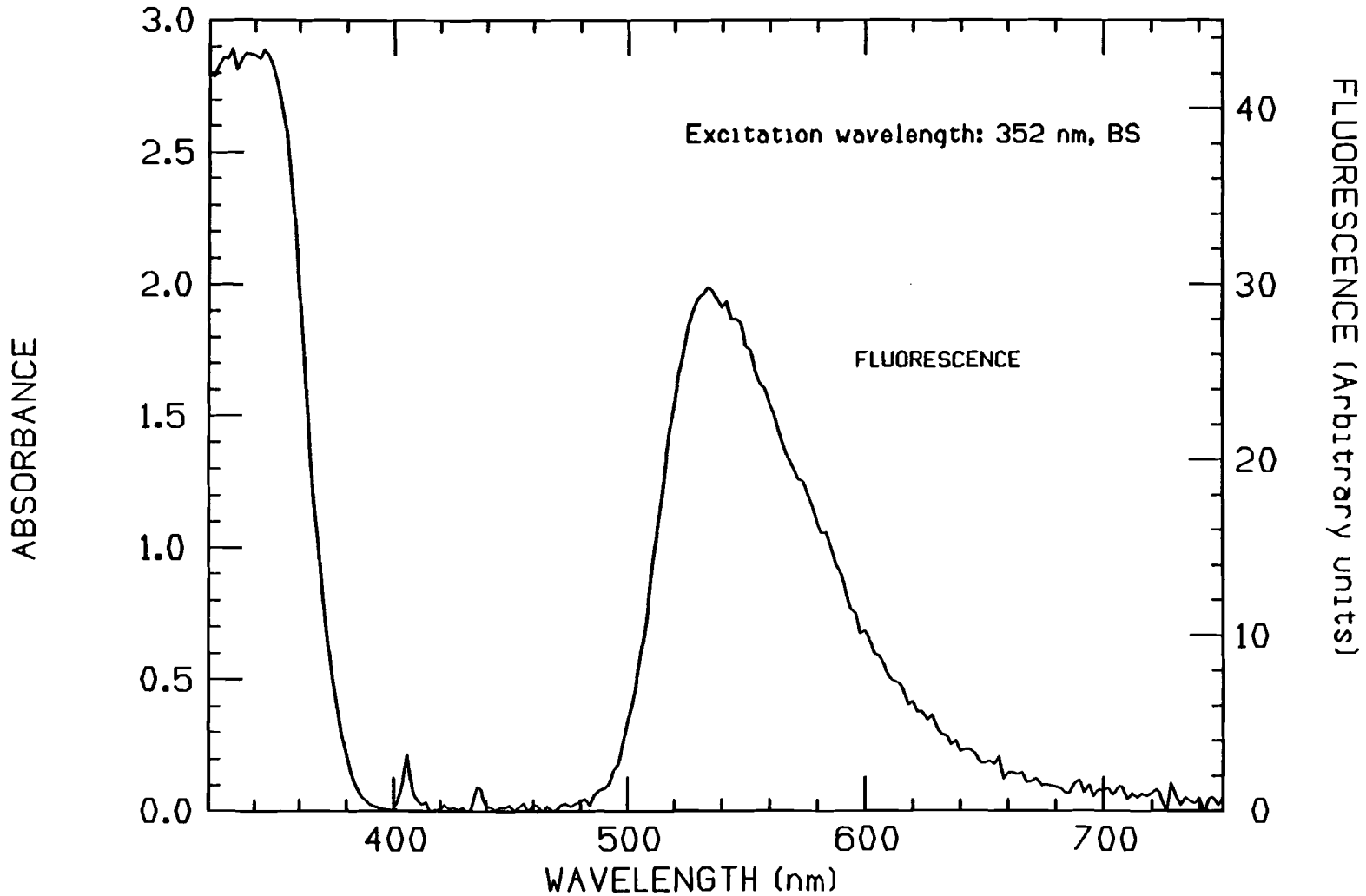

Figure 57. Absorption and emission spectra of 2MO3HF in PS.

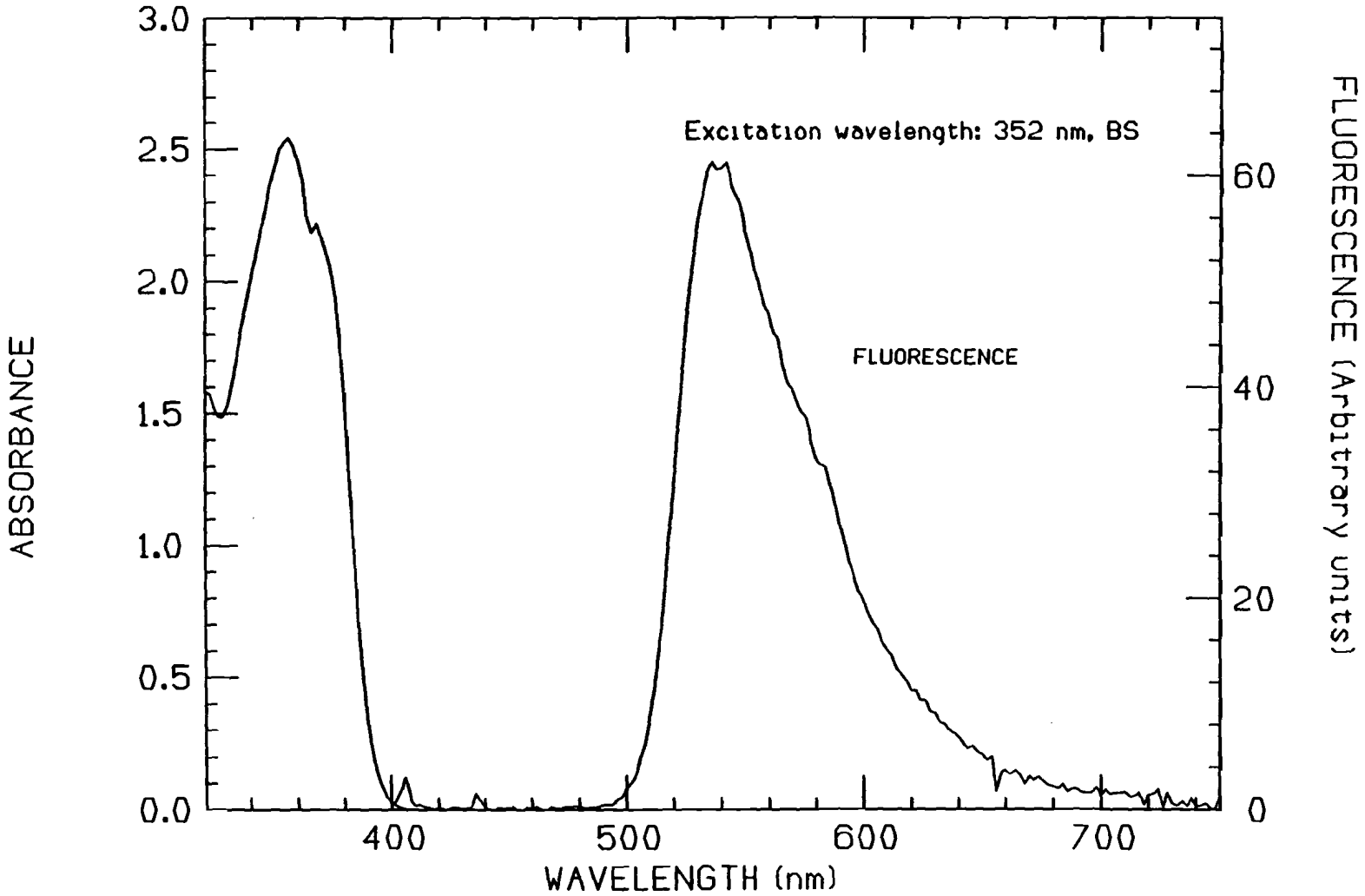

Figure 58. Absorption and emission spectra of 4MO3HF in PS.

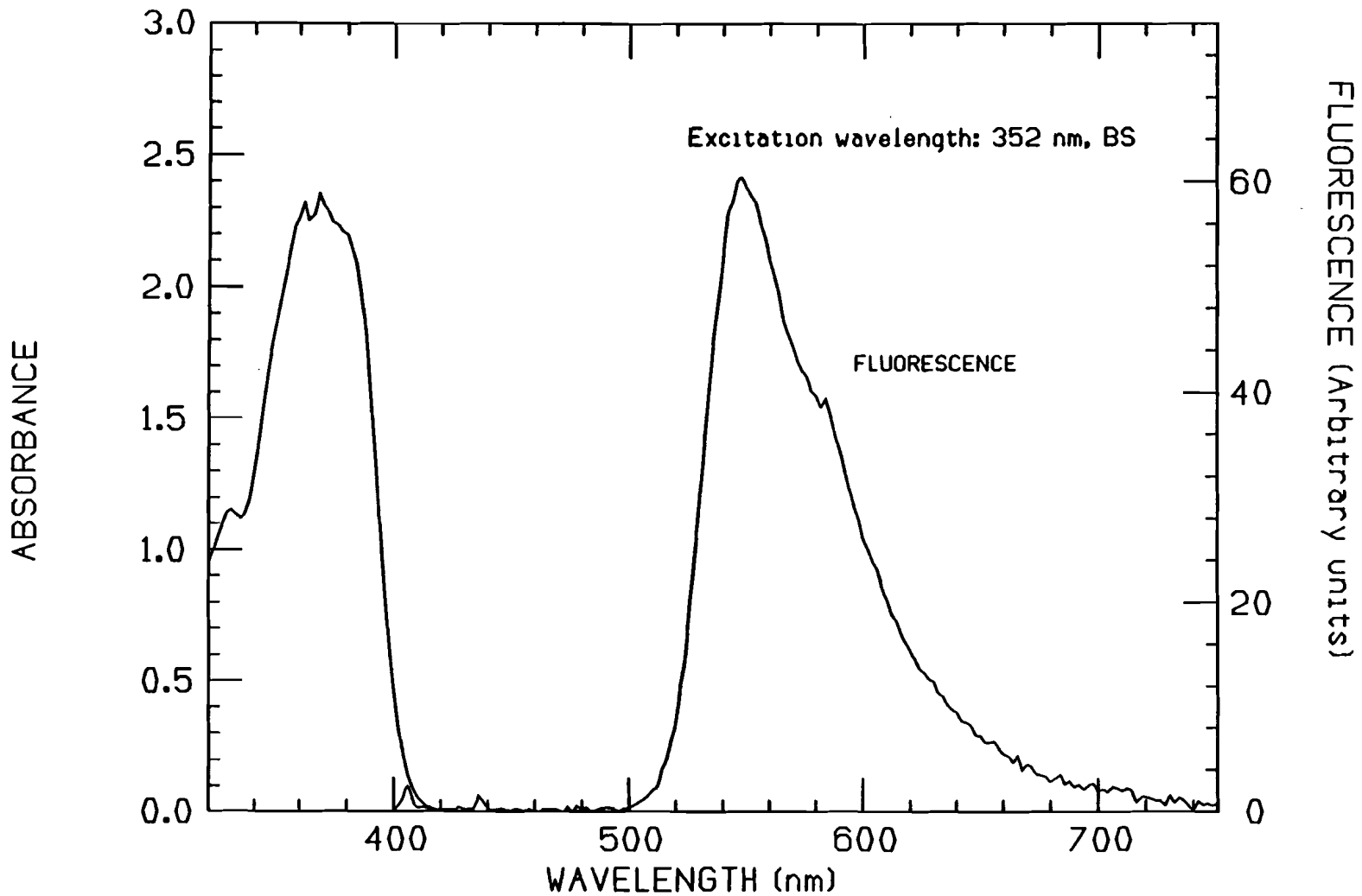

Figure 59. Absorption and emission spectra of 4MS3HF in PS.

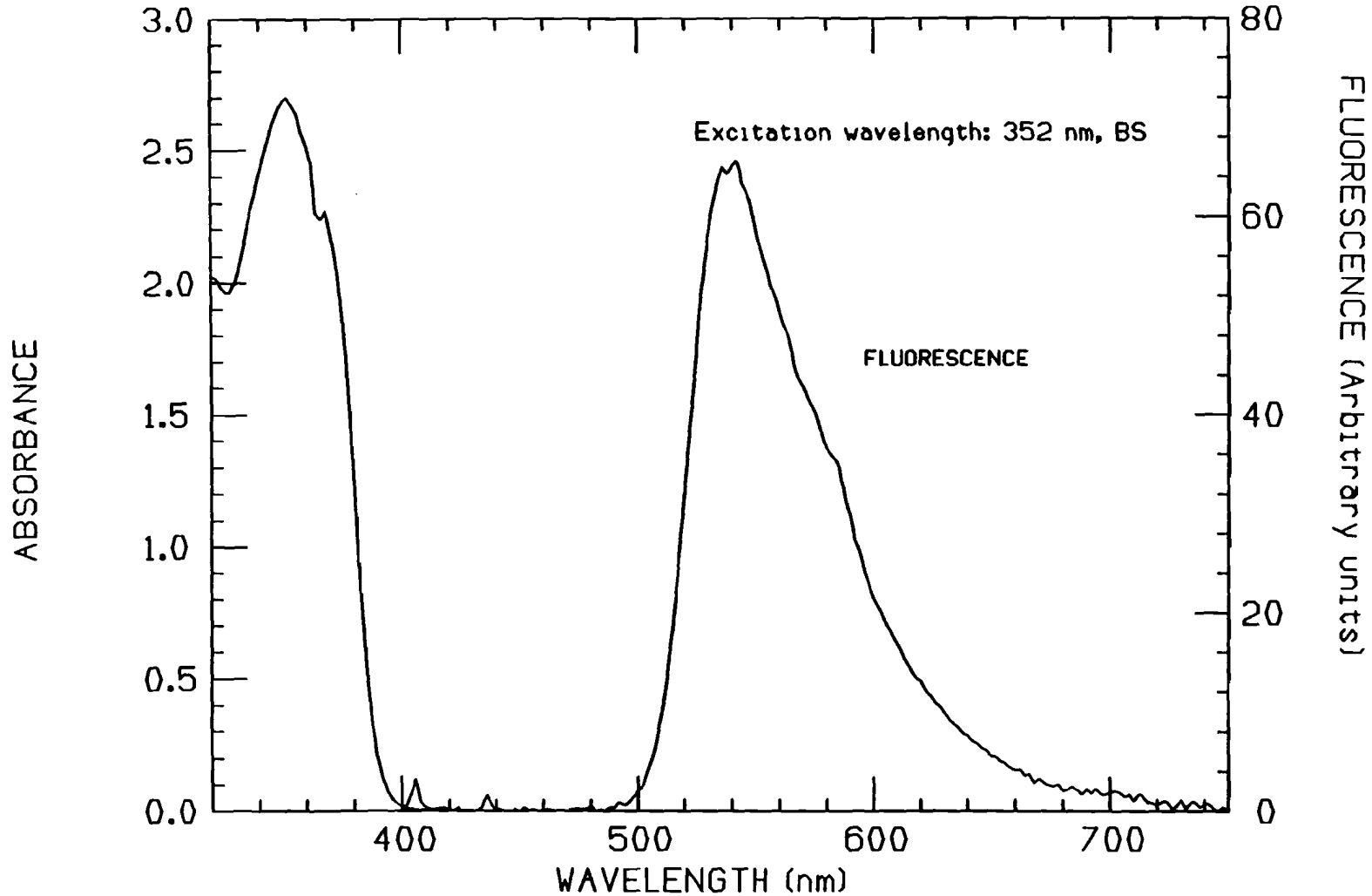

Figure 60. Absorption and emission spectra of 4PO3HF in PS.

APPENDIX B

ABSORPTION AND EMISSION SPECTRA OF IRRADIATED HBT AND 3HF DERIVATIVES IN POLYSTYRENE

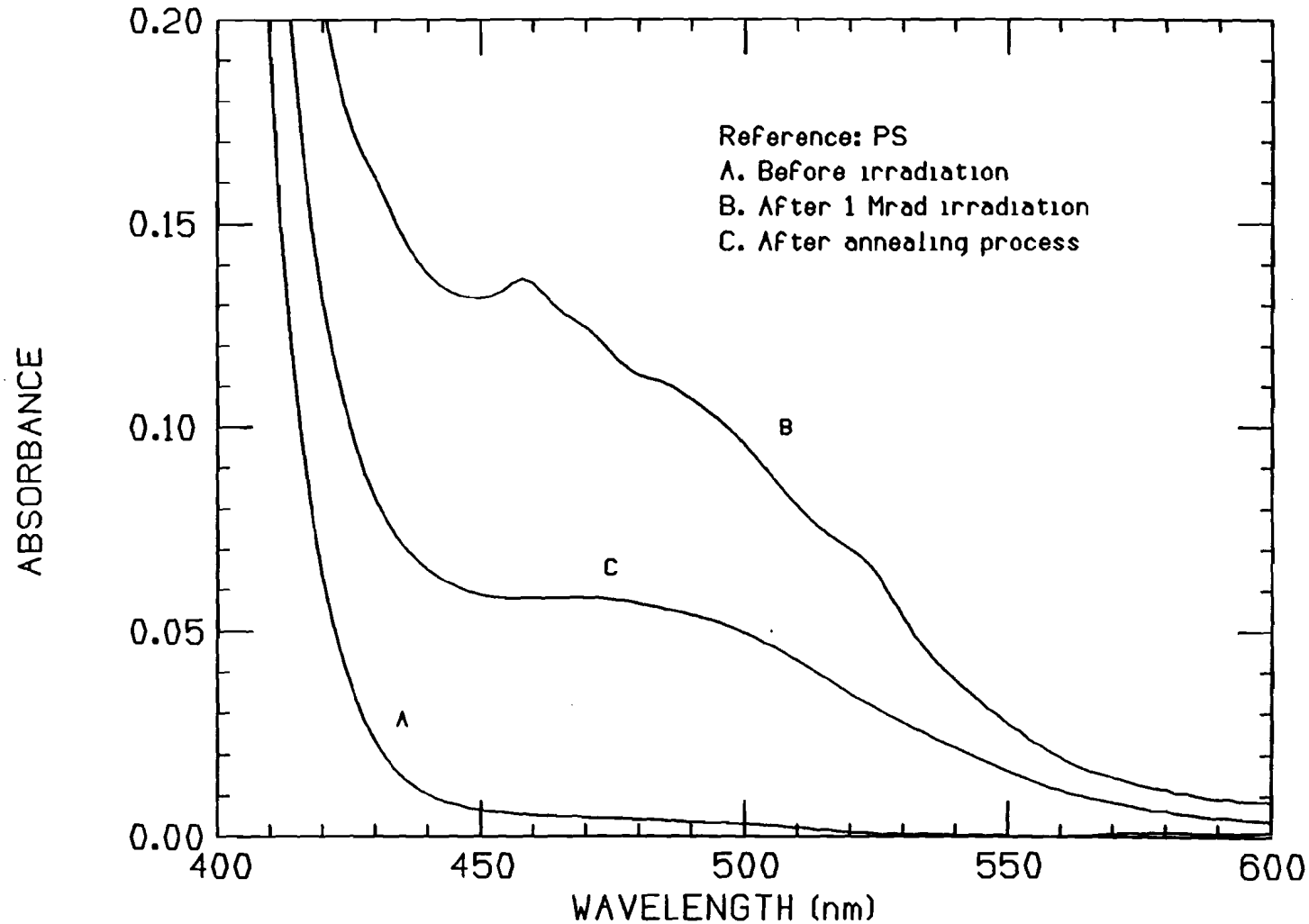

Figure 61. Absorption spectra of irradiated 3CHBT/PS.

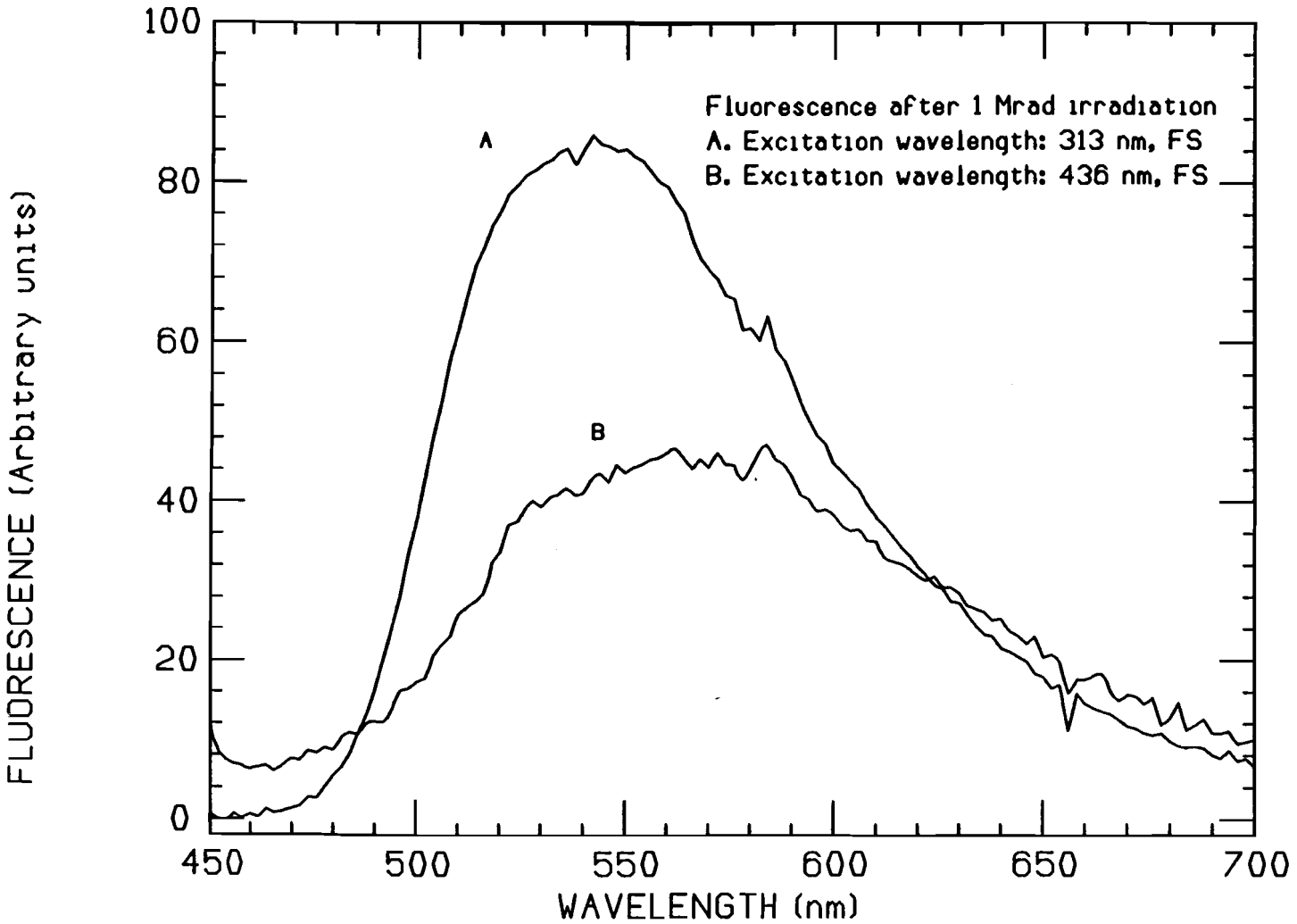

Figure 62. Fluorescence spectra of irradiated 3CHBT/PS.

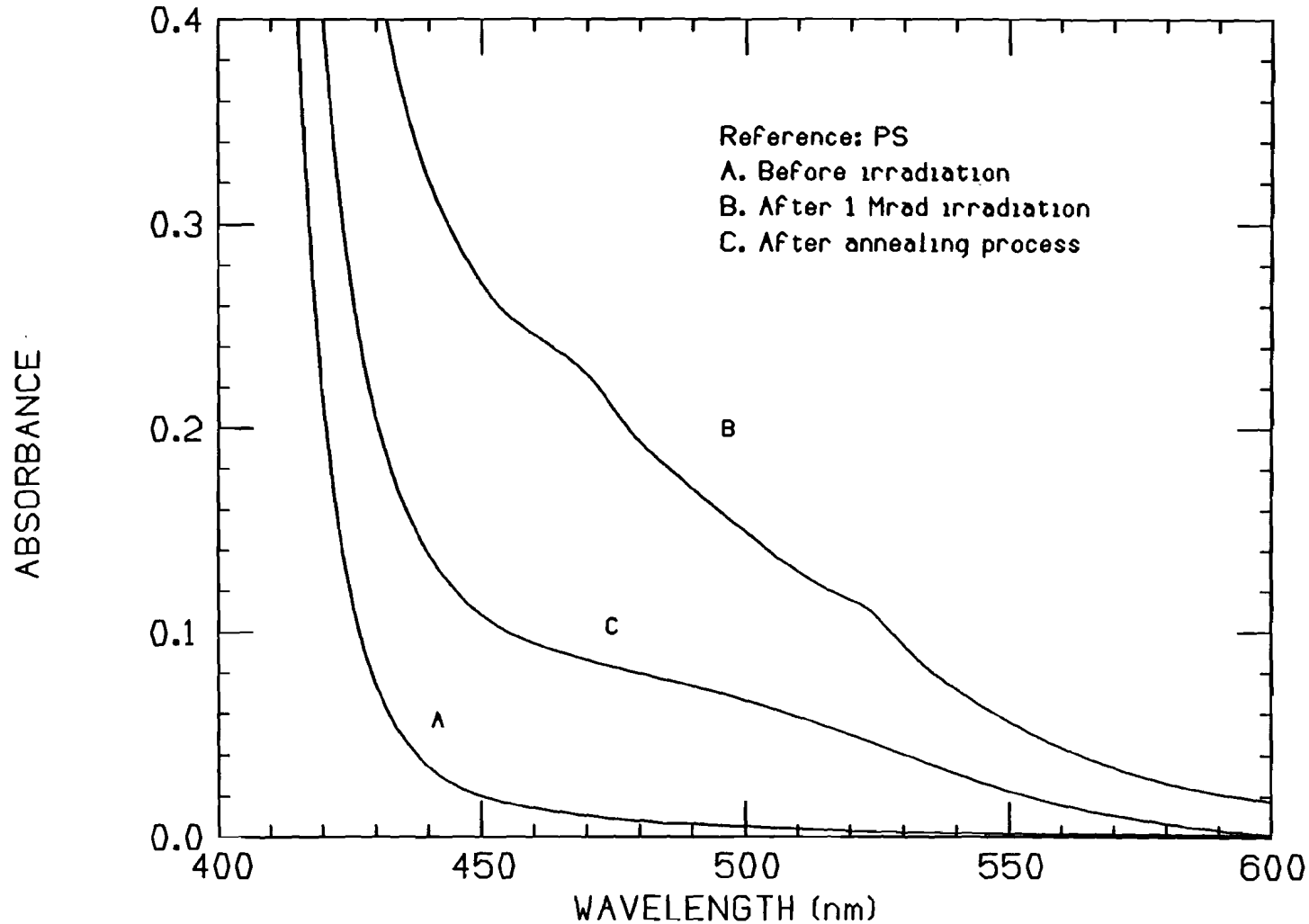

Figure 63. Absorption spectra of irradiated 3PHBT/PS.

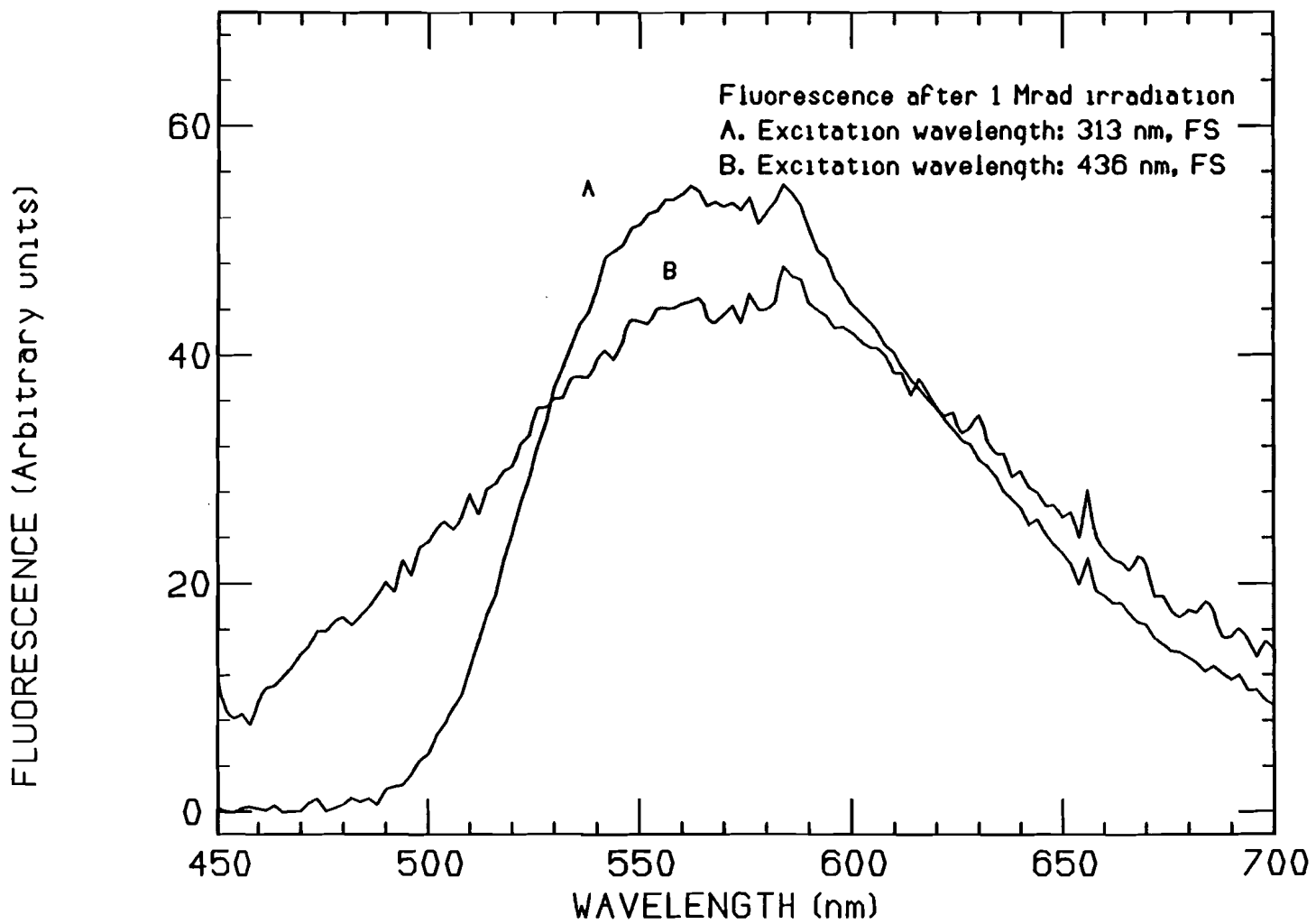

Figure 64. Fluorescence spectra of irradiated 3PHBT/PS.

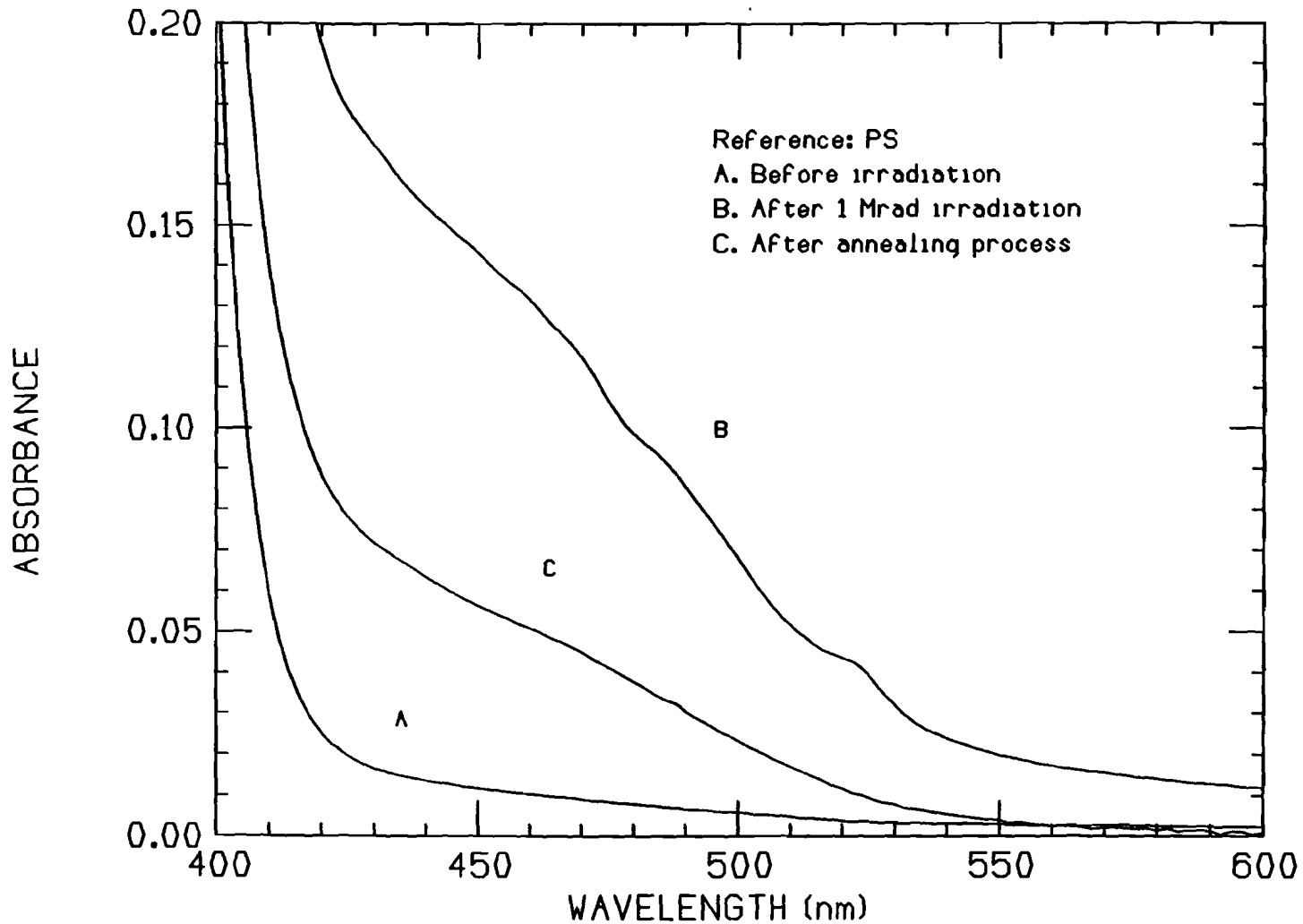

Figure 65. Absorption spectra of irradiated 4MHBT/PS.

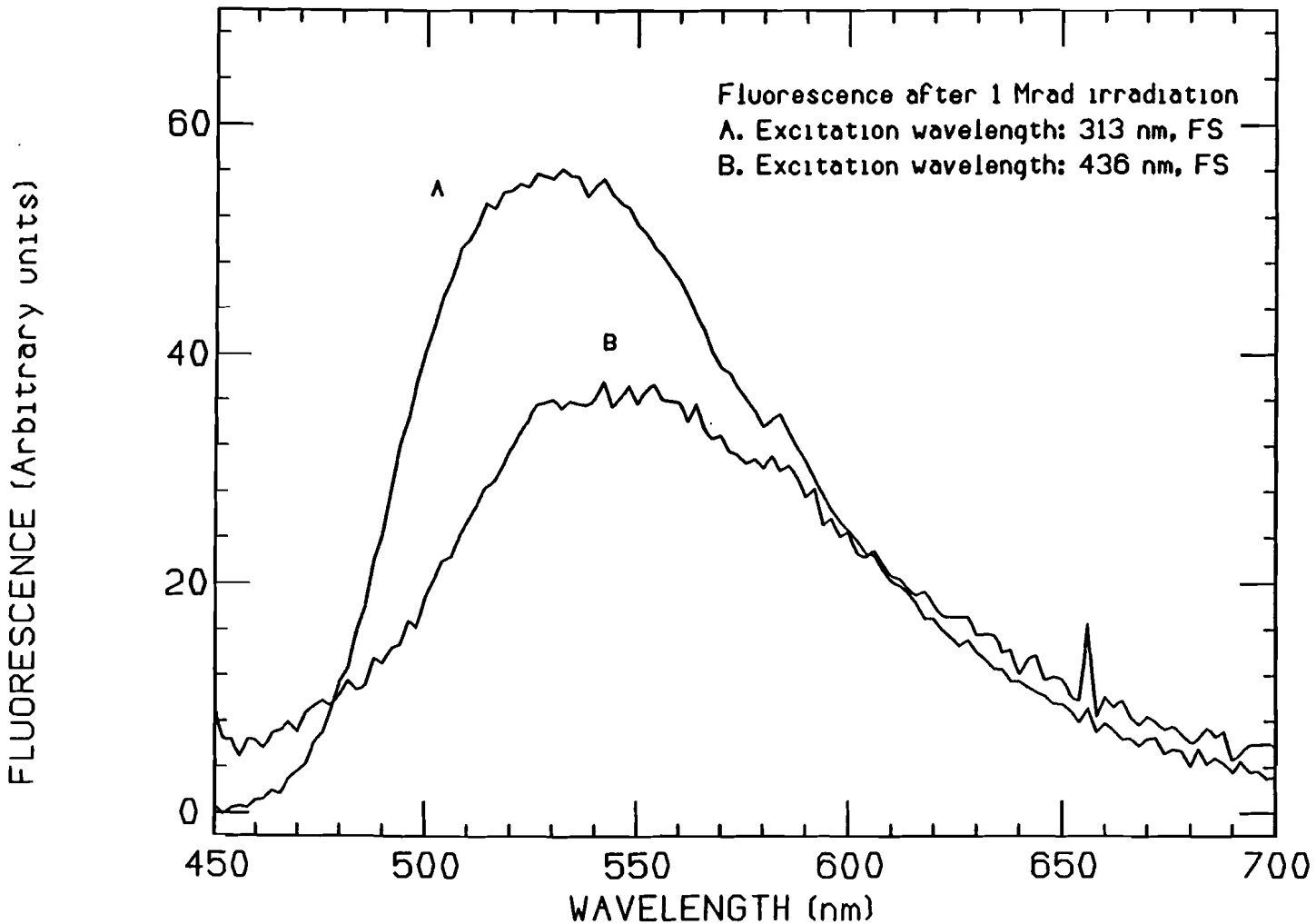

Figure 66. Fluorescence spectra of irradiated 4MHBT/PS.

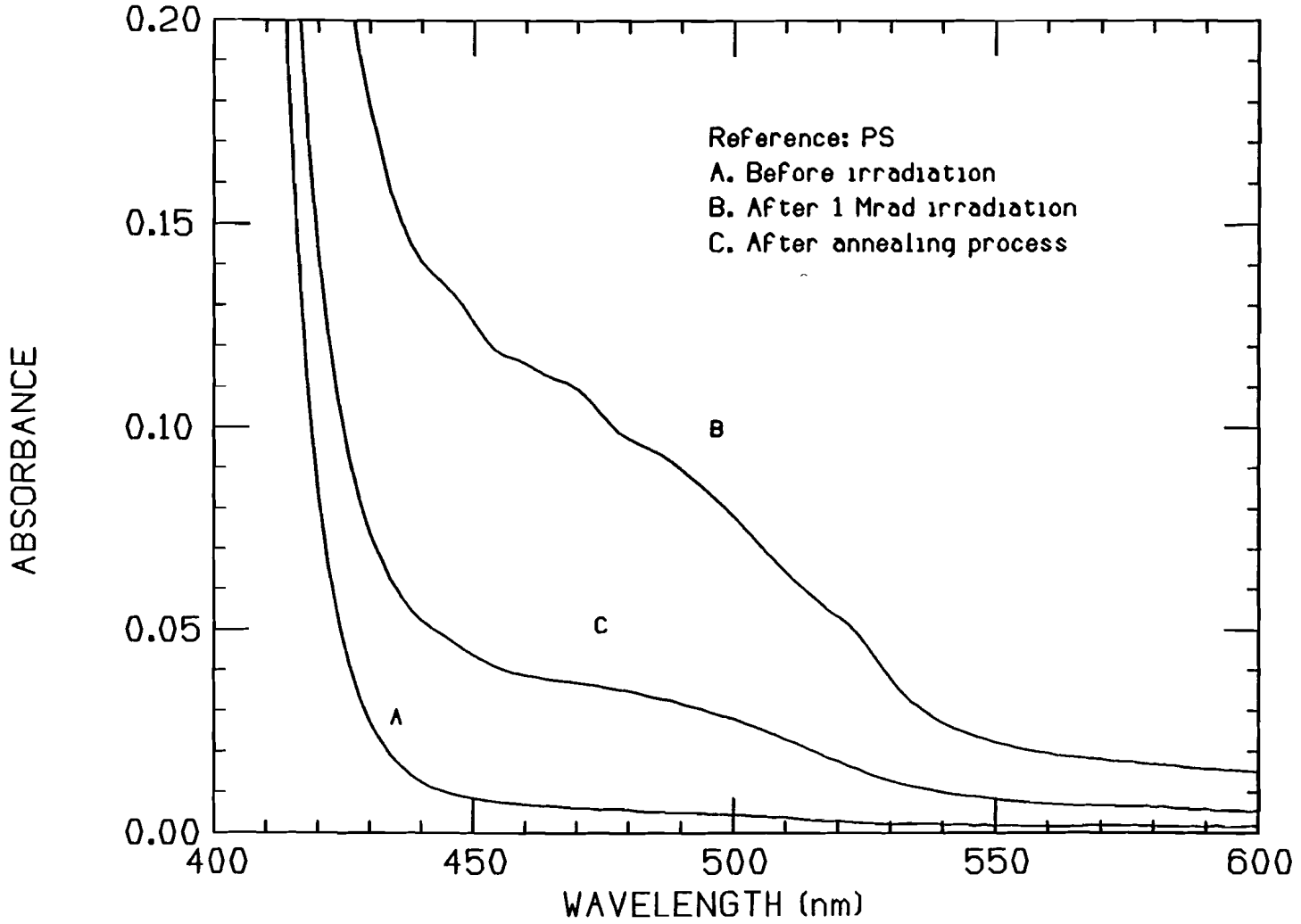

Figure 67. Absorption spectra of irradiated 5MHBT/PS.

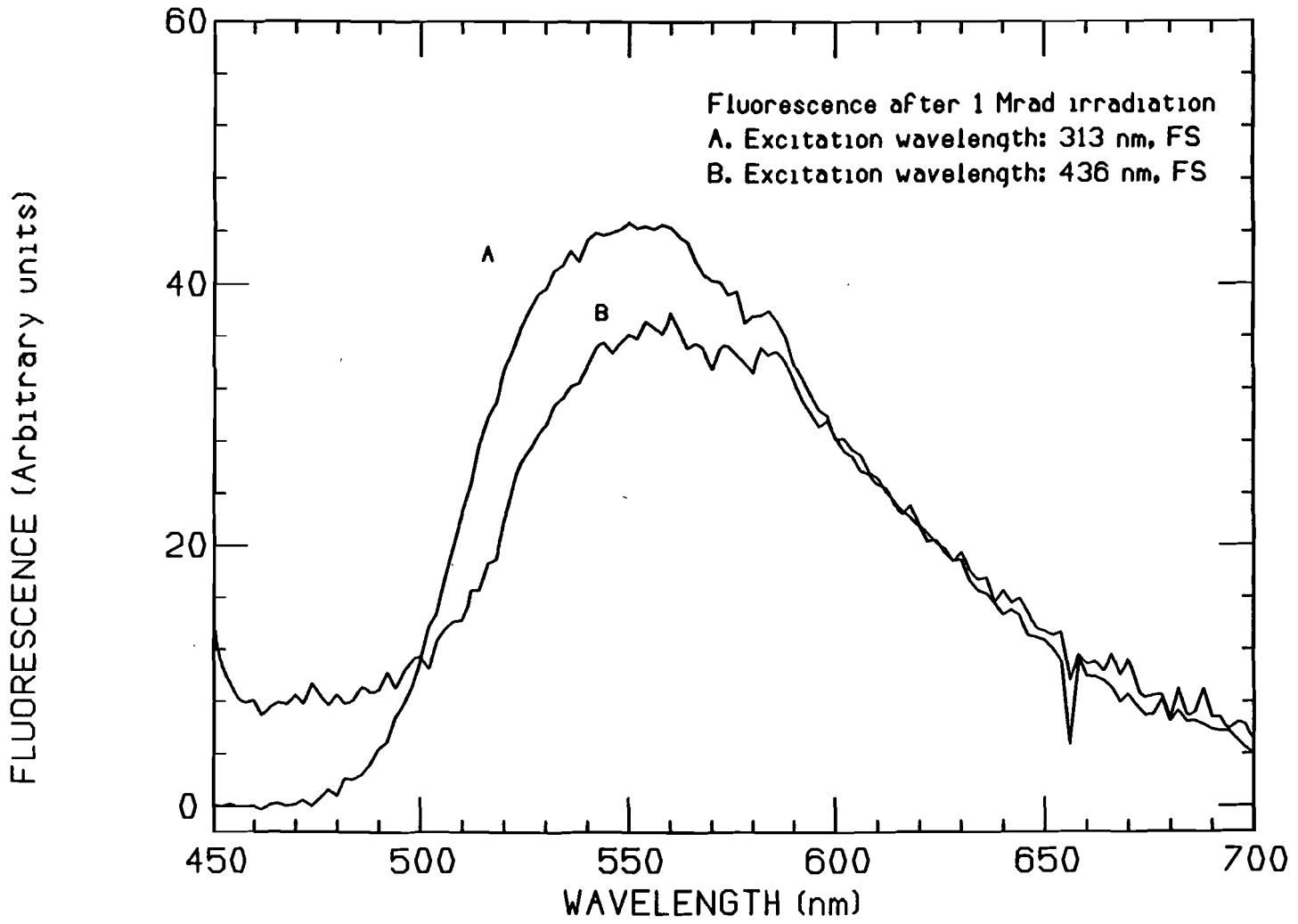

Figure 68. Fluorescence spectra of irradiated 5MHBT/PS.

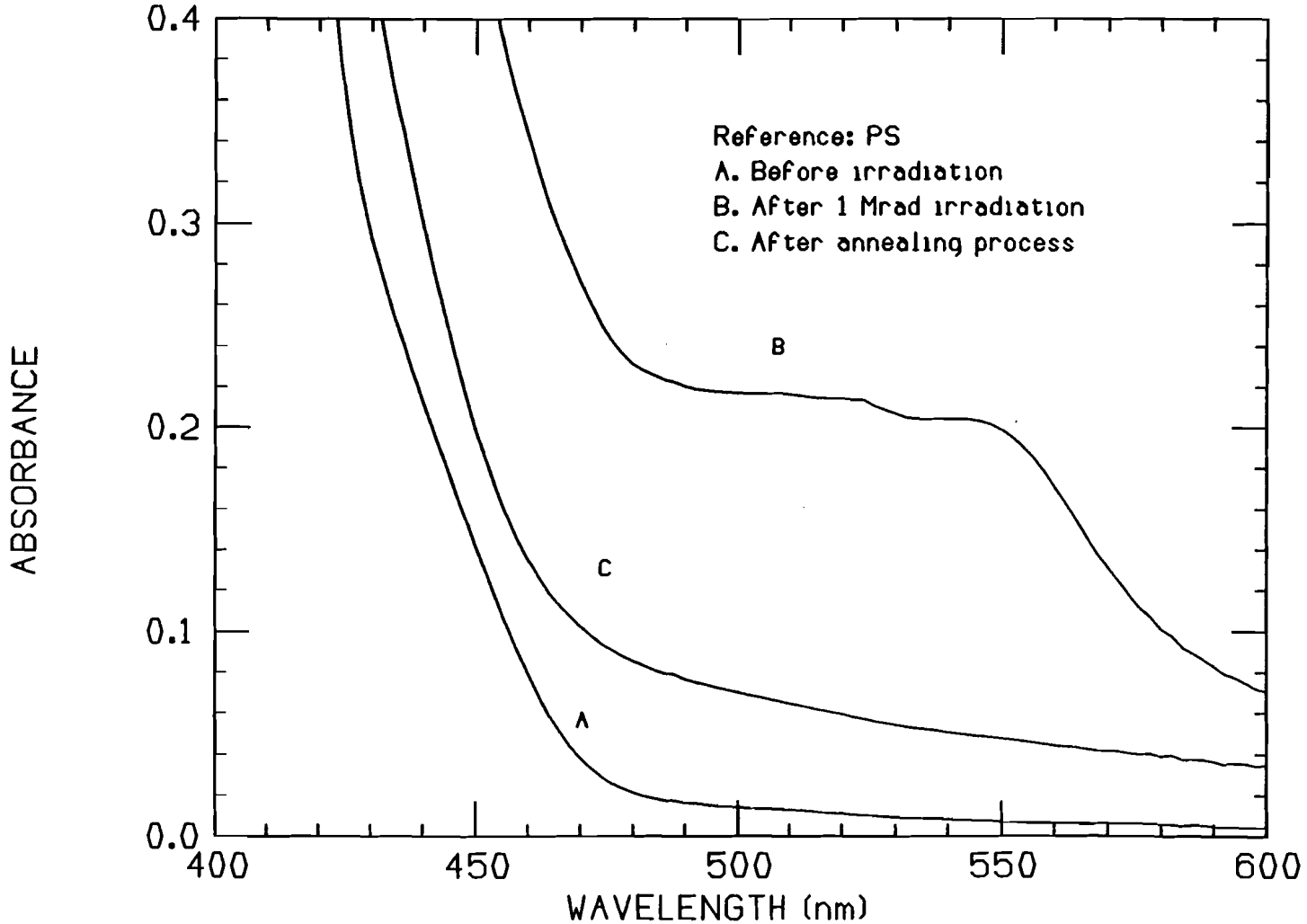

Figure 69. Absorption spectra of irradiated 5PHBT/PS.

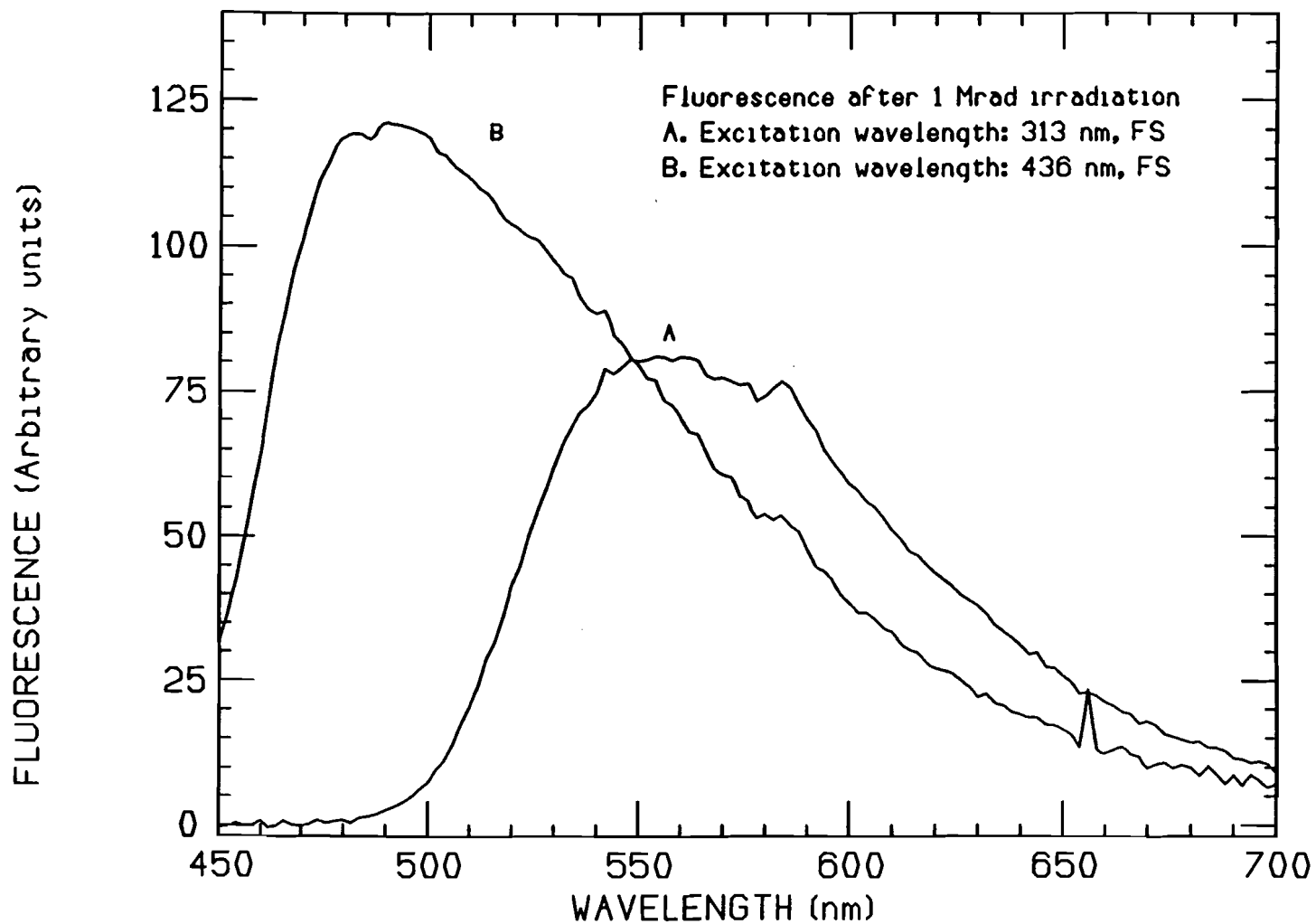

Figure 70. Fluorescence spectra of irradiated 5PHBT/PS.

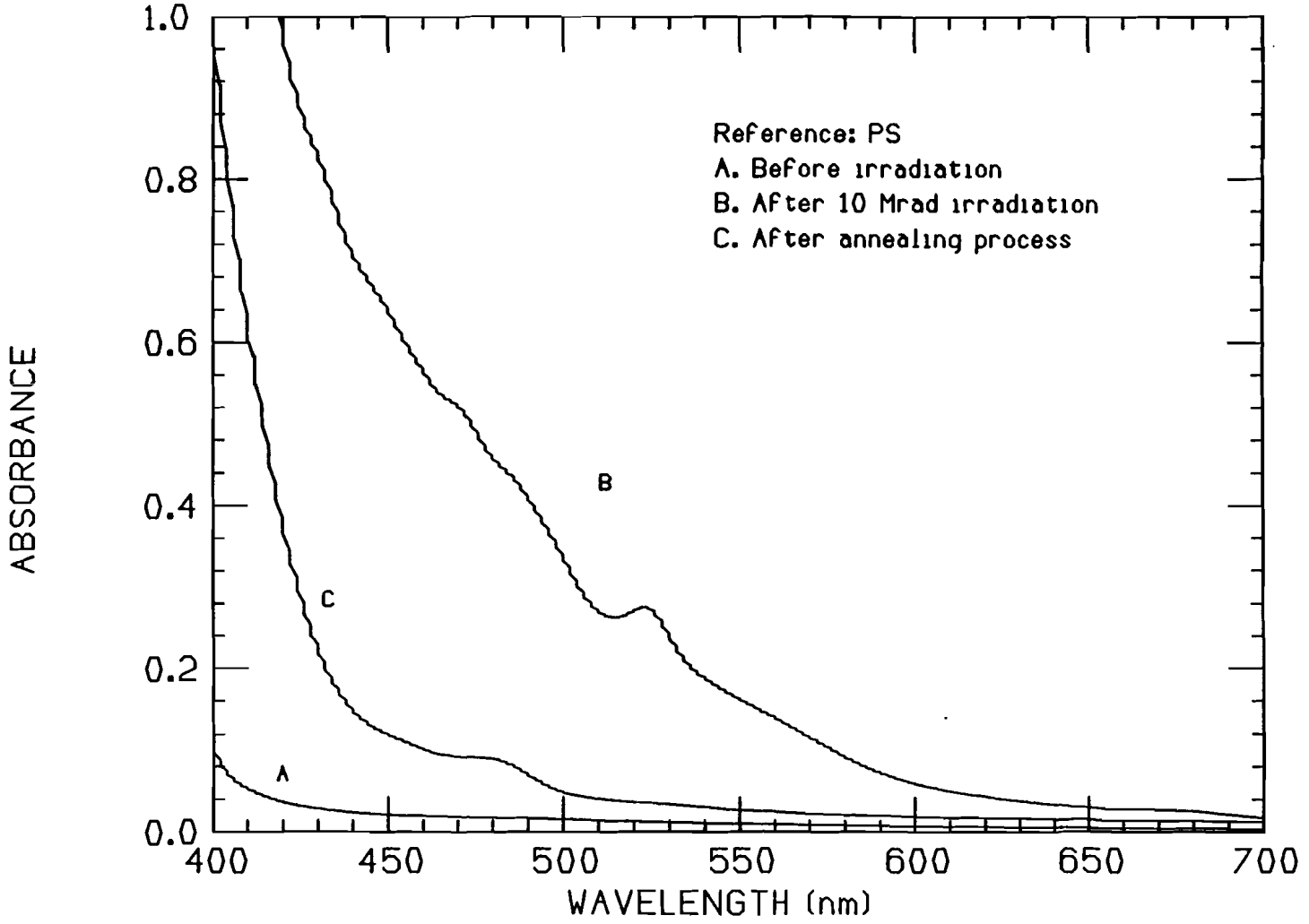

Figure 71. Absorption spectra of irradiated 2M3HF/PS.

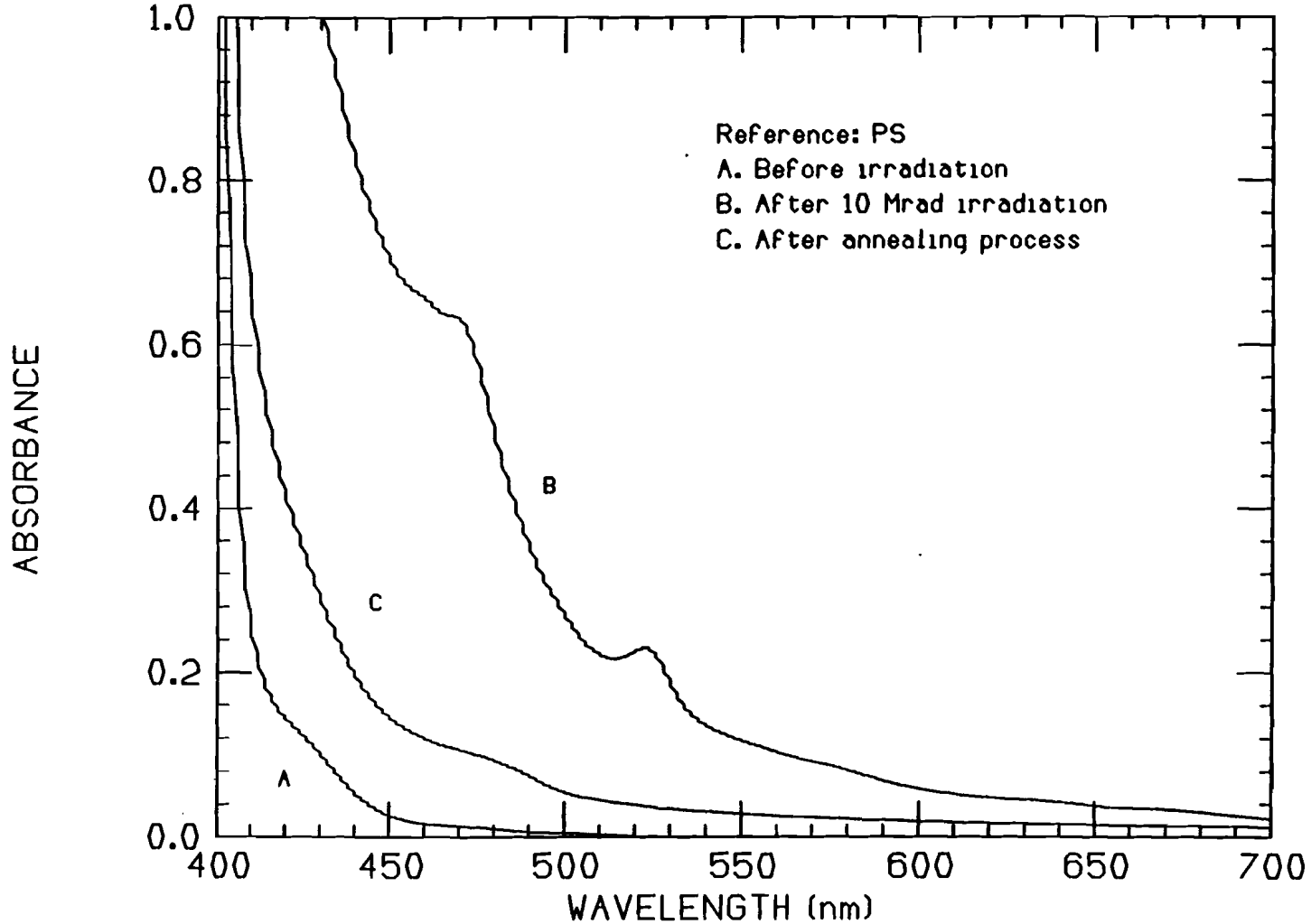

Figure 72. Absorption spectra of irradiated 4M3HF/PS.

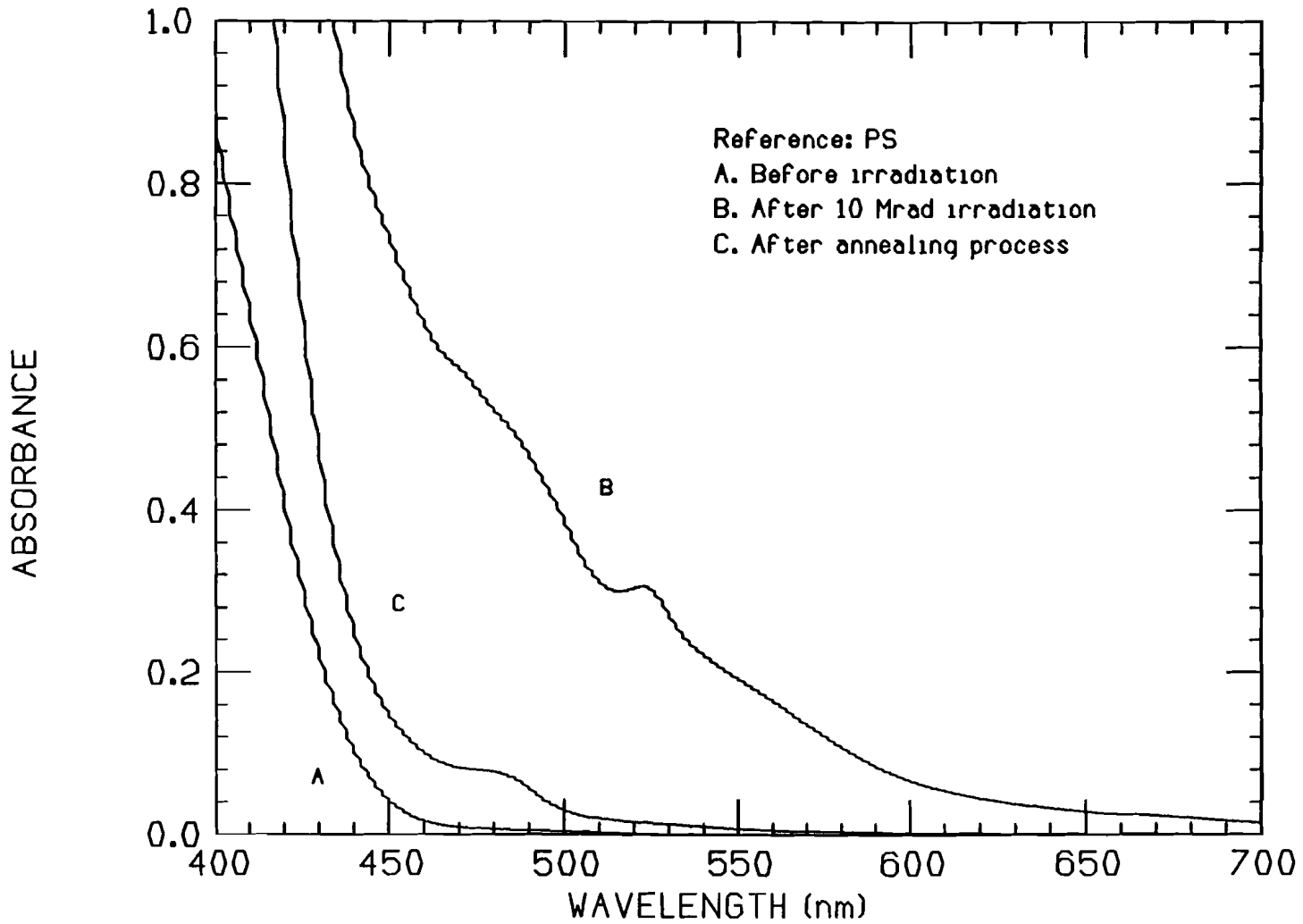

Figure 73. Absorption spectra of irradiated 25M3HF/PS.

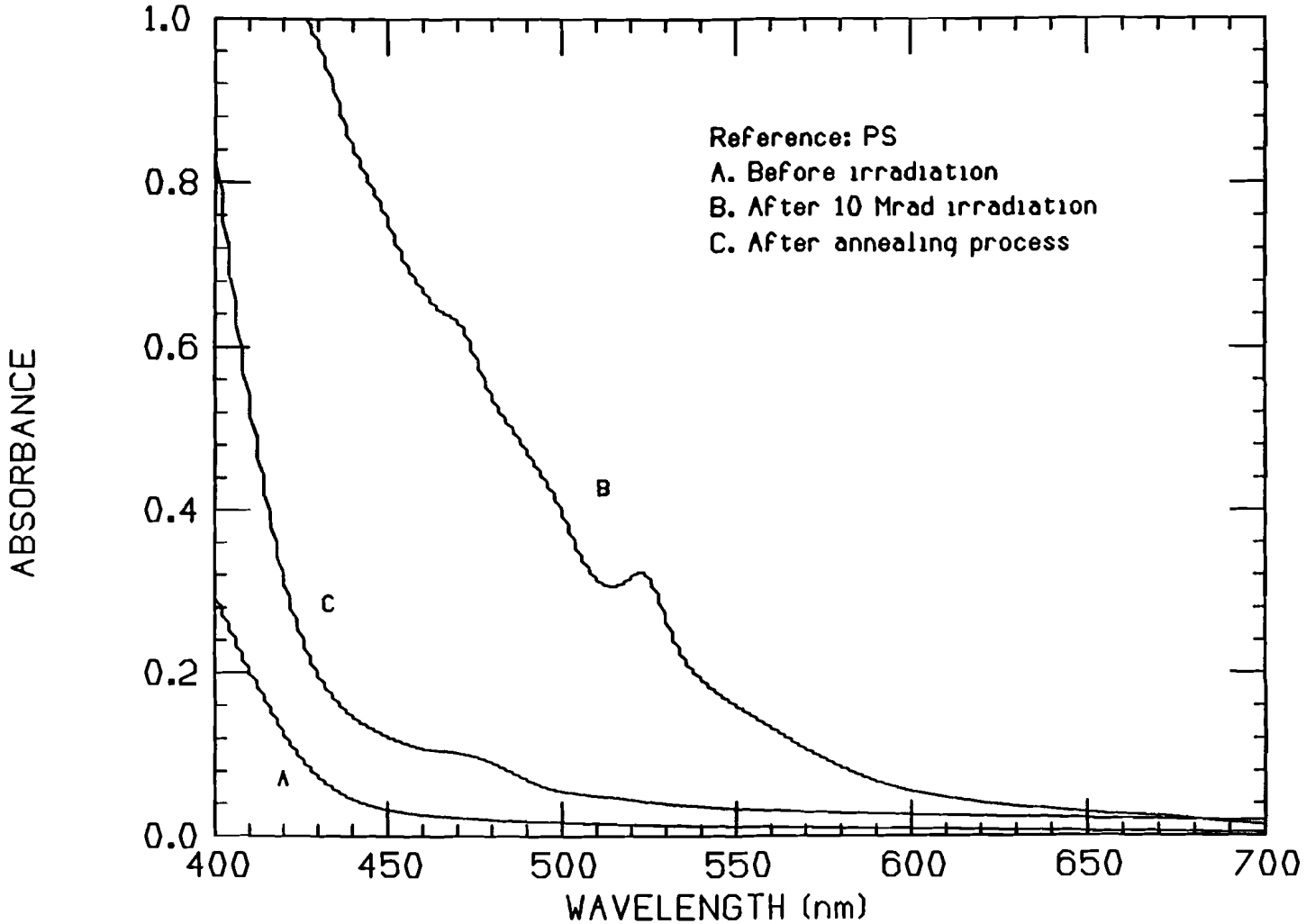

Figure 74. Absorption spectra of irradiated 2C3HF/PS.

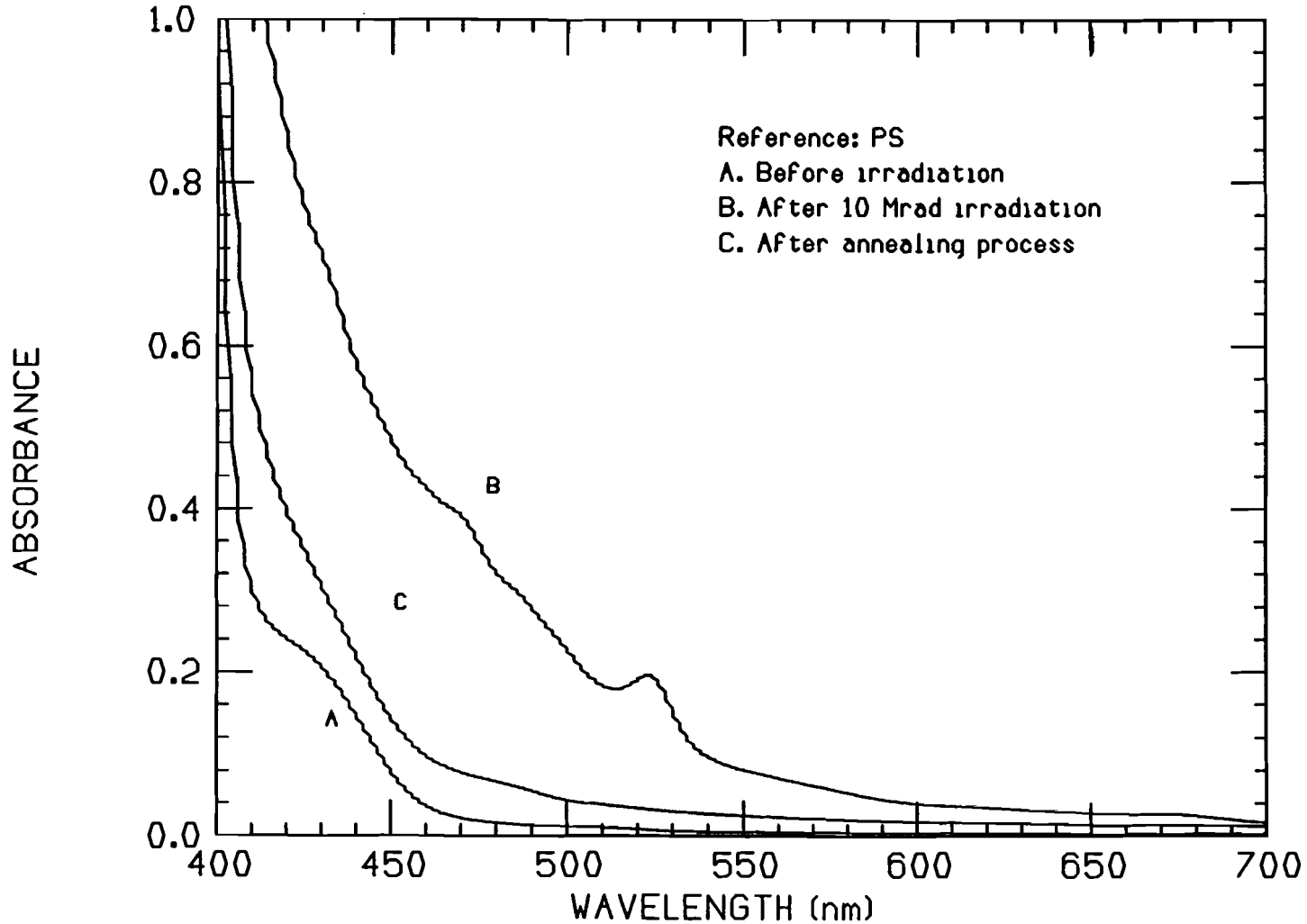

Figure 75. Absorption spectra of irradiated 4C3HF/PS.